1992

Mechanical Behavior of a Continuous Fiber Reinforced SiC/RBSN Ceramic Composite

Nancy M. Narbut
University of Massachusetts Amherst

MECHANICAL BEHAVIOR OF A CONTINUOUS FIBER REINFORCED SiC/RBSN CERAMIC COMPOSITE

A Thesis Presented

by

NANCY M. NARBUT

Submitted to the Graduate School of the
University of Massachusetts in partial fulfillment
of the requirements for the degree of

MASTER OF SCIENCE IN MECHANICAL ENGINEERING

May 1992

Department of Mechanical Engineering

MECHANICAL BEHAVIOR OF A CONTINUOUS FIBER REINFORCED SiC/RBSN CERAMIC COMPOSITE

A Masters Thesis Presented
by
NANCY M. NARBUT

Approved as to style and content by:

Shantikumar V. Nair

Shanti V. Nair, Chair

John E. Ritter, Member

James A. Donovan, Member

Thomas R. Blake, Department Head
Department of Mechanical Engineering

ACKNOWLEDGMENTS

I would like to thank Professor Nair for his encouragement in continuing my studies and for all of his support, guidance, and understanding as my advisor. I also thank Jim Kohl, who started this research so long ago, and Ramesh Ramakrishnan for their friendship and infinite patience when I first started working in the lab. Tsung-Ju Gwo and Hong-Gun Kim also deserve considerable thanks and recognition for their contributions to this thesis as well as for their friendship along with my other labmates Ming-Liang Shiao, Peter Z. Q. Cai, and Yu-Lin Wang.

I would also like to thank Professor Ritter and Professor Donovan for serving on the committee; Glenn Sundberg from Norton Company for supplying the material for my research; Professor Russell for all his help and encouragement, especially in the job search; and Dawn Murphy and Jim Webb for their friendship in my adopted lab. I final and very important thanks goes to my family who have made all of this possible.

ABSTRACT

MECHANICAL BEHAVIOR OF A CONTINUOUS FIBER REINFORCED SiC/RBSN CERAMIC COMPOSITE

MAY 1992

NANCY M. NARBUT, B.S.M.E., UNIVERSITY OF MASSACHUSETTS

M.S.M.E., UNIVERSITY OF MASSACHUSETTS

Directed by: Professor Shanti V. Nair

The purpose of the following research was to obtain an understanding of both ambient and elevated temperature mechanical behavior of a SiC fiber reinforced RBSN composite. At ambient temperature, applicability of available mechanics models to describe the stress-strain curve were examined. Emphasis was also placed on fracture toughness, R-curve behavior, and toughening mechanisms as well as the applicability of available fracture mechanics models to describe toughening behavior. At elevated temperature, an attempt was made to characterize the short term and long term effects on the composite. The material used was a RBSN reinforced with large diameter continuous SiC fibers. A limited investigation of the mechanical behavior of a commercially available RBSN monolith was also performed for comparison purposes with the reinforced material.

At ambient temperature the composite exhibited noncatastrophic failure and analysis of the results suggested that fiber pullout as well as elastic fiber bridging effects may both provide significant contributions to the overall toughness, with the

overall potential for toughness calculated to be on the order of 54 MPa·m$^{1/2}$. Analysis of the toughness based on these mechanisms was complicated, however, by the large amount of delamination that took place in this composite. Toughening occurred as fiber pullout, bridging, and mixed mode failure at room temperature. At elevated temperatures, crack initiation under constant load occurred, after a delay period, in the matrix at temperatures on the order of 1000° C, but occurred in the fiber itself as the temperatures increased past 1350° C. The elevated temperature cracks were normal to the reinforcing fibers and were associated with unbroken bridging fibers in the crack wake. Furthermore, it was observed that the fibers pulled out of the matrix in a time-dependent fashion, thus making bridging a time dependent process during elevated temperature exposure.

TABLE OF CONTENTS

LIST OF TABLES

LIST OF FIGURES

CHAPTER 1

INTRODUCTION

Reaction-bonded silicon nitride (RBSN) is an attractive candidate for structural applications because of it ease of fabrication, low thermal expansion, high specific strength, minimal shrinkage during processing, and good environmental stability due to the absence of sintering additives. It is formed by heating a silicon powder compact, which may be, for example, in the shape of a component, to a temperature between 1250° and 1450°C in a nitrogenous atmosphere [1]. Although the solid volume changes by ≈22% the change in the dimension is negligible. Even with these low processing temperatures, studies have shown RBSN to have promising thermo-mechanical properties, including a good creep resistance in air. However, despite its numerous advantages, investigations have shown that the fracture toughness of RBSN is only about 2-3 $MPa \cdot m^{1/2}$ with no reported R-curve behavior - a desirable material property in which the toughness increases with the size of the crack. The high residual porosity, approximately 20% for a typical commercial RBSN, is also of concern since the strength, according to some researchers [2] may be determined by the size of the largest pores present. In addition, others have stressed the importance of the interconnectivity of this porosity because of its ability to contribute to internal oxidation during creep [3].

With the major disadvantage of RBSN being its low toughness, many attempts have focussed on the reinforcement of RBSN with high modulus fibers [4,5,6,7,8,9],

particulates [10], or whiskers [11,12] in an effort to increase the toughness. The low processing temperatures and the low value of thermal expansion allow for the incorporation of second phases with a minimum of degradation and residual stress. Ideally, reinforcement would provide a composite that shows R-curve behavior and non-catastrophic failure as well as an increase in toughness. Continuous fibers have shown promise [4,5,6,8] in providing these composite properties and materials containing fiber reinforcements have been the focus of much recent study [13].

The potential for improving the properties of RBSN has already been clearly demonstrated for the case of continuous fiber reinforced RBSN. Investigators have shown significant improvements in both strength and work-of-fracture (area under the stress-strain curve) over that of RBSN [6]. The sensitivity of property improvements to the nature of the fiber/matrix interface has also been emphasized [14]. However, detailed studies, such as those on fracture toughness and R-curve behavior and of the relevant toughening mechanisms are still lacking for continuous fiber reinforced RBSN composites. Studies on elevated temperature behavior are even more limited. As yet there is only limited information on, or understanding of, the elevated temperature failure modes and the creep rupture behavior of fiber reinforced RBSN composites.

The purpose of the following proposed research is to obtain an understanding of both ambient and elevated temperature mechanical behavior of a SiC fiber reinforced RBSN composite. At ambient temperature, applicability of available mechanics models to describe the stress-strain curve will be examined. Emphasis will also be placed on fracture toughness and R-curve behavior and the applicability of

available fracture mechanics models to describe toughening behavior. At elevated temperature, an attempt will be mode to characterize the creep rupture behavior of the composite. The applicability of empirical predictive models for lifetime will be investigated. The material used will be a RBSN reinforced with large diameter continuous SiC fibers. An investigation of the mechanical behavior of a commercially available RBSN monolith will also be performed so as to provide a comparison with the reinforced material.

CHAPTER 2

LITERATURE SURVEY

2.1 Ambient Temperature Mechanical Behavior of SiC/RBSN Composites

2.1.1 Mechanical Behavior in the Fiber Direction in Unidirectional SiC Fiber Reinforced RBSN Composites.

The mechanical behavior in the axial direction of an ideal aligned continuous fiber - brittle matrix composite is characterized by noncatastrophic failure that exhibits a first matrix cracking stress, analogous to a yield point, and a non-linear stress/strain curve, see Figure 2.1. The point of first matrix cracking (FMC) is represented by point A on Figure 2.1. The value of the first matrix cracking stress and first matrix cracking strain can both be higher for the composite than for the monolithic material [15]. The first matrix cracking stress has been the subject of extensive study [13] in part because of its use as a design stress in many applications [13]. Models for estimating the first matrix cracking stress have been developed by several investigators [4,16,17,18,19,20] and are discussed in Section 2.3.

Once matrix crack initiation occurs, the subsequent non-linear stress-strain region represents repeated, or multiple, matrix crack formation [15]. The absence of composite failure from any single matrix crack is representative of flaw tolerant behavior that is frequently associated with bridging of matrix cracks by the continuous fibers [15]. Point B on the Figure 2.1 represents the start of fiber failure. Fibers will break randomly until the onset of fiber bundle failure which corresponds to the onset

of composite failure. The ultimate tensile strength of the optimized composite may be many times that of the corresponding unreinforced monolithic material. Following the ultimate tensile strength, additional work may be expended on the "tail" region of the stress-strain curve as a result of fiber pull-out from the matrix. The work of fracture, or the total area under the stress-strain curve, can be considerably enhanced as a result of the presence of the continuous reinforcing fibers.

The type of brittle-matrix continuous fiber composite behavior described above is known to occur only if the fiber/matrix interface is optimal [13]. If the interface is either too weak or too strong, the stress/strain curve exhibited will be similar to that of a monolith. Catastrophic composite failure would ensue once a crack initiates in the matrix. With an optimized interface, the matrix crack can be bridged by unbroken fibers as shown in Figure 2.2. The sufficiently weak interface then provides sufficient compliance to allow for fiber bridging. Too strong of an interface results in fiber fracture, whereas too weak of an interface precludes any closure forces on the matrix crack.

Impressive improvements in mechanical properties have already been realized for the case of reaction bonded silicon nitride reinforced with continuous fibers [4,7]. Two of the most comprehensive studies have been done by Bhatt and coworkers [4,5,22,23,24] and by Corbin and coworkers [6,7] with the earlier studies being by the latter. Corbin et al. [6] studied the influence of fiber type and also the type of fiber-matrix interface on mechanical behavior of their RBSN composites in bending. Both fine (≈10μm) and large (≈150μm) diameter SiC fibers were used. The fine diameter

SiC fibers used were Nicalon, both ceramic and standard grade, and Tyranno fibers and two experimental fibers, MPDZ and HPZ, supplied by Dow Corning. Tyranno fibers contain approximately 3% titanium in order to improve high temperature stability [25]. The large diameter fibers used were the Textron SiC fibers. Nicalon fibers are Si-C-O polymer (organometallic) derived fibers and consist of microcrystalline Beta-SiC in an amorphous matrix containing Si, C, and O with up to 20% porosity. The diameter of the fibers is small, less than 15μm, and the fibers have high strength, approximately 2.3 GPa. The major disadvantage of these fibers is their inherent instability above 1200°C. In fact, use temperatures are usually limited to 1000°C. This instability, however, is known to have some advantage [7]. It has been reported [7] that when limited degradation occurs, a very thin carbon layer will form at the interface. The development of this layer has played a critical role in the development of NICALON/glass composites [25].

The Textron SiC monofilaments in these studies are processed by deposition of Beta-SiC by a CVD process onto a 35μm carbon fiber core. In contrast to the Nicalon, these monofilaments have potential for use above 1200°C. The fibers are then provided surface coatings which consist of a mixture of SiC and amorphous carbon. These surface coatings provide a reaction barrier which may help protect the fiber from oxidative damage. In the Corbin study, the SCS-6 fiber had a coating of 3μm in thickness whereas the SCS-2 fiber had a coating of 1μm in thickness. Both these fibers, as used in the studies of Corbin et al. [6], were single coated fibers. This was in contrast to the double coated SCS SiC fibers which contain two coating layers

that were subsequently developed. The double coated fibers were used in later studies and are reviewed below. Figure 2.3 shows surface layers of SCS fibers. In the SCS-0 fiber the C-rich portion is on the coating surface whereas in the SCS-6 fibers the C-rich region is within the surface layer thereby ensuring better protection of this layer during composite processing. As can be seen, in the double coated SCS-6 fiber there are two C-rich layers encased within the surface coating. The average room temperature tensile strength of these fibers was 73.0 GPa.

In the Corbin et al. [6,7] studies, for the fine fiber case, the RBSN composites were processed by first preparing a fiber mat which was infiltrated with a mixture of fine (1-3μm) silicon powder and binders. Specimens were laminated, sintered and nitrided (heated in a nitrogen rich atmosphere for a specific amount of time) to result in an approximately 30 vol% fiber reinforced RBSN. The processing requirements for nitridation of a RBSN composite were 1) that the matrix be fully nitrided, and that 2) that the fibers suffer minimal degradation at the nitriding temperatures.

Both short (8hrs) and long (48hrs) nitridation schedules were used in the processing of the reinforced Nicalon composites. In the RBSN reinforced with ceramic grade Nicalon fibers, a large (≈2μm) reaction zone formed between the fiber and the matrix when subjected to the longer nitridation schedule. It was found that this reaction zone served to deflect matrix cracks along the interface to result in crack bridging by fibers. Consistent with this, the material was found to exhibit non-linear noncatastrophic behavior, see Figure 2.4. With the shorter cycle, no significant

interface formed, the material exhibited a linear stress-strain curve, and the failure was catastrophic.

The standard grade of Nicalon fiber reinforcements gave rise to somewhat thinner interfacial zones when compared to ceramic grade Nicalon. In the former, toughened behavior was also obtained with a longer nitridation cycle. Behavior of MPDZ fibers, see Figure 2.5, and the ceramic grade Nicalon were similar. Again, a carbon zone (2μm) developed around the fiber during the longer nitriding cycle which was not observed during the shorter cycle. Extensive pullout was observed and attributed to the formation of an interfacial zone. With the HPZ fiber reinforced RBSN, a large gap (3μm) developed between the fiber and the interface under the long cycle and a smaller gap also occurred when the short cycle was used. There was no evidence of any fiber/matrix bonding. It was concluded that for this composite to be of use, a very different nitridation cycle would have to be developed. The results of the Tyranno fiber reinforced material showed behavior similar to the trends shown by the other materials in this study, namely, brittle catastrophic behavior with a short nitridation cycle and tough composite behavior with the long cycle. Long nitridation times allowed for the formation of an effective interfacial zone which did not develop with a short cycle. In all of the above materials in the Corbin et al. study [7], although toughened behavior was observed in some cases, the first matrix cracking stress of all of the materials was low ($\approx$ 125 MPa). This was attributed to the presence of large flaws in the RBSN matrix caused by the difficulty in obtaining macrostructural uniformity.

In a parallel study, Corbin et al. [7] modified the Nicalon fibers by the application of different CVD coatings in an attempt to obtain an interface that would optimize toughening. Coatings that were used as interface modifiers included carbon, Al_2O_3, SiC, and Si_3N_4. These coatings were found not to be significantly damaged by the processing steps. For the unreinforced RBSN and for the Al_2O_3, SiC, and Si_3N_4 coated fiber composites, the failure was brittle with little pullout and the coatings stayed strongly bonded to the matrix. The interface in these cases was not observed to provide for a crack deflection path.

It was found that only the carbon coated Nicalon fibers resulted in a composite that did not fail in a brittle manner. With a carbon coating, the fibers were able to carry the load even after matrix failure and the interface protected the fiber from matrix cracks. The stress-strain curve for the Nicalon fiber with the carbon interface showed linear behavior to approximately 0.2% strain and then subsequent nonlinear behavior. Examination of the fracture surfaces of these composites showed significant pull-out of the fibers from the matrix. First matrix cracking stresses were on the order of 125 MPa.

Some of the carbon rich coating layer on the fibers was consumed during composite processing as a result of the infiltration of Si into the interface. The presence of a sufficiently thick residual carbon rich layer on the fibers was found to be crucial in order to obtain toughened behavior. Behavior of the coated fiber composites was in contrast to the uncoated fibers in which a useful interface formed during processing.

In the SiC monofilament reinforced RBSN, Corbin et al. [6] found that, in bending, cracks that initiated in the SCS-2 fiber reinforced RBSN propagated through the interfacial zone into the Beta-SiC filament thereby damaging the filaments and reducing their effectiveness. For the case of the SCS-6 fiber reinforced RBSN, cracks that initiated in the matrix deflected along the fiber as a result of delamination at the carbon layer. Since matrix cracks were deflected, the filaments were protected and retained their strength. The stress-strain curve of SCS-6 fiber reinforced RBSN obtained by Corbin et al. [6] is shown in Figure 2.6 and can be contrasted with their results for the corresponding case of the carbon coated Nicalon fiber reinforced RBSN. Reinforcement with the SCS-6 monofilaments gave a composite with significantly improved properties when compared to the toughened Nicalon fiber reinforced RBSN composites. Both first matrix cracking and ultimate strengths were significantly higher for the SCS-6 fiber reinforced RBSN. For the SCS-6/RBSN, composite strengths were significantly higher than that for an RBSN monolith used as a comparison material. This was not the case for the Nicalon/RBSN. Furthermore, for the SCS-6 fiber reinforced case, the work of fracture values were increased several times over that of the Nicalon fiber reinforced composite and increased by about 20 times over that of the RBSN monolith.

Because of the demonstrated advantages of the use of the Textron SCS-6 SiC monofilaments on reinforcing RBSN, subsequent studies by other investigators have involved use of these fibers for reinforcement for RBSN. The most comprehensive recent studies are by Bhatt and coworkers [4,5,22,23,24,26,27,28]. Bhatt [5]

conducted experimental studies in bending on RBSN reinforced with uniaxially aligned SiC fibers of three different types; SCS-0, SCS-6 single coated and SCS-6 double coated, in vol% ranging from 20 to 40 percent. A study was also conducted in tensile loading of RBSN reinforced with single coated SCS-6 fibers [8].

The nitridation times employed for the SiC/RBSN were either 40 or 72 hours. After nitridation, differences in fiber/matrix bonding with the three composites were revealed under high magnification. The carbon rich coating of the SCS-0 fiber was seen to have reacted and formed a chemical bond with the matrix. The SCS-6 fibers remained intact. The interfacial region of the SCS-6 fibers was also found to contain voids and delaminated areas which indicated a weak fiber/matrix bond. Matrix porosity was also found to increase with increased nitridation time, being 39% for nitridation at 1200°C for 40 hours and 32% for nitridation at 1350°C for 40 hours. The SCS-6 single coated composite which was nitrided in a nitrogen and hydrogen atmosphere at 1200°C showed high as fabricated strengths and noncatastrophic failure. In contrast, SCS-0 composite nitrided in the same atmosphere at 1350°C showed poor mechanical properties. Loss of fiber coating and fiber/matrix reactions during processing were theorized as possible explanations.

Results of testing in four point bending revealed no significant strength differences between the SCS-6 single and double coated fiber reinforced composites. The strengths obtained were both significantly greater than that of the SCS-0 material. Table 2.1 shows some of these values. The SCS-6 fiber reinforced composites also exhibited toughened behavior. The SCS-0 composite did not, as shown in Figure 2.7.

The non-linear behavior above 220 MPa for the SCS-6 composites coincided with the onset of matrix cracking normal to the fiber axis. At higher stresses, regularly spaced matrix cracks appeared, as observed after unloading. Random fracture of fibers accompanied ultimate failure. Ultimate flexural surface stress at failure of 9.5 times over that of unreinforced material was reported and the flexural first matrix cracking stress was 2.7 times greater. The average room temperature failure stress was 593 MPa [8]. The average crack initiation stress was 245 MPa which is larger than the average strength of monolithic RBSN at this porosity level which is approximately 200 MPa.

Strength results on batches nitrided at 1200°C showed no degradation even for long nitridation times. At 1350°C however, strength properties were significantly lower. Investigations of the causes of this behavior suggest that environmental attack of the fiber coating occurred during nitridation. Optimum results occurred from reinforcing RBSN with SCS-6 fibers nitrided at 1200°C in a nitrogen atmosphere where ultimate strength levels of 530 MPa were reached.

Due to the numerous disadvantages of bend testing which include mixed mode failure, studies in tension were also conducted by Bhatt [8] and results of the studies done under tensile loading also showed toughened composite behavior. The data indicated that the composite was significantly stronger and failed at a higher strain than the monolith and also that an increase in strength was gained with increase in fiber volume fraction. The matrix failure strain was approximately the same, however, because of the large diameter of the SiC monofilaments. It was concluded that first

matrix cracking strengths may be improved by increased fiber volume fraction and reduction of matrix porosity. Porosity of the matrix has been shown to have a significant effect on the strength of the composite material [4]. Decreasing the porosity has the effect of increasing the modulus of the matrix and may also increase the fracture strain of the matrix.

To further investigate the effect of fiber volume fraction, Chulya, Gyekenyesi, and Bhatt [22] examined the effect of fiber content on large diameter SiC/RBSN systems using samples of various fiber vol%. It was shown that if the fiber content was small, fiber pullout did not guarantee noncatastrophic failure even if a weak interface existed. The transition from catastrophic to noncatastrophic failure occurred at between 16-19% fiber content. It was also shown that fiber volume fraction did little to influence first matrix cracking strain but did influence the first matrix cracking stress and the ultimate composite fracture strength [4]. On this basis it was concluded that the onset of first matrix cracking was a strain controlled process. For a weaker fiber/matrix bond, increased debonding was stated to increase this critical strain and thereby increase the magnitude of first matrix cracking stress.

2.1.2 Transverse and Interfacial Mechanical Properties of SiC Fiber Reinforced RBSN Composites

Although a weak interface is required for optimal axial mechanical properties, the transverse properties may be potentially degraded. Accordingly, previous studies have carefully focussed on assessing transverse properties in conjunction with axial

properties. Chulya et al. [22] employed bend specimens containing 23 vol% SiC fibers in RBSN to evaluate transverse properties. The transverse bend strength was found to be low, approximately 76 MPa, indicative of weak interfacial bonding. Inspection of the fracture surface revealed interfacial splitting as the source of failure. This splitting occurred between the carbon-rich surface coating of the fiber and the matrix.

The transverse strength of a fiber reinforced SiC/RBSN composite was also measured indirectly by changing the orientation of the fibers relative to the axial orientation of tensile specimens by Bhatt and Phillips [24]. The $[0]_8$ (unidirectional, 0 degrees, eight plies) specimens studied contained eight plies with the fiber volume fraction being approximately 30%. The stress-strain plots of the differently oriented specimens were compared to that of the monolith. The $[0]_8$ was clearly much stronger than any other orientation. Accordingly, the unidirectional reinforced composite laminates were shown to have highly anisotropic in-plane properties.

A direct indicator of transverse mechanical behavior is the interlaminar shear strength which assesses the strength and failure behavior of internal interfaces. Researchers have found [29], that the short beam flexure test, a common shear test for a variety of materials, often fails to provide accurate interlaminar shear data for ceramic composites due to the mixed-mode nature of the failure. Based on ASTM D3846, the opposed double notched compression test for interlaminar shear has shown promise with ceramic composites. Two notches extend from opposite sides to the midplane of the specimen as shown in Figure 2.8. Compression loading avoids tensile

failure. This double notched specimen was used by Bhatt and Phillips [20] to measure the interlaminar shear of a SiC/RBSN unidirectional composite. Two sets of specimens were made; one with the notches made along the thickness direction (along the hot pressing direction) and the other with the notches made along the width direction (normal to the hot pressing direction). For the former, the interlaminar shear strength value was 40 MPa and for the later, 100 MPa. This difference was attributed to the location of the notches relative to the fibers. For specimens with notches cut along the thickness, the notches end on the same fiber row and failed in shear. For the specimens cut in the width direction, the failure mode was a combination of compression and shear. Data on interlaminar shear strength was not directly related to the transverse mechanical behavior of the composite in these two orientations.

Interfacial shear strength, τ, which is a measure of the fiber/matrix interface strength has also been studied for these composites by fiber push-out tests on SiC/RBSN composites. Values of τ on the order of 40-55 MPa was measured for materials fired to 1200°C [30]. Bhatt [20] calculated the interfacial shear strength, τ, indirectly by measuring the spacing between matrix cracks and then applying the Averston, Cooper, and Kelly model, (ACK), and the theoretical results derived from it, which are described further in Section 2.3. This gave for τ a much reduced value of 18 MPa. The value of τ can vary with processing changes. For example, clamping stresses due to residual stresses, which will be described later in more detail, created during processing from differences in fiber/matrix thermal expansion properties may be present which can alter the measured interfacial shear, τ.

2.1.3 Fracture Toughness and Toughening Mechanisms in SiC Fiber Reinforced RBSN Composites

Fracture toughness can be thought of as the resistance to crack growth, and, for linear elastic materials, is the parameter that also govems the strength of the material. The toughness of monolithic RBSN is on the order of 2-3 $MPa \cdot m^{1/2}$. As of yet, there has been little work done on evaluating the toughness and toughening mechanisms of SiC/RBSN. There has also been no reported studies of R-curve behavior in SiC fiber reinforced RBSN composites.

Bhatt and Phillips [20] examined failure behavior ahead of a blunt notch in their unidirectional SiC fiber reinforced RBSN. They observed delamination of the fiber/matrix interface parallel to the fiber direction ahead of the notch tip. This appeared to include propagation of cracks from the notch in a direction normal to the fibers. They attributed this to a lower fracture energy for the SiC(f)/matrix interface compared to the fracture energy of the matrix. The effect of this delamination was a suppression of through-the-thickness cracking, load redistribution from cracked areas into undamaged areas and prevention of premature fiber failure.

The degree of toughening also depends on the residual stresses, caused by processing, in the composite material. For example, Cao et al. [16] emphasized that both the residual stress and the interfacial sliding stress are significant in influencing the matrix cracking strength. Bhatt [22] reports for NASA SiC/RBSN that the coefficients of thermal expansion up to 1450°C were 4.2E-6 and 3.8E-6 /°C for the fiber and matrix, respectively. Strain mismatches will occur when the composite is

cooled from the processing temperature to room temperature thus creating residual stresses in the material. Residual stresses occur both in the radial and axial direction, i.e. normal and parallel to the fiber. Residual radial stresses which leave the interface in tension are preferable because the thermal contraction of the fibers will be higher than that of the matrix. If the service temperature is lower than the temperature where the residual stresses go to zero, radial tensile forces will exist at the fiber-matrix interface at or below the service temperature. This gives the fibers a better chance of pulling out. If, on the other hand, the fibers were to contract less than the matrix, compressive radial stresses may develop at the fiber-matrix interface and fiber pullout will become very unlikely [31]. Compressive axial stresses, however, can be a source of extra strength for the matrix [22].

Fracture toughness studies have been conducted on other continuous fiber reinforced composite systems [32]. Kodama et al. [33] experimentally showed, using SiC(f)/HPSN, that fracture toughness increased as the fiber/matrix frictional stress increased, but if the frictional stress became too high then the toughness was usually no better than that of the monolithic material. Figure 2.9 shows this experimental result.

The only available studies of R-curve behavior in a continuous fiber reinforced ceramic composite are that by Zok et al. [32] in glass ceramic composites. Here the reinforcing fibers were in the cross-ply (0/90) orientation. The R-curve results from their work is shown in Figure 2.10. The mechanism of the R-curve was attributed mainly to energy dissipation by pull-out of the fibers in the wake of the crack.

The possibility of more than on operating fracture mode must be taken into consideration when attempting to make any conclusions about the toughening mechanisms of a certain system tested under specific conditions. Also according to Zok et al. [32], fiber reinforced brittle matrix composites exhibit competing fracture modes which depend on a number of factors including the specific arrangement of fibers, the properties of the fiber/matrix interface, the fracture characteristics of the fibers, the presence of notches and the test configuration. Other modes exhibited by practical continuous fiber reinforced ceramic matrix composites include mode II, mixed mode I/II, and failure in compression [34]. Mixed mode or change in failure mode can also release additional energy. One problem with testing in bend is that fiber reinforced composites, when tested under flexural loading, can fail in either compression, tension, shear, or a combination of these modes. Results from bend testing must be interpreted with this in mind.

2.2 Elevated Temperature Behavior of SiC/RBSN Systems

Existing studies have focussed mainly on the effects of short term degradation under elevated temperature exposures, namely, the effect of temperature on composite strength. Jablonski and Bhatt performed tensile strength tests at elevated temperature up to 1500° C in air [8]. Tests were performed in tension to eliminate the mixed mode fracture of bend testing. The composite used for their study was a 30 vol% uniaxial SCS-6/RBSN. Properties were measured at 25° C, 1300° C, and 1500° C and the results are tabulated in Table 2.1. Most dramatic was the loss of the ultimate

tensile strength and the increase in failure strain with increased temperature. The crack initiation conditions did not appear to be as dramatically influenced.

Figure 2.11 shows the stress-strain curves at these three test temperatures. At 1300°C the material exhibited a matrix cracking strain of approximately 0.10%, with an accompanying major load drop. After the second load drop, the stress carrying capacity of the material was reduced by a factor of two. The ultimate strain was only .115% which was due to the fibers being poorly bonded, pulling out easily thereby contributing little to composite strength. The composite contained many secondary cracks which were found running both parallel and perpendicular to the fiber axis. Fracture parallel to the stress axis was caused by shear in the fiber matrix interface.

At 1500°C, there was no clear indication of a first matrix cracking stress and the stress-strain became nonlinear at approximately 0.10% strain which indicated either matrix yielding or matrix fracture. The material appeared to exhibit some plastic flow. The ultimate strain was on the order of 0.60% and since the matrix was somewhat ductile, the fibers stayed bonded to the matrix and did not easily pull out. Because of the strong fiber bonding, cracks were found to run through the fibers instead of circumventing them. A large debond region which extended up to 7mm in the center of the specimen indicated poor through the thickness strength. The length of fiber pullout was less than that at 1300°C. Modulus values for the composite were 20% and 26% lower than the room temperature values for the samples tested at 1300°C and 1500°C respectively. At all temperatures, however, in spite of the strength degradation, SiC/RBSN appeared to demonstrate non-catastrophic behavior.

At elevated temperature, there have been no studies investigating the relationship of strength to interlaminar or interfacial properties. In one study by Morscher et al. [35], the temperature dependence of the interfacial shear strength, τ, of SiC/RBSN was investigated using fiber push-out tests. They observed that τ increased as the temperature increased. They attributed this to residual stresses. At ambient temperatures, fiber/matrix interfaces are subjected to residual tension, whereas this tensile stress is relieved at elevated temperatures. The reduction of this tensile stress was stated to increase the effective value of τ.

There are no available studies on long term degradation of continuous fiber SiC/RBSN. The closest material to SiC/RBSN in which some data is available is HPSN reinforced with continuous SiC fibers. All of these studies involve the characterization of the bulk creep behavior at elevated temperatures. Holmes [36], in studies on tensile creep behavior of HPSN reinforced with large diameter (SCS-6) silicon carbide fibers, observed during testing the occurrence of small, gage-section extensions of approximately 0.3 to 1.0 μm that occurred as instantaneous strain jumps during steady state creep. Possible mechanisms for this behavior include the random fracture of individual fibers or the cracking of the matrix and the subsequent arrest at the fibers. It was concluded that irreversible microstructural damage occurred during the creep of these materials. Microstructural observations showed that extensive fiber pullout, from 0 to 6 mm, accompanied creep failures at low stresses. This possibly indicated a decrease in interfacial shear strength during long term creep testing. Significant radial separation along the fiber/matrix interface, up to almost 8 μm,

occurred in the low stress creep samples and was possibly due to radial contraction of the fibers. At higher stresses the maximum pullout length was reduced to about 1 mm which is on the same order as monotonic tensile loading.

Additional work on creep in fiber reinforced silicon nitride composites have been conducted by J.-M. Yang, R. B. Thayer, et al. [37]. They presented monolithic/composite comparisons of creep behavior in silicon nitride and its fiber reinforced composites. Testing was done in four point bend between 1100°-1450°C and at stresses ranging from 60-350 MPa. Creep strains for the composite did not exceed 1.25% for test times up to 150 hours. It was found that the steady-state creep rate was two orders of magnitude slower for the composite and that the failure mechanisms, concluded from microstructural analysis, were grain boundary sliding leading to void growth and coalescence. Initial creep of the composite was dominated by the matrix, followed by a transition where load was transferred to the fibers thereby causing stress relaxation in the matrix. Due to load transfer to the fibers, stresses in the matrix did not reach a level where microcracking could take place. Eventually, the high stresses in the fibers caused by this load transfer caused the fibers to randomly break thereby transferring the load back to the matrix which sustained further creep deformation. The cycle then repeated with intact fiber segments supplying the restraining forces needed to allow the matrix to relax. Steady-state creep in the composite was attributed to an equilibrium established between the rate of load transfer to the fibers and subsequent fiber rupture. The process of deformation was summarized as repetitive matrix stress relaxation/fiber rupture/load transfer through the

matrix. This was in contrast to monolithic silicon nitride where creep strains could be attributed to subcritical crack growth.

2.3 Equations and Models

It is one goal of this thesis to determine the applicability of micromechanical models to strengthening. The following sections discuss various equations and models and the behavior that they are attempting to describe.

2.3.1 Stiffness

The stiffness of the composite is roughly the linear combination, based on the rule of mixtures, of the values of the fiber and the matrix. For example, if f is the volume fraction of fibers, and E_m and E_f are the modulus of the matrix and the fiber respectively, then the modulus of the composite is

$$E_c = f E_f + (1 - f) E_m \qquad (1)$$

as long as the fibers are aligned along the loading direction. Other composite material properties, however do not always follow this rule. Often, such as in the case of strength and toughness, more significant gains can be made than predicted by Equation (1).

2.3.2 First Matrix Cracking Stress

Bhatt [4], introduced a strain controlled fracture initiation criterion which provides the first matrix cracking stress, σ_{fmc},

$$\sigma_{fmc} = e_{fmc}^{*} (E_f G + E_m (1 - G)) \quad (2)$$

e^{*}_{fmc} is the critical strain at which the crack initiates. No theoretical explanations were provided for e^{*}_{fmc}. Other variable are V_m and V_f which are the volume fraction of the matrix and the fiber, respectively.

The bulk of existing models for σ_{fmc} is based on the steady state cracking stress for a continuous fiber reinforced composite. Several micromechanical models have been developed that estimate the first matrix cracking stress. These include models by Aveston, Cooper, and Kelly (ACK) [18] , Budianski, Hutchinson, and Evans (BHE) [38], and by Sutcu and Hillig (SH) [19]. These models have been shown to work well where values of the sliding stress are less than or equal to 20 MPa.

The predicted value of the first matrix cracking strength can be calculated using the following equation [39],

$$\sigma_m{}^{c} = 2.3 \left(K_m \right)^{\frac{2}{3}} \left[\tau E_f f^2 \frac{\left(1 - \frac{E_f f}{E_m (1-f)} \right)^2}{E_m R} \right]^{\frac{1}{3}} - \sigma_m{}^{R}, \quad (3)$$

where τ is the shear resistance of the fiber/matrix interface, f is the volume fraction of fiber, R is the fiber radius, E_f and E_m are respectively the fiber and matrix moduli, $\sigma_m{}^{R}$ is the axial residual stress in the matrix and can be calculated based on Hsueh and Becher, [40], namely

$$\sigma_m^R = \frac{-f\,\sigma_f^R}{(1-f)}, \tag{4}$$

in which, σ_f^R is the axial residual stress in the fiber given by,

$$\sigma_f^R = A\left\{\left[\frac{1+\nu_f}{E_f}+\frac{(1+f)(1+\nu_m)}{(1-f)E_m}\right]\alpha_m - 2\left[\frac{\nu_f}{E_f}+\frac{f\,\nu_m}{(1-f)E_m}\right]\alpha_f - \left[\frac{(1-\nu_f)}{E_f}+\frac{1}{E_m}\left(\frac{1+f}{1-f}+\nu_m\right)\right]\alpha_f\right\}\Delta T, \tag{5}$$

where,

$$A = \left[\frac{(1+\nu_f)(1-2\nu_f)}{E_f^2}+\frac{f\,(2-\nu_f-\nu_m-4\nu_f\nu_m)-1+\nu_m}{(1-f)E_f E_m}+\frac{f\,(1+\nu_m)(1-f-2f\,\nu_m)}{(1-f)^2 E_m^2}\right]^{-1}, \tag{6}$$

and ν, α, and ΔT are the Poisson's ratio, thermal expansion coefficient, and temperature difference respectively.

2.3.3 Initiation Toughness and Toughening Models

Contributions to the steady state toughness occur via a number of different mechanisms. One of these is fiber pull-out, which provides frictional dissipation. Another is debonding of the fibers which generates new surface and contributes positively to the toughness by pulling away fibers from the matrix, creating debond surfaces, and dissipating the residual strain energy by the creating stress-free surfaces in the vicinity of the crack. Debonding can occur at either the crack front and/or the crack wake, see Figure 2.12. Partial debonding may already be present if the thermal

expansion of the fiber is greater than that of the matrix which would leave the interface in a state of residual tension [41]. Debonding is very important in that debonding must occur for any toughness increases to be realized. Frictional sliding also governs the toughening of a material. In addition, energy can be dissipated by acoustic waves created during the cracking of the composite.

These effects are indicative of resistance-curve behavior, increased toughness with crack size, because each contribution, according to Evans [13], is only fully realized when the fibers fail and pull out. Sliding and pullout contribute to toughness only if the fibers are rough and friction is provided by "asperity contact" [41]. Crack bridging is the primary contributor to toughness in the presence of friction. The amount of toughness increase with crack extension is sensitively dependent on the fiber/matrix interface since the behavior of this interface determines the amount of pull-out and debonding that occurs. Bridging of cracks in the crack wake can also contribute to toughening. Bridging is possible due to the presence of frictional shear resistance along the fiber/matrix interface in unbonded composites and preferential debonding of the reinforcement-matrix interface in bonded composites [42]. Figure 2.13 shows the various contributions to steady-state toughness.

Some of the available toughening models, each stressing a different aspect of toughening, are explained below. For failure ahead of the notch in a room temperature single edge notched bend specimen (SENB) the initiation toughness may be predicted according to [43]

$$K_c = K_m \times \frac{E_c}{E_m}. \tag{7}$$

The subsequent R-curve, based on pull-out, K_R, based on fiber pullout as being the major contributor to the overall toughening, can be derived to be [32]

$$K_R = \frac{4\tau f (\bar{h})^{1.5}}{R} (\frac{2}{\pi})^{0.5} [(\frac{\Delta a}{\bar{h}})^{0.5} - (\frac{2}{\pi})^{0.5} \frac{K_o(1-\nu_c^2)}{E_c(\bar{h})^{0.5}} (\frac{\Delta a}{\bar{h}})^{0.5}] + K_o , \tag{8}$$

where τ is assumed to be constant during the fiber pullout; $\bar{h}$ is the average length of fiber pullout; Δa is the crack growth distance after initiation. The predicted intrinsic steady-state toughness based on the pullout model can be given by

$$K_{ss1} = \sqrt{K_o^2 + \frac{E_c f \tau (\bar{h})^2}{R (1-\nu^2_c)}} , \tag{9}$$

where K_o is the initial fracture resistance and all other terms have their usual meaning.

When the major toughness contribution to the R-curve comes from elastic fiber bridging of matrix cracks and crack wake debonding of fiber/matrix interfaces, the results for the steady-state toughness, using a recent model, [42] are dependent on the fiber fracture strength, σ_f, fiber radius, R, and the fiber/matrix interface toughness, G_c. The steady-state toughness, K_{ss2}, in this case can be given by

$$K_{ss2} = \sqrt{\frac{(K_m E_c)^2}{E_m^2} + \frac{E_c \Delta G}{1-\nu_c^2}}, \tag{10}$$

where, ΔG is the toughness increase due to fiber bridging and can be obtained [42],

$$\begin{aligned}\Delta G = & \frac{8f\tau^2 l_d^{c^3}}{3E_f R^2 \Omega^2 (2-\Omega)^2}\left[\frac{A}{(1-\Omega)^2} - (1-\Omega)\right] \\ & + \frac{Rf\sigma^3_f}{3E_f\tau}\left[1-\frac{B}{(1-\Omega)^2}\right] - \frac{RfT^3_c}{3E_f\tau}\left[1-\frac{1}{(1-\Omega)^2}\right] \\ & + \frac{8f\tau^2 l_c^2 l_d^c}{R^2 E_f \Omega(2-\Omega)} - \frac{8f\tau^2 \Omega l_c^3}{3R^2 E_f[\Omega(2-\Omega)]^{0.5}(1-\Omega)^2},\end{aligned} \tag{11}$$

in which,

$$\Omega = \left(1 + \frac{fE_f}{(1-f)E_m}\right)^{-1},$$

$$l_c^2 = \frac{RE_f G_c \Omega}{\tau^2},$$

$$A = \left[(1-\Omega)^2 + \Omega(2-\Omega)\left(\frac{l_c}{l^c_d}\right)^2\right]^{\frac{3}{2}},$$

$$B = \left[(1-\Omega)^2 + \Omega(2-\Omega)\left(\frac{T_c}{\omega_f}\right)^2\right]^{\frac{3}{2}},$$

$$l_d^c = \frac{\sigma_f R}{2\tau}\left(1-B^{\frac{1}{3}}\right),$$

$$T_c = \left[\frac{4E_f G_c}{R(2-\Omega)}\right]^{0.5}.$$

2.3.4 Empirical Stress-Rupture Equation

In monolithic ceramics as well as in one ceramic composite [44], the commonly used empirical stress-rupture equation has the form

$$\sigma^n \, t_f = constant \tag{13}$$

where σ is the applied stress and t_f the failure time and n, we call a stress-rupture exponent. Monkman and Grant showed that the empirical equation, Equation (13), can be justified on the basis that failure is a strain controlled process primarily dominated by steady state creep. Under such conditions they showed that

$$\dot{\varepsilon}_s \, t_f = constant \tag{14}$$

where $\dot{\varepsilon}_s$ is the steady state creep rate given by

$$\dot{\varepsilon}_s = A\sigma^N \tag{15}$$

where N is the creep stress exponent. By substitution of Equation (15) into Equation (14), N = n for strain controlled and steady-state creep dominated failures.

Accordingly, by measurement of the stress-rupture exponent, n, it is possible to obtain information on the nature of the long term failure process.

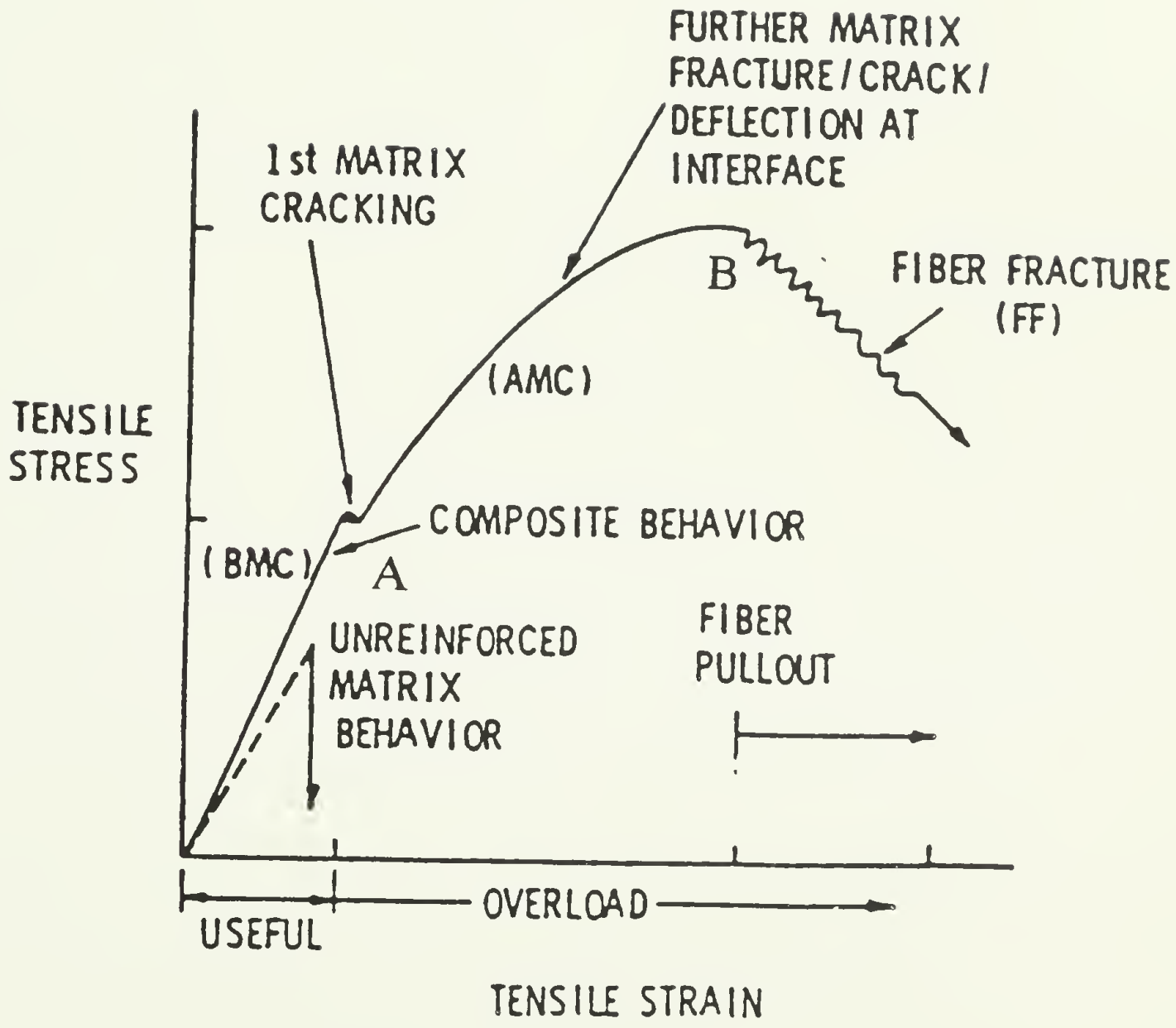

Figure 2.1 Typical ideal stress/strain curve of a fiber reinforced ceramic composite. (A) denotes the area of first matrix cracking while (B) denotes the ultimate strength and area of fiber pullout and subsequent fracture. After ref. [15]

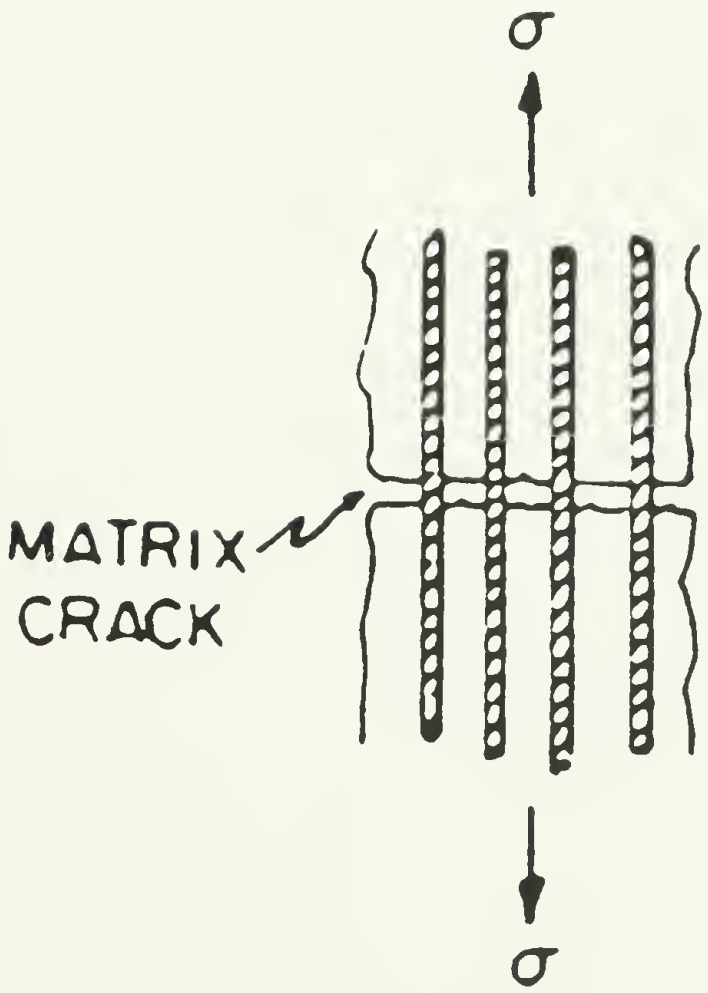

Figure 2.2 Fibers bridging a matrix crack. After ref. [21].

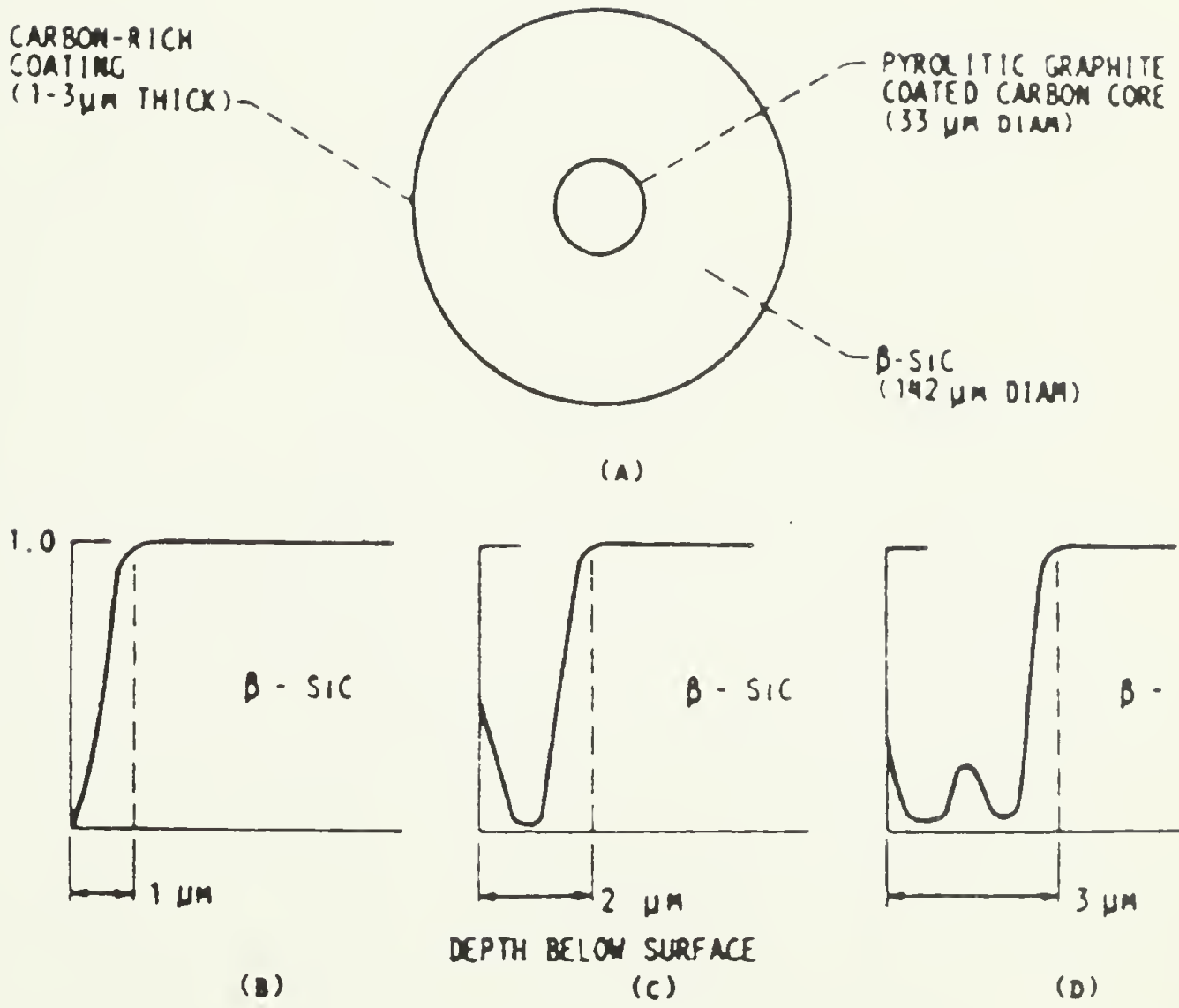

Figure 2.3 Schematic of SCS fibers. (A) typical cross-section of coated (CVD) SiC fiber, (B), (C), and (D) are the composition profile of carbon-rich coating near the surface of SCS-0, SCS-6 (single coated) and SCS-6 (double coated) SiC fibers respectively. After ref. [5].

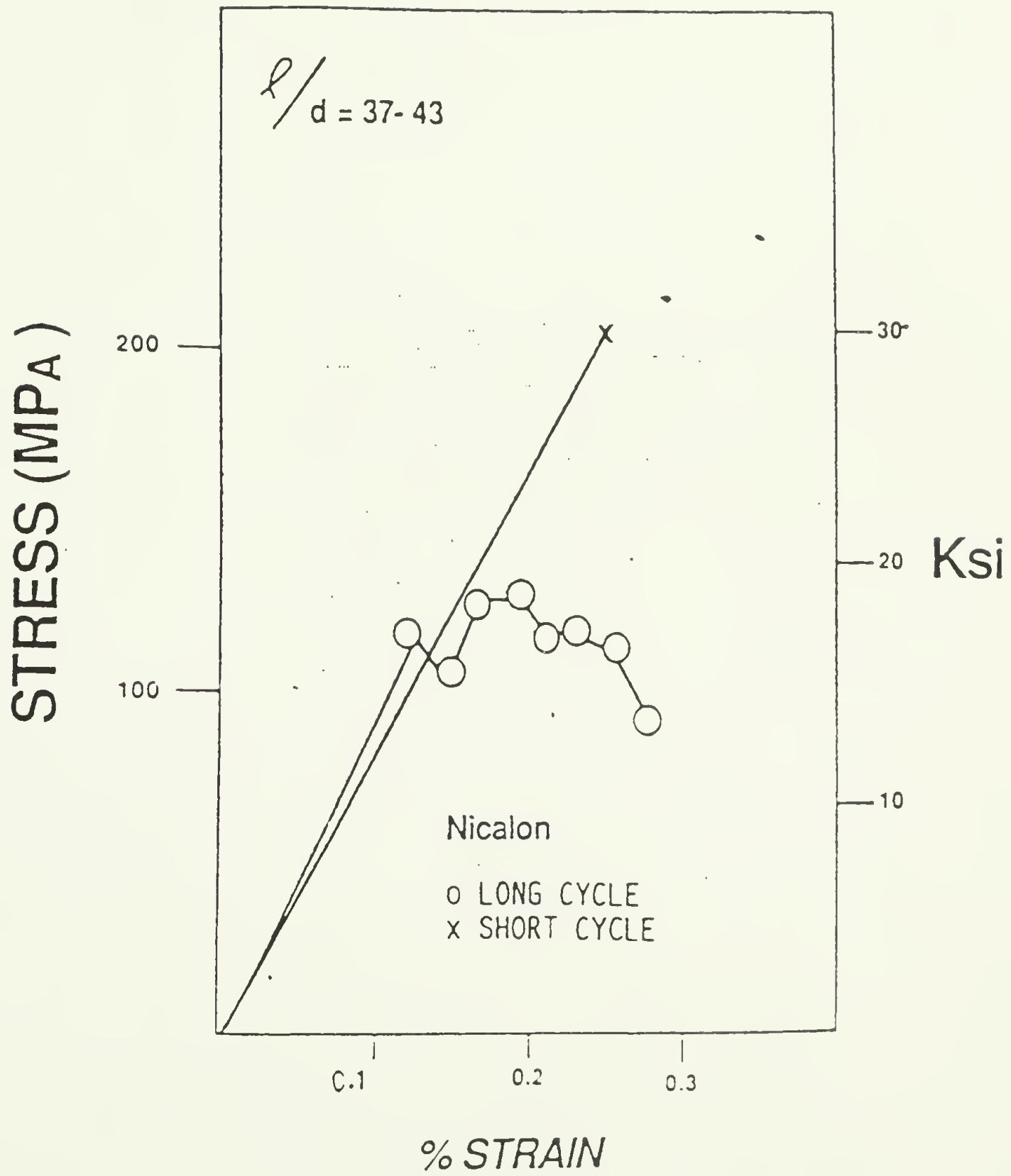

Figure 2.4 Stress/strain curves for Nicalon fiber reinforced composites, both long and short term nitridation schedules. After ref. [7].

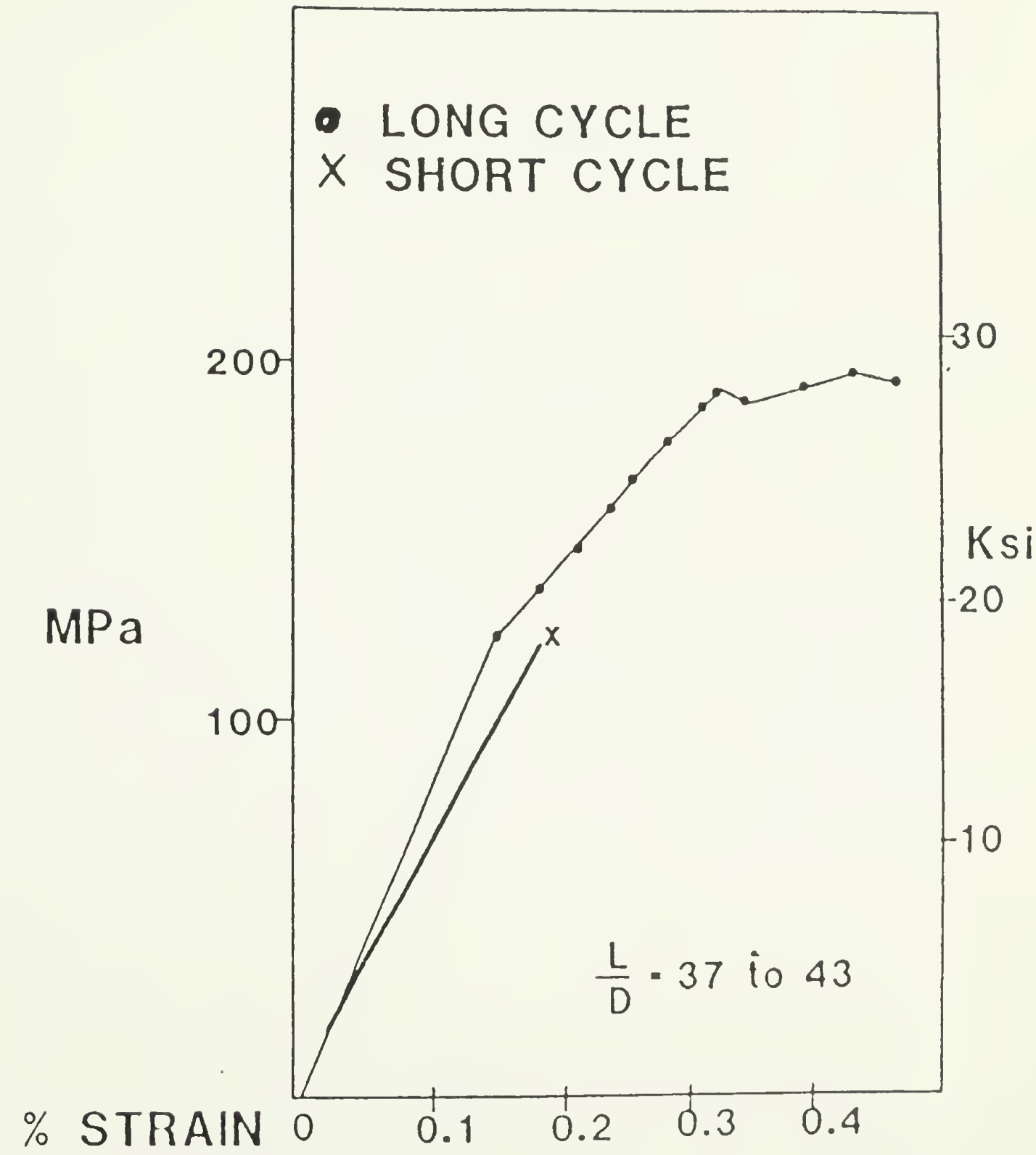

Figure 2.5 Stress/strain curves for MPDZ reinforced composites, both long and short nitridation schedules. After ref. [7].

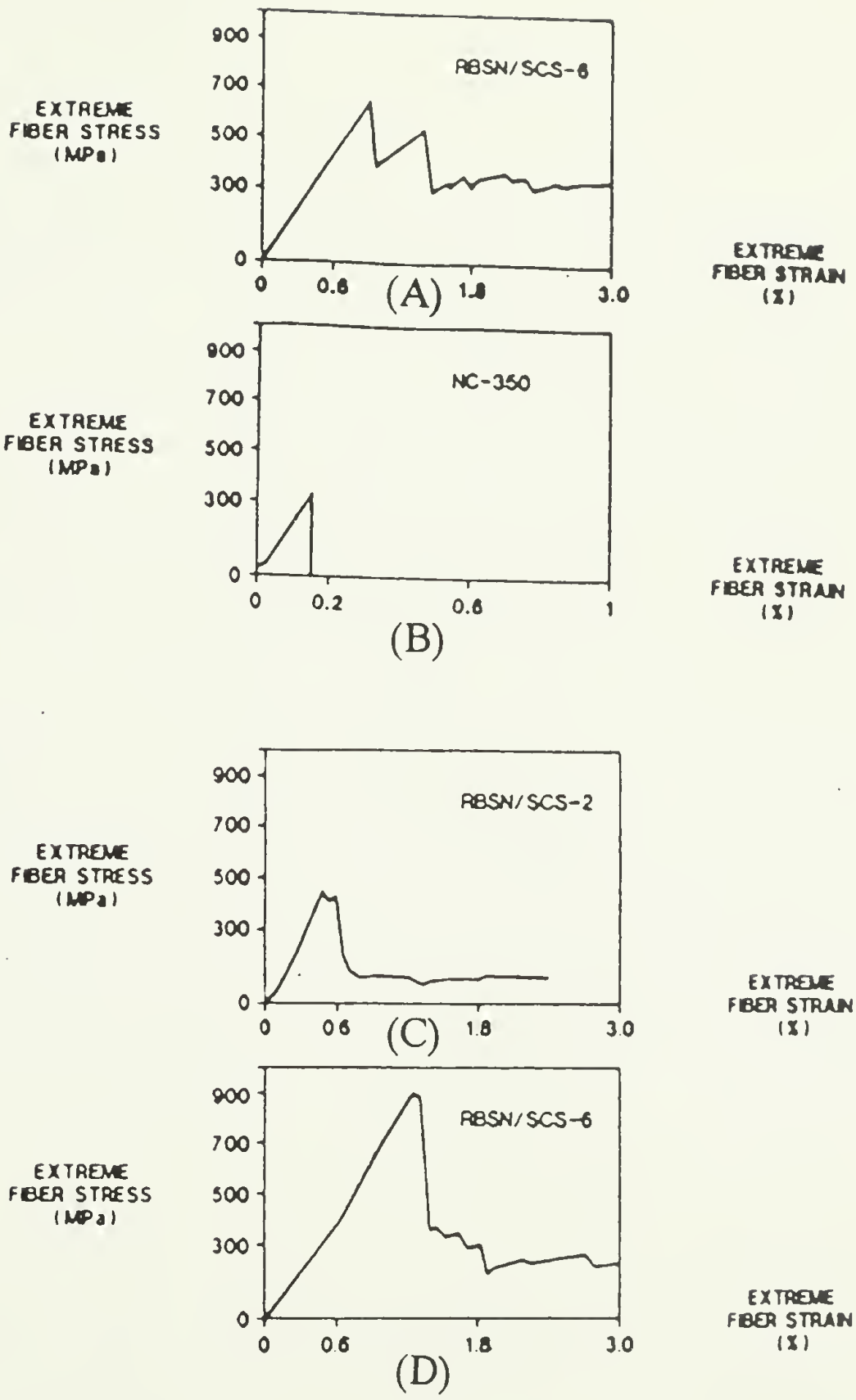

Figure 2.6 Stress/strain curves for RBSN monoliths and SCS reinforced RBSN. (A) RBSN/SCS-6, (B) RBSN monolith, (C) RBSN/SCS-2, (D) RBSN/SCS-6. Note the increased work of fracture (area under the stress/strain curve) for the SCS-6 reinforced composites over both the monolith and the SCS-2 reinforced composite. After ref. [6].

Table 2.1 Tensile Properties of SiC/RBSN as obtained by Bhatt. After ref. [8].

Property	25°C	1300°C	1500°C
Modulus (GPa)	193	154	143
Crack Initiation Strain (%)	0.130	0.0957	NA
Crack Initiation Stress (MPa)	245	160	NA
Ultimate Strain (%)	1.035	0.115	0.592
Ultimate Stress (MPa)	593	172	169

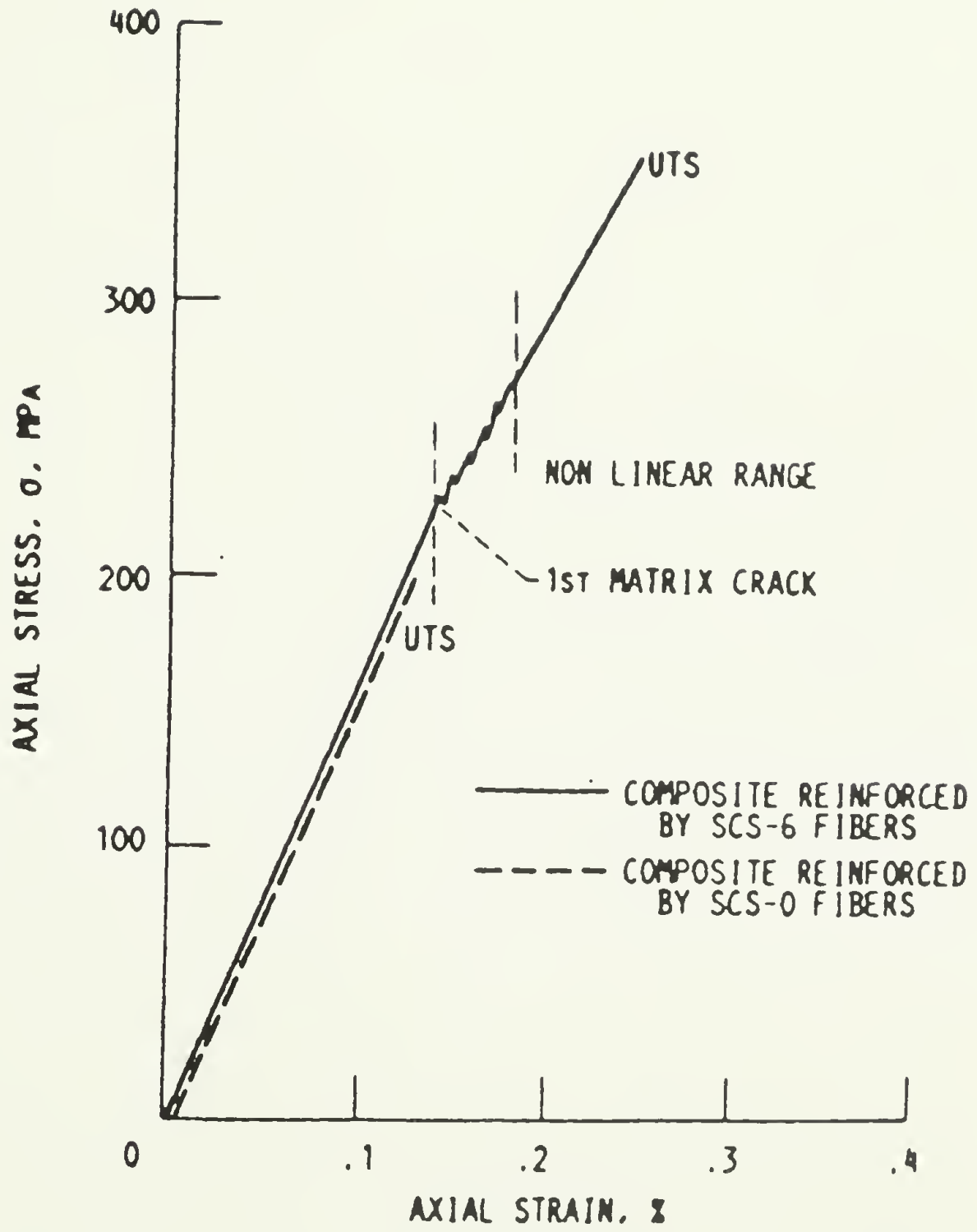

Figure 2.7 Effect of fiber coatings on the axial stress-strain behavior of 23 vol% SiC/RBSN composites. Note the increased strain to failure using the coated SCS-6 fibers over the SCS-0 fibers. After ref. [27].

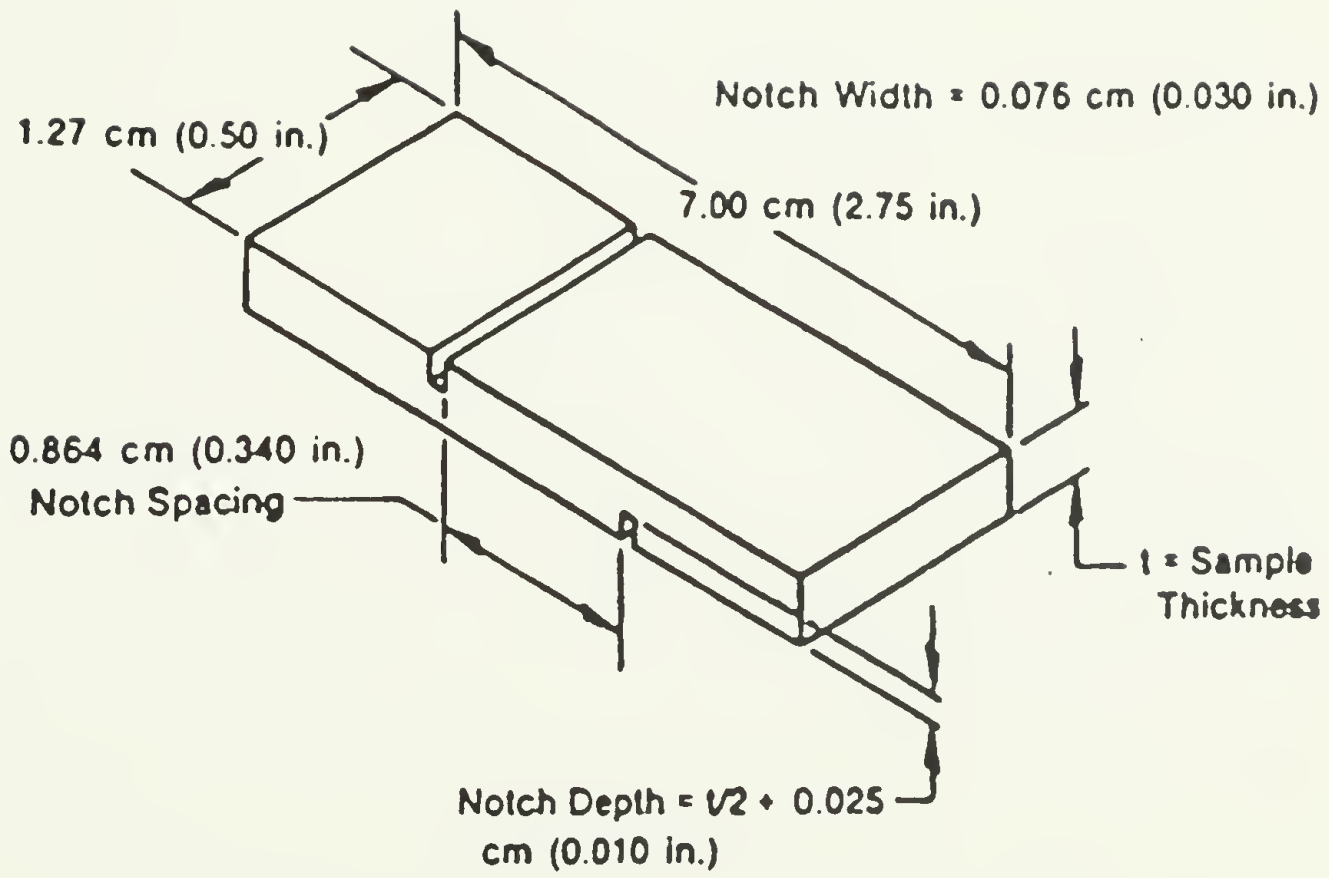

Figure 2.8 Double notched interlaminar shear test specimen. This configuration was used by Pratt and Whitney with the test being performed in compression. After ref. [29].

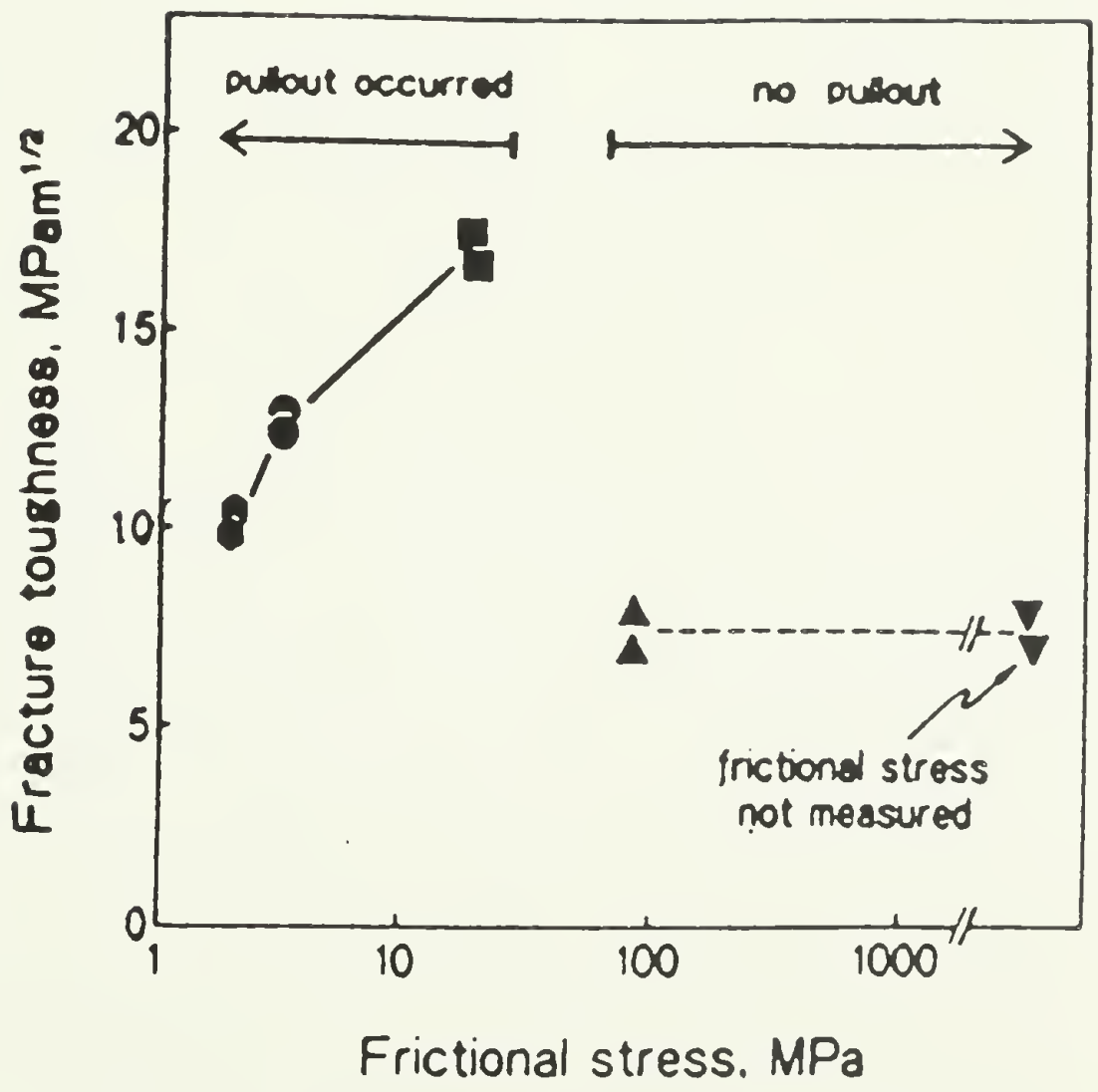

Figure 2.9 Relationship between interfacial frictional stresses and fracture toughness of SiC-monofilament reinforced silicon nitride matrix composites. After ref. [33].

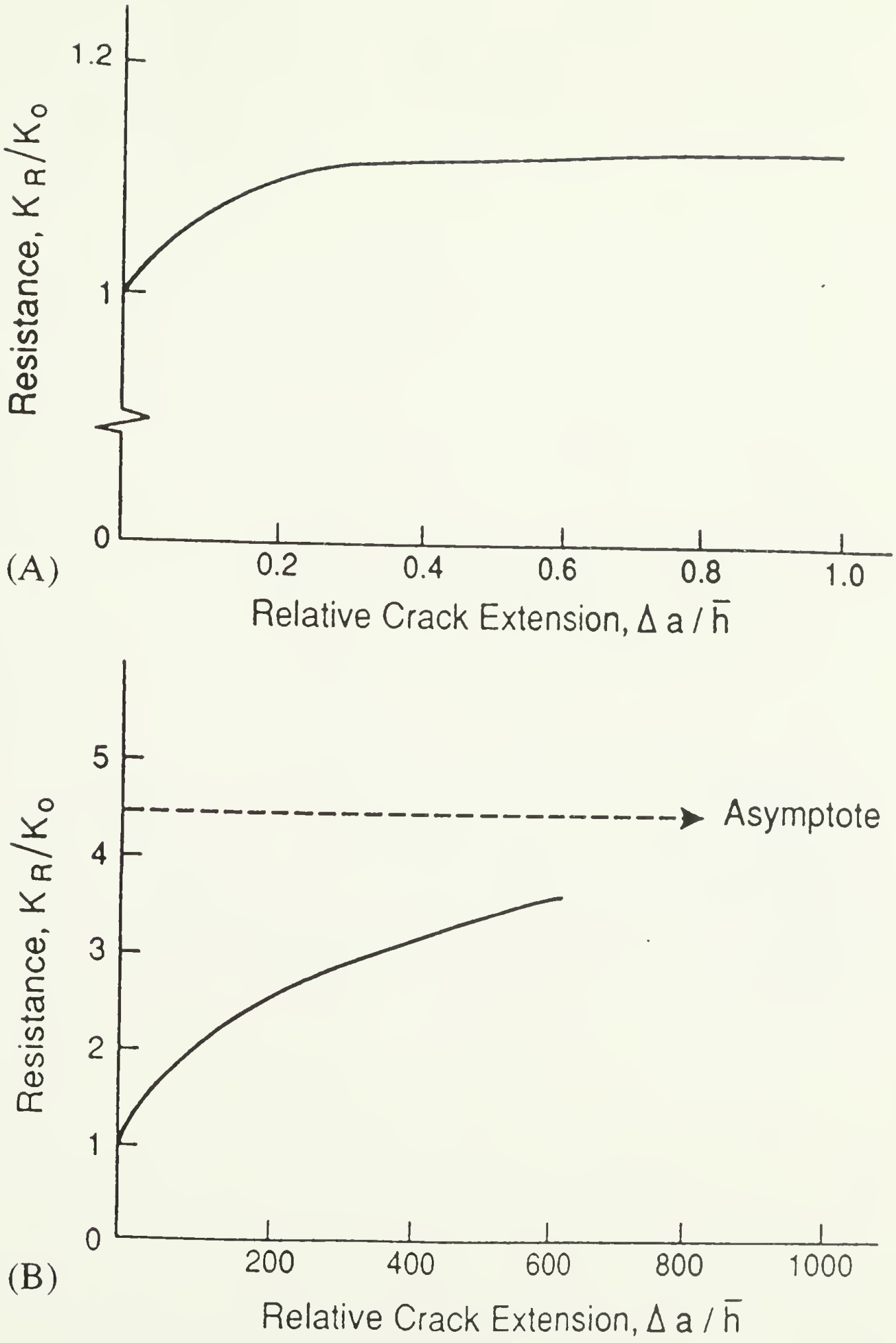

Figure 2.10 The resistance curves caused by (A) bridging fibers (with no pull-out) and (B) pull-out of fractured fibers. After ref. [32].

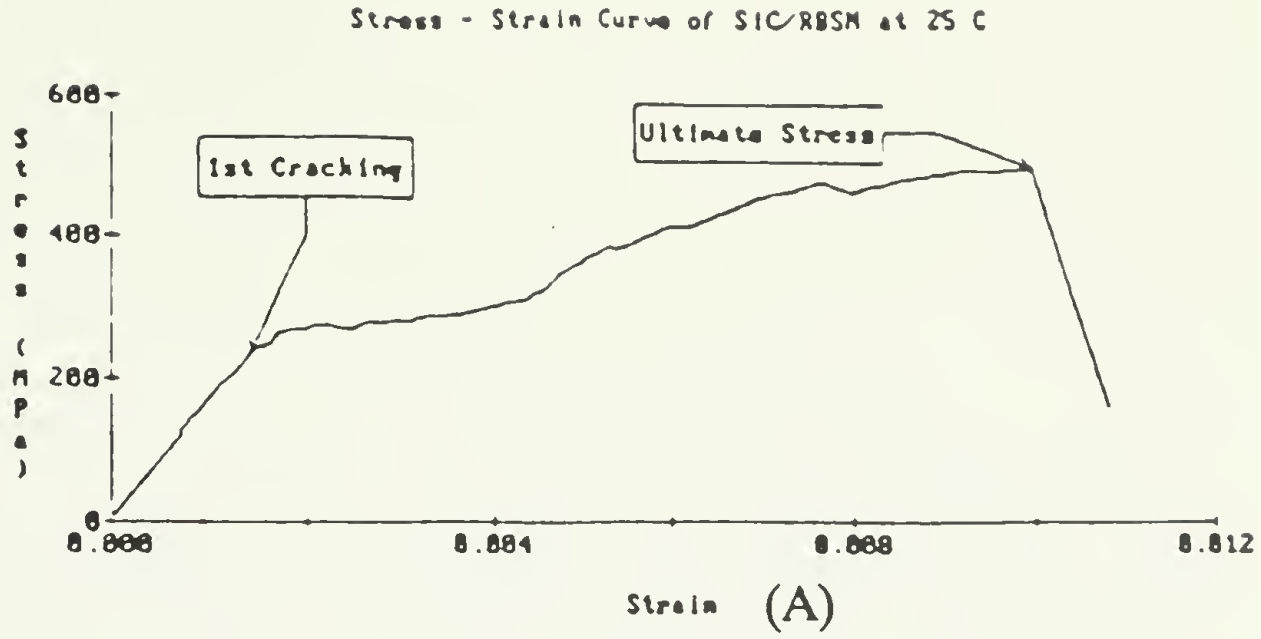

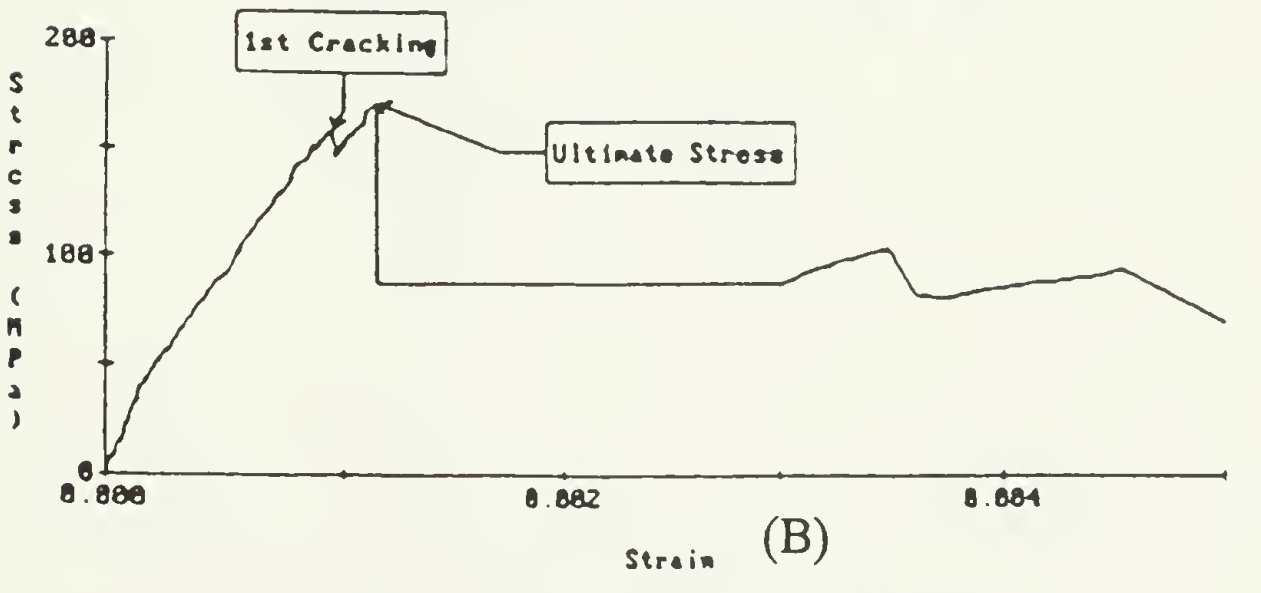

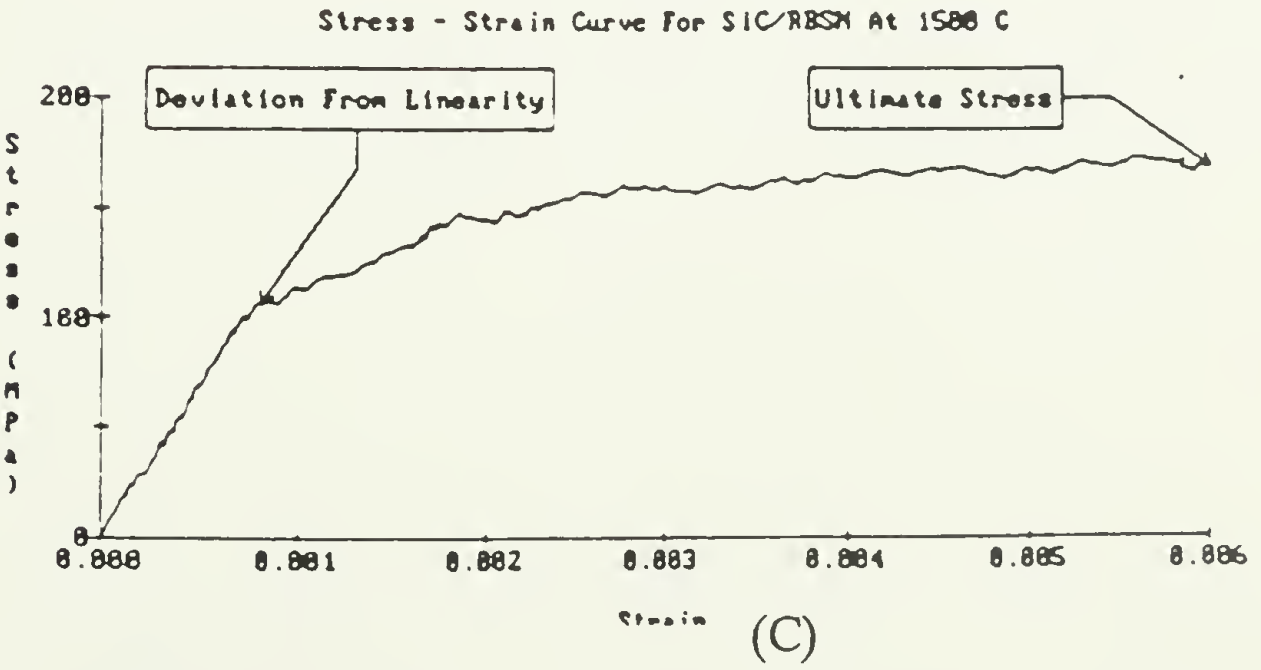

Figure 2.11 Stress/strain curves for SiC/RBSN at (A) 25°C, (B) 1300°C, and (C) 1500°C. Noise produced by the furnace at 1500° C produced the waviness of (C). After ref. [8].

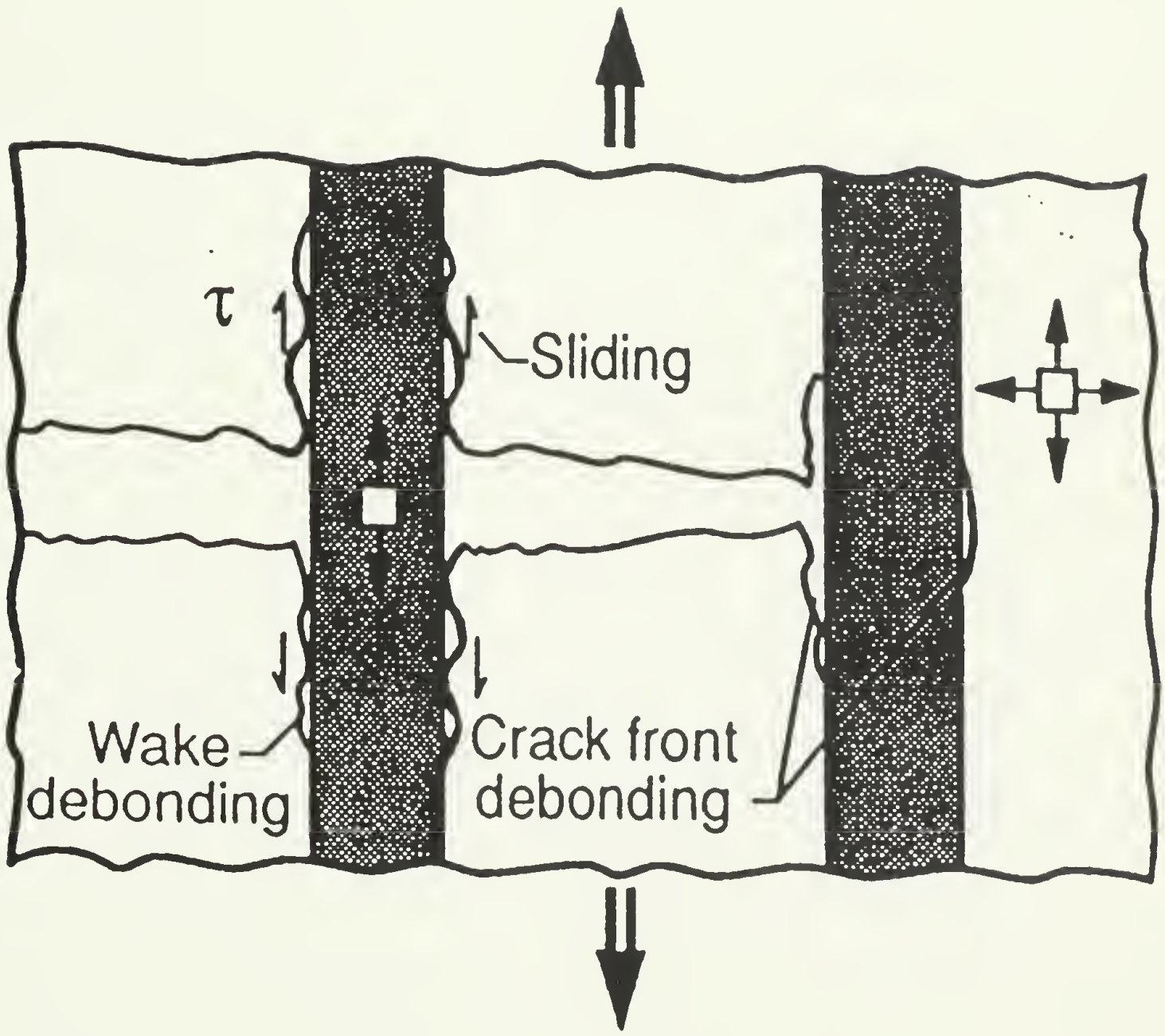

Figure 2.12 Schematic illustrating the initial debonding of fibers at the crack front, as well as fiber debonding and sliding in the crack wake. After ref. [13].

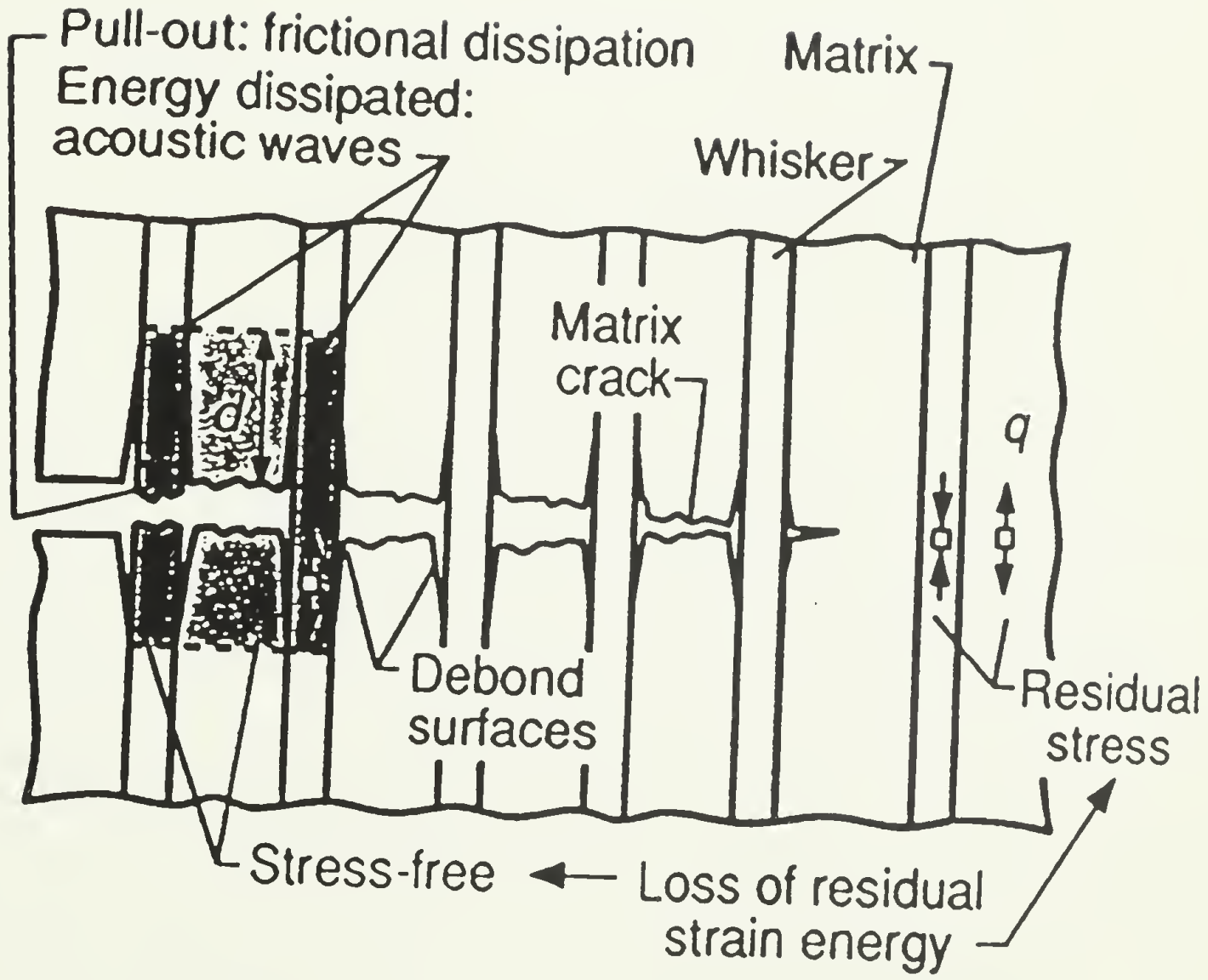

Figure 2.13 Schematic indicating the various contributions to the steady-state toughness. After ref. [13].

CHAPTER 3

EXPERIMENTAL PROCEDURES

3.1 Materials

3.1.1 SiC/RBSN

The SiC/RBSN investigated in this study was manufactured and supplied by the Norton Company. It contained 20 vol% uniaxially aligned Textron SCS-6 monofilaments which, as stated in Chapter 2, are approximately 140μm in diameter and contain two carbon rich surface layers. The processing of this material has been described in the literature and is shown in Figure 3.1. [5].

The reported porosity levels for this particular material as measured by three samples using a water immersion technique gave an average matrix porosity level of 36% with a corresponding matrix density of $2.0x10^3$ kg/m^3. These porosity levels were fairly substantial. Residual Si, as measured by X-ray diffraction, gave results of less than detectable levels or less than 1 percent in all cases.

The material was delivered mostly in the form of MOR bars measuring 3x4x50 mm or 3x8x65 mm. Billets supplied and cut by the manufacturer are 9b, 9c, 9d, 13a, 13c, 11a, 11c, 14b, 12b, and 10a. Except for the section dealing with long term elevated temperature behavior, batch numbers for experimental studies were randomly selected. Several samples were cut from each billet and the excess material was also made available. The manufacturer's designations for the materials are used throughout this text. It should be noted that the appearance of the MOR bars varied

with samples being cut along various planes, some of which exposed fibers on the surface while others did not or only exposed part of the fibers, and some specimens also had more large voids on the surface than others. The possible influence of these differences will be discussed in the later chapters.

All samples were polished to a 1-6 μm finish using diamond paste and were optically observed before testing. A cross-sectional view of the composite microstructure, Figures 3.2 (a) and (b) reveal that the fibers are uniformly distributed throughout the RBSN matrix. A higher magnification view of the interface, Figure 3.3, reveals that both C-rich surfaces are visible and were not degraded during the nitridation step. Some samples were found to contain some very large, around 50 μm, voids, see Figure 3.4.

3.1.2 Comparative Monolithic RBSN

A commercially available refractory grade RBSN was used as a comparative material in this study. The two available billets of this material were cut into several MOR bars, polished to an appropriate surface finish, and then tested at room and high temperature in bend. The typical apparent porosity of this material was 25%.

3.2 Experimental Studies

3.2.1 Ambient Temperature Studies

3.2.1.1 Composite Strengthening

The properties of strength and interlaminar shear of the SiC/RBSN composite material were investigated. An attempt was made to relate the strength and toughness to the interlaminar properties. Characterization of composite strengthening was attempted by employing both bend and tensile tests to investigate the first matrix cracking stress and ultimate tensile strength as well as the strain to failure of the composite. Samples for mechanical property evaluation were tested with the fibers aligned in the longitudinal direction.

Testing in four point bend using bend bars 3x4x50 mm in size made up the majority of the information obtained in this study. The fixture used for all bend tests was made of silicon carbide with Si/SiC rollers and was used for temperatures up to 1400° C. The span to height ratio was, in most cases, 13.33 with the inner span of the four point bend fixture being 10 mm and the outer span 40 mm. Mechanical tests in bend were performed using an Instron model 1321 electromechanical unit with a typical crosshead speed of approximately 0.2 mm/min. Some tests were preformed at 0.5 mm/min. A schematic of the test fixture is shown in Figure 3.5. Strengths were determined using the equations for an elastic beam in bending, namely,

$$\sigma = \frac{My}{I} \tag{16}$$

where M is the moment, y is the distance from the neutral axis, and I is the moment

of inertia. The modulus of the composite was determined using an unnotched specimen in tension and with the same set-up as described in part B.

To investigate interface properties, several configurations of the interlaminar shear specimen, two opposed offset notches, as used in the literature [24,29] were tried until one which produced acceptable results was found. Figure 3.6 shows the final configuration. Sample 13c-11 was cut into seven interlaminar shear specimens with internotch spacings of approximately 1.85 mm. Specimen depth was 3.00 mm. Sample 13c-2 had a internotch spacing of approximately 1.1 mm. The results from these tests were also evaluated for applicability since it is not only the interface that is being tested but also the matrix. The tests were performed in compression with a constant displacement of approximately 0.2 mm/min. The value of the interlaminar shear strength was considered the highest load divided by the area sheared.

The goal of the above mentioned tests was to be able to gain an understanding of composite strengthening. This is done via the evaluation of the applicability of the models presented in Chapter 2 and by an investigation into the relationship between strength and interlaminar properties. These goals were facilitated by examination of the fracture surfaces using optical microscopy and SEM. A JEOL JSM-5200 scanning electron microscope was used for the SEM work and optical microscopy was conducted using and Olympus AHBT microscope.

3.2.1.2 Composite Toughening

An attempt was made to evaluate both toughness and R-curve behavior using a single edge notched tensile bar with aluminum end tabs as shown in Figure 3.7. Evaluation of the R-curve was also attempted using a SENB sample by interrupting the test at several intervals and observing the specimen under the optical microscope. Tensile tests were performed using an Instron 1330 servohydraulic test system with hydraulic grip arrangement and a typical loading speed of approximately 440 N/min. Displacements were measured using an extensometer that was attached to the specimen and strain gages were used to verify alignment. An attempt to observe crack extension in situ during loading was made using a Questar model QM-100 long distance microscope. The results were recorded using a VHS video recorder.

For initiation toughness measurements, the single edge notched bend test, SENB, was employed. Notches approximately 0.5 mm in width were inserted into bend bars giving a notch depth to specimen height ratio on the order of 0.25. Again, the sample size was 3x4x50mm. The notches were inserted with a diamond wafering blade and were approximately 200μm in width. The procedure was the same as the MOR test described in the last section and the rate was approximately 0.2 mm/min. In addition to ambient temperature SENB, tests were also conducted at 1000° C, 1200° C, and 1300° C and the results of these tests are discussed in the next section. The initiation fracture toughness was calculated from the SENB data according to the equation

$$K_I = \frac{6Ma^{1/2}}{bw^2}\, y \qquad (17)$$

$$where \quad y = A_0 + A_1(a/w) + A_2(a/w)^2 + A_3(a/w)^3 + A_4(a/w)^4 + \ldots$$

and where M is the applied moment, b is the thickness, w is the width, and a is the notch depth. The load at the onset of load/displacement nonlinearity was used to calculate the initiation toughness.

The applicability of the different models that describe toughening was then made. Each possible contribution to toughening was considered. This was done by analyzing the above results in conjunction with in situ observations and fractographic analysis.

3.2.2 Elevated Temperature Studies

3.2.2.1 Short-term Behavior

Short term testing at elevated temperature included tests of strength, initiation toughness, and interlaminar shear. The applicability of existing models to strength was also evaluated. The apparatus for elevated temperature tests consisted of an Instron model 1321 electromechanical unit in conjunction with a molydisilicide high temperature "tube" furnace that wrapped around two SiC rods that attached to the Instron. This is shown schematically in Figure 3.8.

For the modulus of rupture test, MOR, samples were tested in four point bend from room temperature to 1400°C using the Instron in displacement control. The displacement rate was 0.5 mm/min. For the high temperature tests, the samples and

the SiC test fixture were heated to temperature and allowed to equalize before the test was run. Strengths were calculated using the strength of materials equations for an elastic beam in bending. Although no high temperature tensile tests were performed, measurements of the initiation fracture toughness using notched specimens in four point bend were attempted using the same technique as previously described in the ambient temperature section.

An attempt was also made to evaluate the R-curve at 1300° C using a SENB specimen in four point bend using the same apparatus as the above tests. Upon the first indication of nonlinearity in the load/displacement record, the sample was cooled and observed under an optical microscope and any crack extension was recorded and measured. This procedure was repeated in an attempt to create an R-curve plot.

Tests of interlaminar shear were also performed at high temperature using the previously mentioned opposed double notch specimen in compression. Again, an attempt was made to correlate the strength to the interlaminar properties. At-temperature tests were done at 1000°, 1200°, and 1400°C. In an attempt to study the effects of high temperature exposure on the interface, another set of specimens was pre-exposed to high temperatures up to 1400°C and then tested in compression at ambient temperature.

To investigate the relationship of strength and toughness at various temperatures to the interlaminar properties both optical and SEM observations were made. A comparison of the data at each temperature was made to see what conclusions could be drawn from the results.

3.2.2.2 Long-term Behavior

Characterization of creep, creep fracture, and elevated temperature lifetime was investigated using the interruption technique described here. To investigate creep crack initiation and growth, prepolished four point bend samples, 3x4x50 mm in size were subjected to constant loads at elevated temperature. Crack initiation and growth observations were made by employing the method of interrupting the tests at various times by cooling under load, to prevent relaxation effects, followed by unloading and optical observation. After observation, samples were then reheated to the test temperature, allowed to equalize, and then the test load was reapplied. This cycle was then repeated several times until the information desired was obtained or the specimen failed. Initial interruptions were around 15-30 minutes at temperature, at load, with approximately 1 1/2 hours taken for heat up and equalization and 2 hours for cool down under load. This interruption technique was also useful for exploring crack growth since in situ observation of bend tests at high temperature was not feasible. Both notched and unnotched samples were tested in this manner. The insertion of Vickers and Knoop indents into some the samples as a possible way to observe crack growth at high temperature was also investigated although obtaining pre-cracks from indents for these materials is often difficult because of the presence of the fibers.

Measurement of the creep strain was made for some of the unnotched bend specimens between interruptions. Two approaches were attempted. One technique involved placing several sets of Vickers indents on the tensile surface of the bend bar. The change in distance between the indents were averaged and used to calculate the

strain of the specimen based on change in length divided by length. This technique was deemed unsuccessful because of the difficulty in finding and accurately observing the distance between the indents consistently each time. The second technique involved measuring the change in focal length of the specimen along its length via the optical microscope. Units on the focusing knob were used to calibrate the height of the specimen along its length. Plotting the distance along the length of the specimen versus the specimen height gave points that were fit with a second degree polynomial curve. The curvature of the specimen was then determined from the curve fit. From this point, the equations from Hollenburg [46] were used to determine the maximum strain of the specimen.

Due to the large amount of oxidation present on the specimens after some of the high temperature tests, an attempt to remove the oxidation layer via acid etching was also by made but there was reason to believe the interface was damaged by the acid. Due to this, this technique was not used therefore small cracks may have remained undetected under an unremovable oxidation layer. The majority of the investigation into crack formation was done using optical and SEM techniques.

Using additional samples from the same as well as different batches as used above, time to failure data as a function of stress and temperature were recorded. The applicability of empirical models, see Section 2.3.4, to lifetime predictions were then investigated. Such lifetime data was obtained for mostly for 1000° and 1400° C although some information was obtained at 1200°, 1300°, and 1350° C also.

The applied stress selected to start this section of the study was 100 MPa, less that the corresponding stress value for first matrix cracking at all temperatures. Thus, it was hoped that both crack initiation and growth could be observed by the interruption procedure discussed.

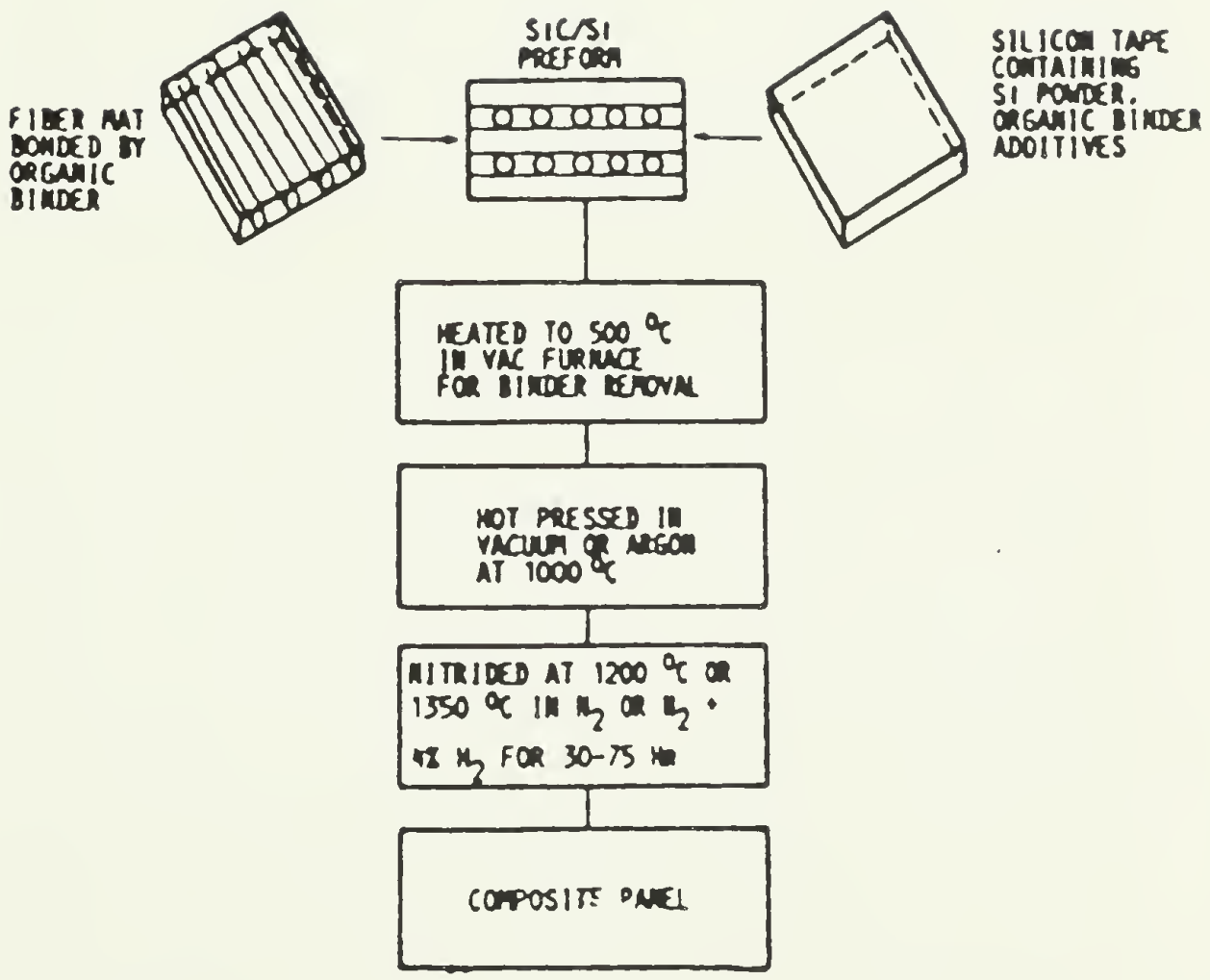

Figure 3.1 Block diagram showing a typical fabrication scheme for the processing of SiC/RBSN composites. After ref. [5].

(A)

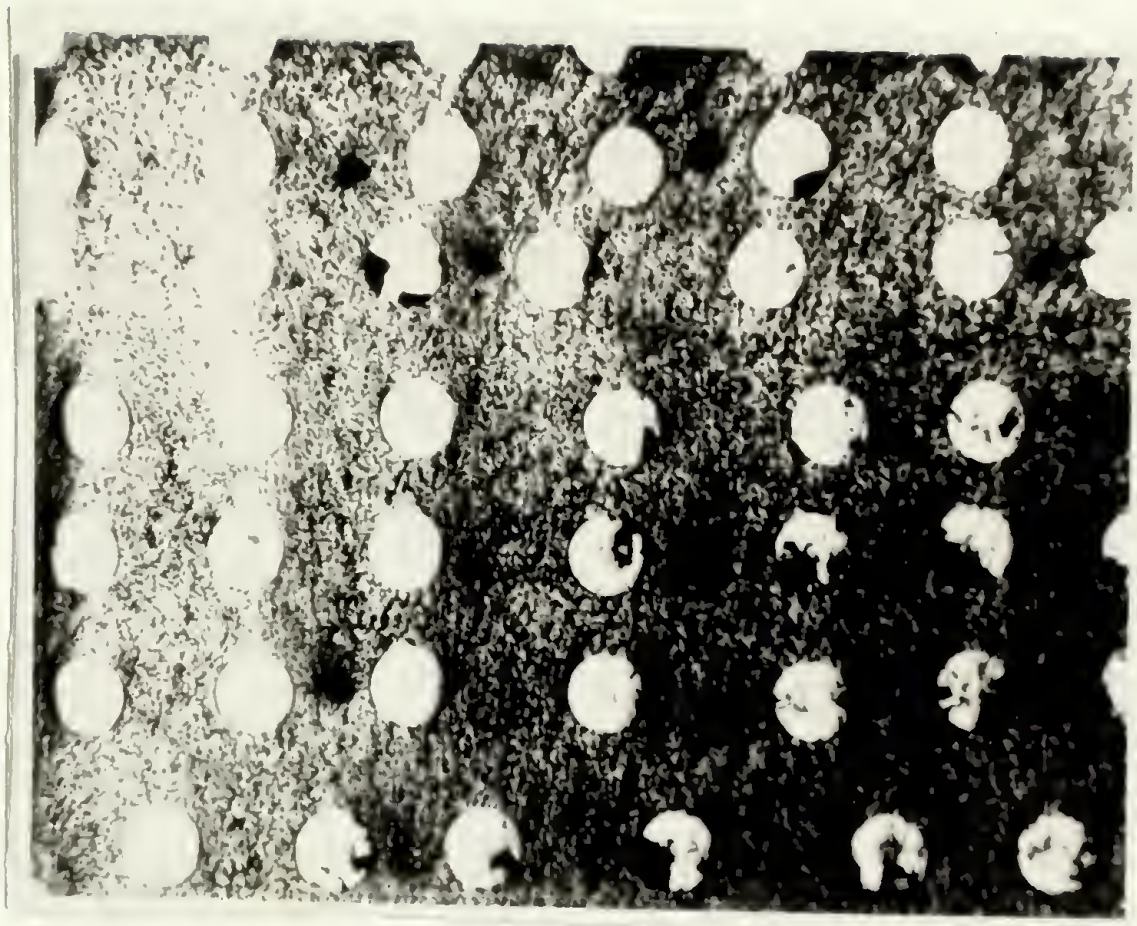

(B)

Figure 3.2 Micrograph of composite cross section showing (A) the uniformity of fiber distribution and (B) a closer look at the fiber cross section.

Figure 3.3 View of the SiC/RBSN composite fiber/matrix interface on a lengthwise slice of fiber showing both C-rich surface layers and the porosity of the matrix.

Figure 3.4 Micrograph detailing two large voids in the composite material.

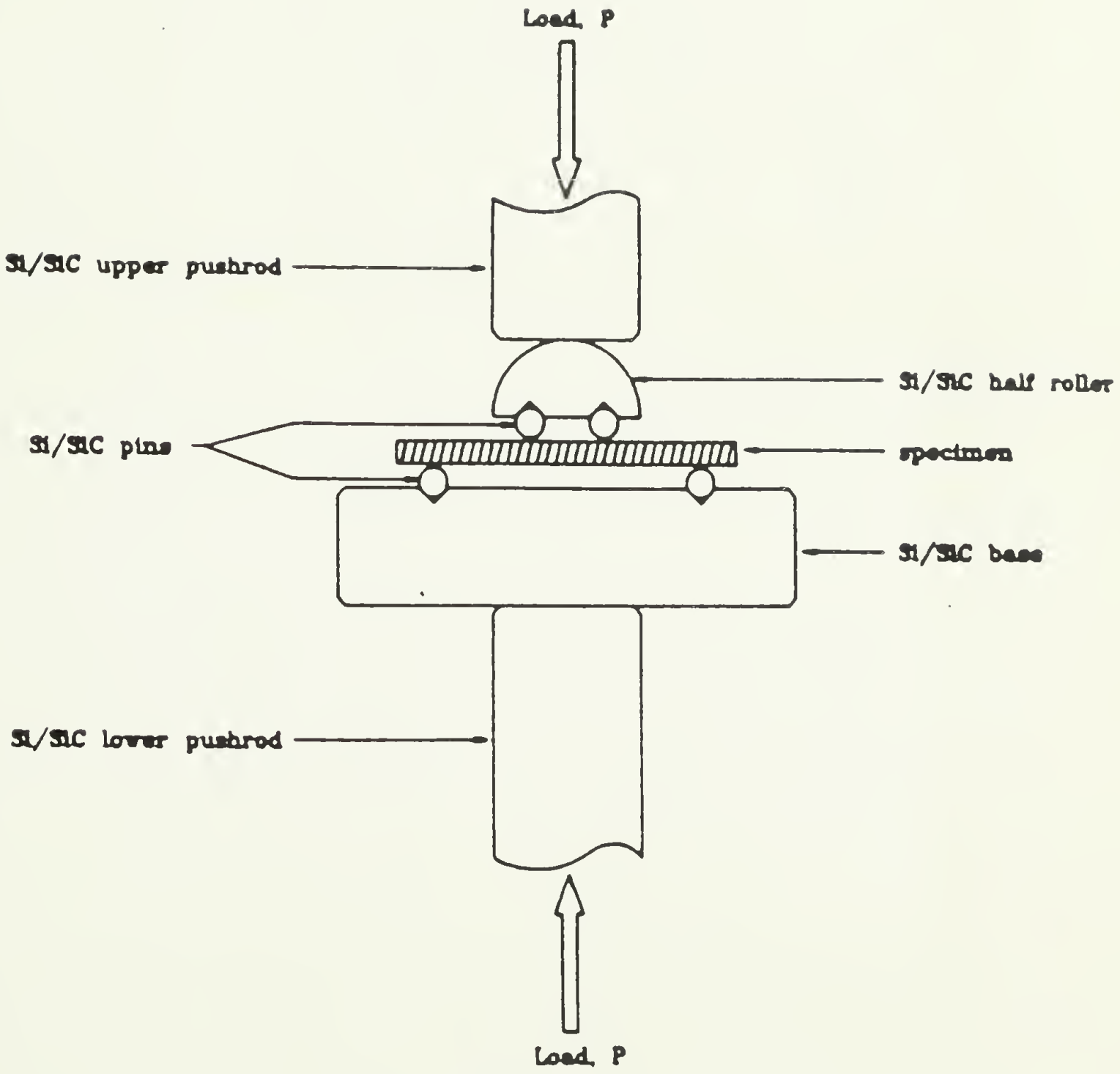

Figure 3.5 Schematic of room/elevated temperature 4-point bend fixture. After ref. [47].

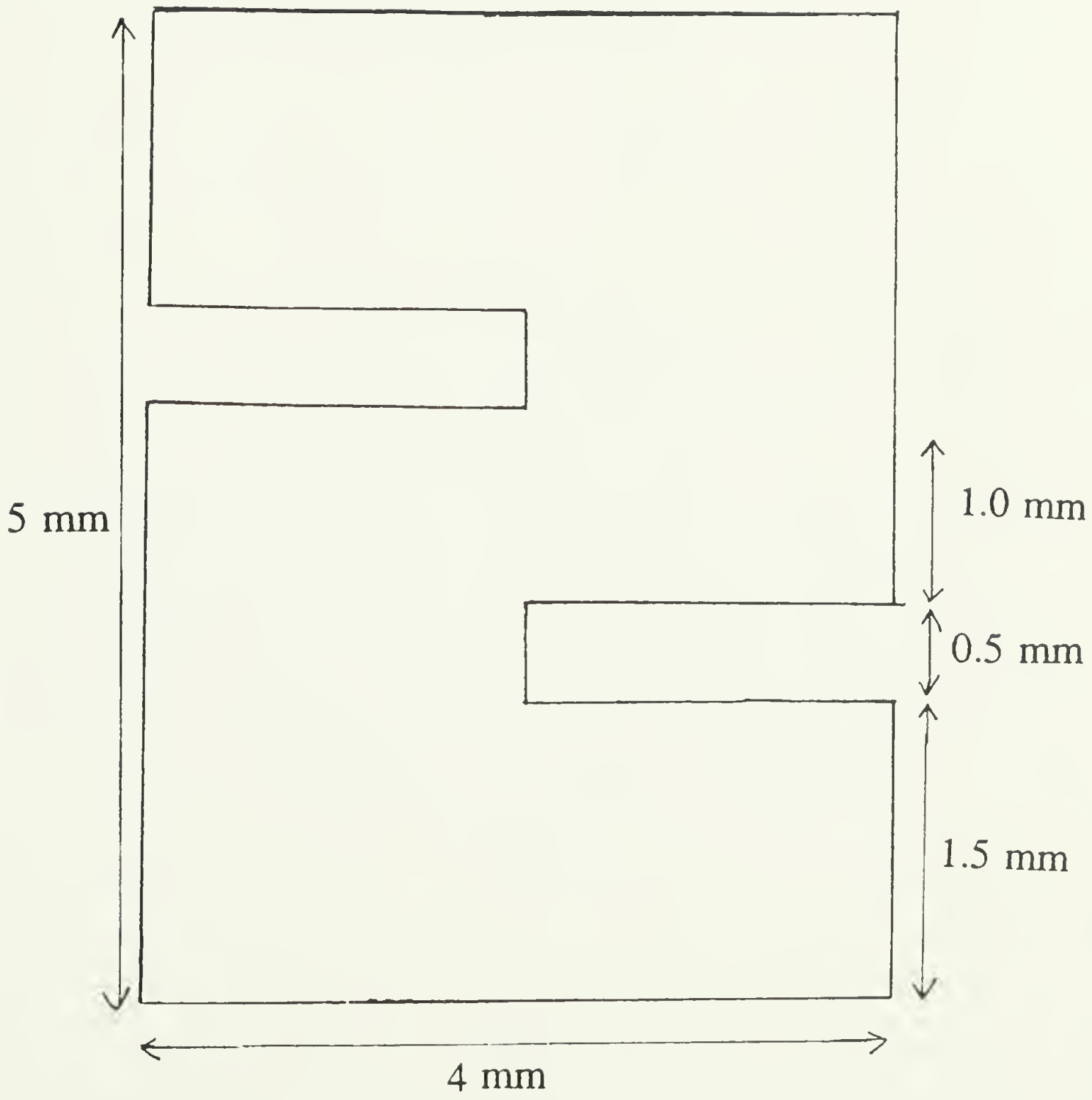

Figure 3.6 Configuration of the interlaminar shear specimen used in this study.

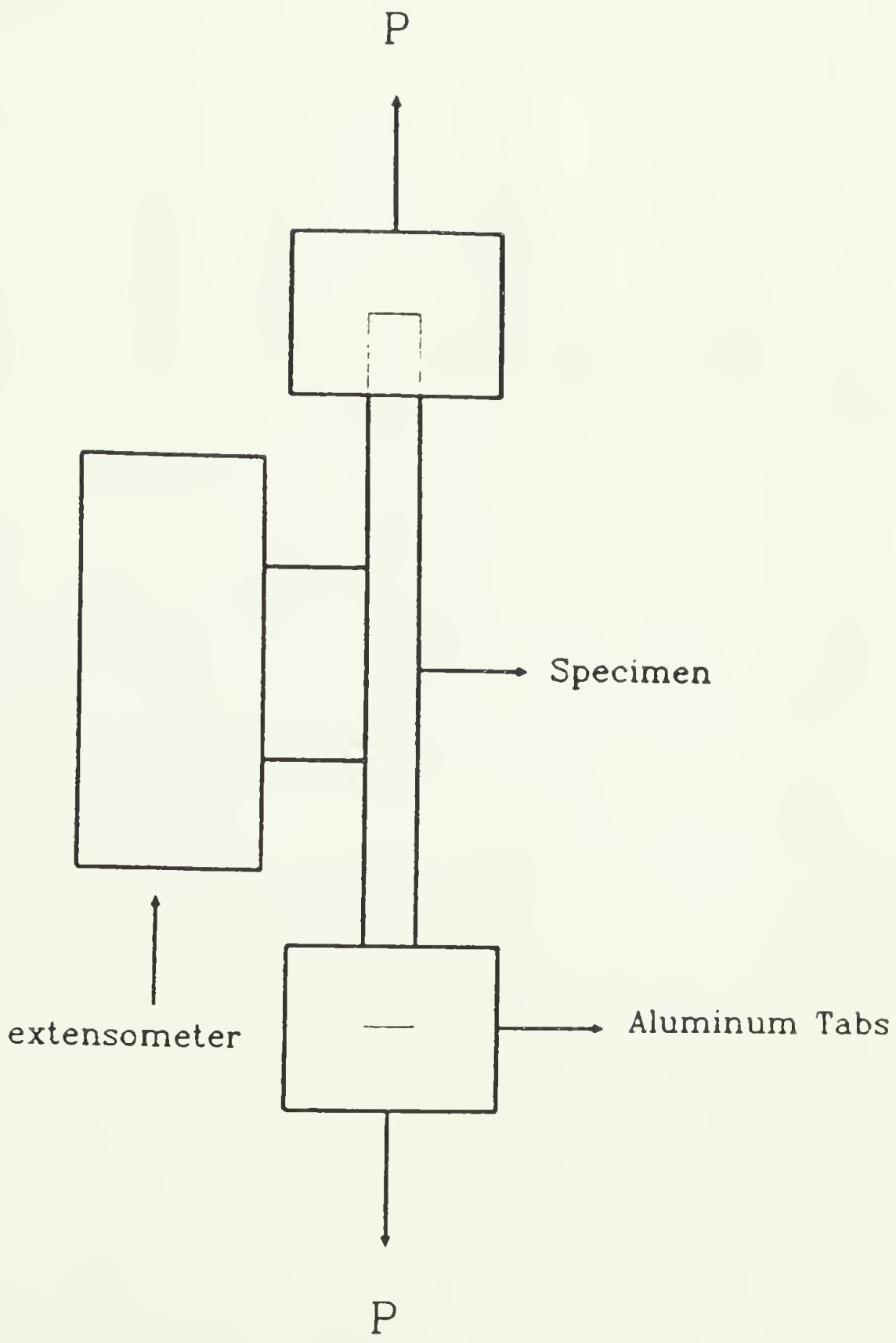

Figure 3.7 Schematic of tensile test apparatus.

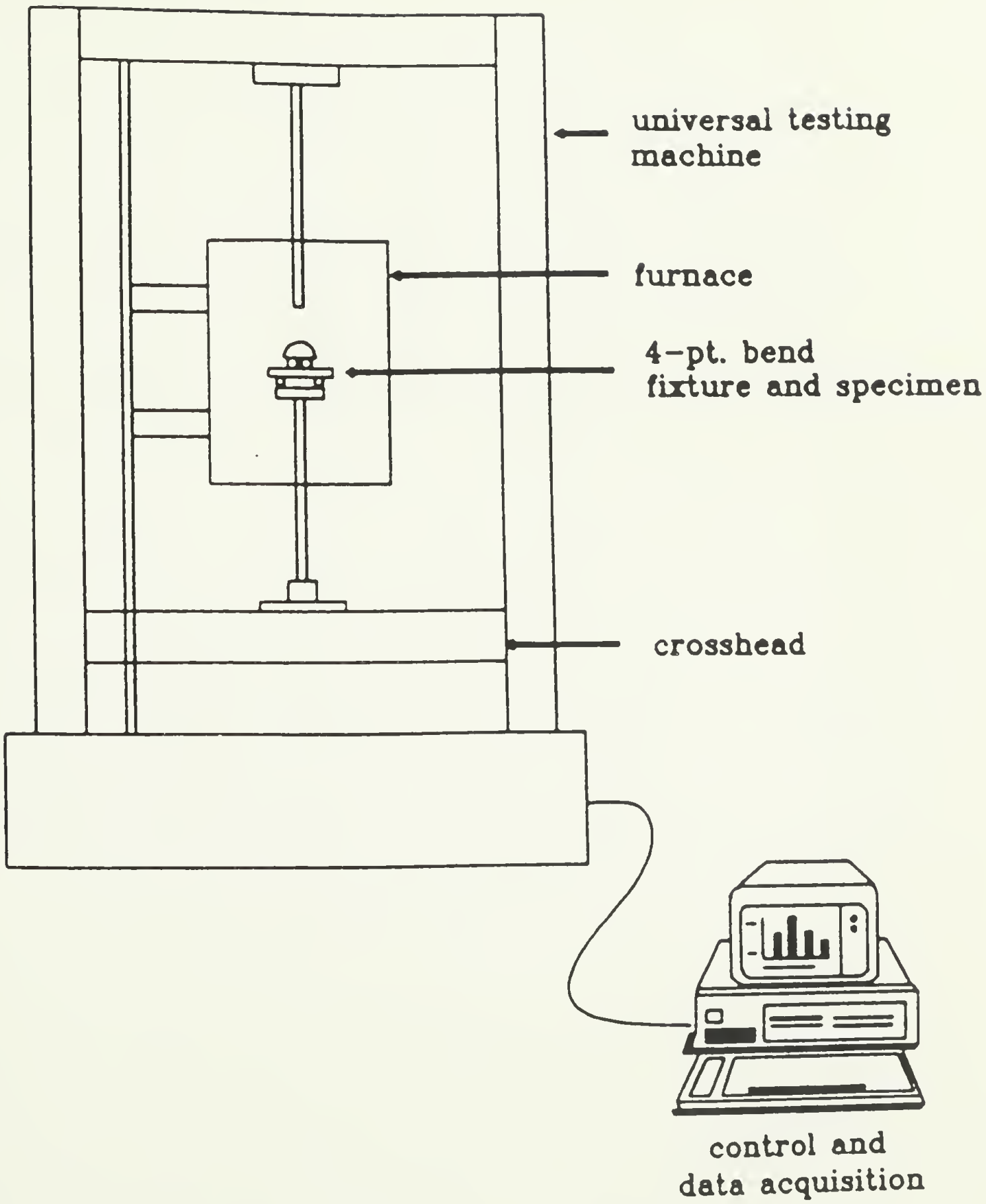

Figure 3.8 Schematic of bending and high temperature apparatus. After ref [47].

CHAPTER 4

EXPERIMENTAL RESULTS AND DISCUSSION

This chapter will document both the experimental data and qualitative observations made during the study of the SiC/RBSN composite as described in the previous chapter. Discussion of the results will be included as well. Ambient temperature results will be presented first and elevated temperature results will follow. Data on the comparative RBSN monolith will also be included throughout the text as well as in the last section.

4.1 Ambient Temperature Studies

4.1.1 Composite Strengthening

Studies of composite strengthening included, as stated in Chapter 3, measurement of the modulus, tensile and bend strengths, and interlaminar shear strength. In the following sections, data will be presented first and qualitative observations will then be stated.

4.1.1.1 Bend and Tensile Strength

Ambient temperature, four point bend, modulus of rupture tests (MOR), performed at a constant displacement rates of 0.5 and 0.2 mm/min, yielded the initiation and failure stresses shown in Table 4.1. The first load drop was often accompanied by an audible noise and the occurrence of first matrix cracking at this

point was substantiated by unloading, observation, and reloading. Initial cracking was often hard to detect because the cracks closed up tightly upon unloading. On several occasions, a small applied load was needed to force open the crack slightly for detection purposes under the microscope. The first matrix and ultimate failure strengths for the composite at room temperature in bend with the layup direction positioned horizontally during testing were 362 and 720 MPa respectively. Figure 4.1 shows a typical curve at ambient temperature. Superimposed on this plot is the load/displacement record of a RBSN monolith of approximately the same dimensions, also tested in bend. Note the large increase in the area under the load/displacement curve for the composite over that of the monolith. The work-of-fracture for the composite was clearly higher and the first failure event in the composite was also at a stress higher than the failure stress of the monolith. Displacement change to failure was also greatly increased.

As compared to the monolith, the load/displacement record of the composite shows many failure events before its noncatastrophic failure. The arrow in Figure 4.1 indicates the characteristic first matrix cracking stress. This was followed by a region of intermittent cracking until eventual failure at some maximum load. Failure proceeded as multiple matrix cracks formed, grew, and opened, leading to fiber failure events. Figure 4.2 shows the edge view of a failed bend sample at room temperature. As noted from samples tested in tension at room temperature where certain fracture features are more observable, a high degree of pullout and debonding was shown to be present and is shown in Figures 4.3 (a) and (b). The pullout lengths varied widely and

were roughly in the range of 100-1000 μm. From the higher magnification view of Figure 4.3 (b) it is clear that the coating layers are still visible on the pulled out fibers indicating that the applicable weak interface at ambient temperatures was somewhere in the outer C-rich layer.

Clearly, failure was noncatastrophic with the total work of fracture increased considerably over that corresponding to first matrix crack formation. This was in contrast to the RBSN monolith which showed elastic behavior up until fracture with clearly catastrophic failure. Because the region of intermittent cracking is generally associated with fiber bridging and pullout and the maximum load with fiber bundle fracture [39], these results are consistent with the presence of sufficiently weak C-rich layers which were not damaged during nitridation.

Figure 4.4 shows the load displacement curve of a specimen tested in the alternate direction which was the vertical orientation of the fiber layers. The strength result for this specimen was lower than for the horizontal orientation, 573 MPa, but the first matrix cracking values were close, 347 MPa compared to 362 MPa for the vertical orientation. At this point an actual orientation effect due to lay-up direction could not be determined or shown conclusively. Again, because of the high variability in strength between the different batches of this material, more tests on a single batch would have to be performed, which was not done due to lack of available material.

4.1.1.2 Modulus

The tensile modulus results from two specimens were 130 and 133.9 GPa with an average of 132 GPa. The predicted value of the composite modulus was evaluated from the rule-of-mixtures equation given by Equation (1). With the known moduli of fiber and matrix, this equation gave a predicted value for the composite modulus of 130 GPa, which was comparable to the measured value. From this we concluded that the interface was sufficiently strong to support ideal load transfer to the fibers at ambient temperatures. In addition, it was also concluded that the composite modulus was significantly limited by the large porosity levels in the matrix.

4.1.1.3 Interlaminar Shear

The room temperature values for the interlaminar shear strength were 85 MPa for two specimens in one batch and 42 MPa for a specimen from a different batch. The load/displacement plots were linear for these ambient temperature tests with complete failure occurring at the maximum load. Significant fiber-matrix debonding was observed occurring as significant gap around the fiber as observed in cross section. This large separation may have been due to the relief of residual tensile stresses at the fiber/matrix interface which are known to occur in fiber reinforced composites as a result of cooling from the processing temperature. In the tested samples, the fiber coating also appeared to be attached to the fiber meaning that the failure occurred at the outer interface which was consistent with the strength testing results. The large difference in room temperature interlaminar shear strength between

batches may have been due to differences in the plane on which the notches were cut as well as batch variation effects.

4.1.2 Composite Toughening Studies- Toughness and R-Curve Behavior

4.1.2.1 Toughness

Loading of notched samples, in both tension and bend, gave a load-displacement result similar to that for the unnotched case that was shown in Figure 4.1, namely, a point of crack initiation followed by intermittent crack extension from the notch with increased load until ultimate failure. A typical result is shown in the tensile load-displacement result of Figure 4.5 where the point of first crack extension from the notch is indicated by an arrow. In situ viewing during load application of a notched tensile sample revealed that the breaks in the loading curve following first crack extension ahead of the notch were indeed associated with continued intermittent crack extension. As a result the toughness value calculated from the load corresponding to the arrow in Figure 4.5 was denoted the initiation toughness. The values of initiation toughness obtained in this study will provide relative comparisons between materials, they were not intended to be taken as absolute values of toughness or initiation toughness.

In the notched tensile specimens, two cracks headed out from the notch at 45° angles, debonded along a fiber layer for a certain distance, broke through the fiber layer and then continued until specimen failure. Final failure of the specimens in tension was accompanied by a high degree of fiber pullout. Considerable delamination

along fiber/matrix interfaces was also readily observable by inspection as shown in Figure 4.6. Again, as in the unnotched case, failure occurred along the outer interface. The initiation toughness at ambient temperature, including SENB data, gave a toughness result for five samples of 3.14 ± 0.2 MPa·$m^{1/2}$. Direct observation revealed that initiation appeared to occur by failure in the matrix ahead of the notch. In some cases, however, initiation was observed as a crack emanating from the notch on one side of the specimen while on the other side of the specimen only the delaminating, mode II, part of the crack could be observed and a connection to the notch could not be seen.

To further study damage progression in a notched specimen at room temperature, a SENB specimen was loaded under constant displacement conditions and the test was interrupted at several intervals. The test was interrupted at the first sign of nonlinearity. At this point, the load on the specimen was 52 N which corresponded to an initiation fracture toughness of 3.7 MPa·$m^{1/2}$. There were no visible cracks when the specimen was observed under the optical microscope. However, upon applying a small opening force to the notch, two cracks, each emanating 45° from the notch sides, were observed. Upon repeated observation of micrographs taken of the initially observed material, a white haze could be seen where the crack was later observed. In any case, it was not known if the actual location of the crack tip was observed. This test demonstrated the often extreme difficulty and uncertainty in determining the presence and nature of cracks in this material. With continued interrupted testing of this specimen, the crack path continued as mode II, moving

perpendicular to the notch to an area far outside of the inner span. No secondary cracks were observable in the material. Figure 4.7 (a) shows this crack emanating from the notch. Figure 4.7 (b) shows the other side of the sample with only a mode II crack with no visible surface connection to the notch. This type of behavior is indicative of notch insensitivity.

4.1.2.2 R-Curve

Figure 4.5 also indicates the load/displacement profile during unloading and subsequent re-loading at a stage prior to specimen fracture. Note that upon reloading continued crack extension occurred at the same load as at which unloading was begun. The reloading curve, however, was not linear, with a hysteresis in the unloading-reloading cycle, which has previously been discussed [34] in terms of fiber pull-out effects. It appears, then, that the R-curve may be associated to some degree with fiber pullout effects. Crack extension with increasing load was confirmed using an interrupted SENB test as was described in the previous section. Crack extension with increasing load bearing capability is indicative of R-curve behavior.

4.2 Elevated Temperature Studies

4.2.1 Short Term Test Results

4.2.1.1 Strength

Modulus of rupture tests were also conducted at elevated temperatures ranging from 1000°-1400°C. Table 4.1 shows the strength results. The first matrix cracking

strengths and the ultimate strengths are plotted in Figure 4.8 from ambient to 1400° C. Figures 4.9-4.15 show the load/displacement curves for these bend tests. While not every specimen showed a first matrix cracking stress, in all cases the load/displacement curve went non-linear at some point before final failure. Non-catastrophic behavior was observed in all specimens at all test temperatures.

The specific nature of the failure behavior the above specimens varied. At room temperature, the failure was characterized by a large amount of matrix cracking with many crack branches. At 1000° C, in all cases, one matrix crack formed on the tensile surface which led to specimen failure. Figures 4.9 - 4.11 show load/displacement curves for 1000° C. For two of the samples, Figure 4.11, there were few events before the ultimate stress was reached while for the other two tests, the behavior was similar to the ambient temperature behavior. Slopes and total displacements were all similar. Fiber bridging and pullout were observed at elevated temperatures as shown in Figures 4.16 (a) and (b) for MOR samples tested at 1000° C. The difference at elevated temperature was, as shown in the enlarged view in Figure 4.16 (b), that the coating appeared to have been left behind in the matrix as fiber pullout occurred. This suggested that at elevated temperature the applicable weak interface may be the inner C-rich layer. This may be have been due to thermal degradation of the outer layer or reaction of the outer layer with the matrix. The possible reactions were not identified in this study.

At 1200°C, a change from single crack formation to multiple matrix cracking on the tensile side was observed. Two specimens tested at 1200° C had one main

branched crack with another having four tensile side matrix cracks in the inner span. Figures 4.17 (a) and (b) show both the edge and tensile side view of a sample after testing. Note the multiple matrix cracking. Another specimen had 2-3 branched tensile surface matrix cracks. Figure 4.12 shows the load/displacement curves for the specimens tested at 1200°C. The slopes are similar and not one of the curves demonstrates a first matrix cracking point. Note that one of the specimens exhibited a much higher strength than the other samples. A specific reason for this was not discovered. Again, batch variations may have played a role.

Increasing the temperature to 1300° and 1350° C, two main cracks appeared in each specimen. Figures 4.13 and 4.14 show the load/displacement curves of 1300° and 1350° C respectively. Increasing the temperature to 1400° C, two separate, similar width cracks appeared on the tensile surfaces of two specimens. The fibers had the appearance of being pulled out of the matrix. One sample tested at 1400° C only had one main inner span tensile surface matrix crack. Its load/displacement behavior, as evidenced from Figure 4.15 was also much different than for the other two samples which exhibited the expected, more plastic, behavior.

Figure 4.8 shows the general trend of decreasing strength with temperature but a relatively steady value of the first matrix cracking stress. It also indicates that while first matrix cracking strengths were fairly stable to relatively high temperatures, ultimate strengths dropped significantly and actually began to approach the first matrix cracking strength at elevated temperatures. This is indicative of significant fiber degradation with increased temperature [47]. Beyond the point of first matrix

cracking, it appears that fibers can be easily accessed by the external environment and may suffer oxidative damage, as discussed elsewhere [48]. Strength of monolithic RBSN also remains relatively constant in this temperature range, which was also witnessed from MOR tests of the comparative monolith. A theory of fiber/matrix bonding at elevated temperature would therefore explain an overall strength decrease.

4.2.1.2 Interlaminar Shear - At temperature and pre-exposed

The results of elevated temperature interlaminar shear tests are shown in Table 4.2 and Figure 4.18. The samples were tested at temperatures to 1400° C in compression. The load/displacement curves for these tests are shown in Figure 4.19. Inspection under optical and stereo microscopes revealed what appeared to be significant debonding at ambient temperature. The matrix appeared to have pulled away from the fiber leaving a large gap around the fiber. Significantly less debonding was observed at the higher temperatures.

Another set of specimens was also made and three of these samples were pre-exposed to temperatures ranging from 1000° - 1400° C for one hour (length of a typical first interruption in long term high temperature testing), and were then tested at room temperature. The results are shown in Table 4.3 and graphically in Figure 4.20. The load/displacement curves are given in Figure 4.21. Failure was observed to be occurring without the extensive delamination and separation occurring at the interface that was seen at ambient temperature. The strengths were all similar and no significant trend or difference between specimens could be observed.

Failure of this ceramic composite system, as demonstrated by the SENB tests both in tension and bend, occurred as mixed mode I and II or purely mode II at room temperature. Although delamination of the fiber/matrix interface occurs in these tests, failure of matrix necessarily occurs also. This is the same type of failure that occurs during an interlaminar shear test. If the composite is considered to have laminate properties, then a consideration of the orientation of the specimen according to the laminate direction is also necessitated - an effect due to the direction that the fiber layers were stacked during processing. MOR and creep tests were conducted in the horizontal layup orientation, SENB and interlaminar shear tests were conducted in the vertical orientation. Therefore, comparisons of interlaminar shear strength and failure should be valid between the interlaminar shear test and the SENB tests where with the MOR and creep tests applicability is difficult to determine. Figure 4.22 shows the relation between the first matrix cracking stresses, ultimate strengths, and the values of the interlaminar shear strength.

4.2.1.3 Toughness

The initiation toughness results obtained from notched bend specimens are shown in Table 4.4. In all cases, a mode I crack that proceeded straight out 0° from the notch and then split into two cracks which delaminated parallel to the fibers. The straight 0° portion of the crack ran approximately three fiber matrix layers long for the specimens tested at 1000° and 1200° and about twice that for the samples tested at

1300° C. The load/displacement curves, see Figure 4.23, in most cases showed a distinct load drop prior to reaching the ultimate load.

Since the largest amount of mode I crack growth before delamination was observed to occur at 1300°, an interrupted SENB was performed at this temperature in order to see if enough information on the mode I crack growth could be obtained to quantify the R-curve of the material. This was not successful. Even after interrupting the test at the first sign of non-linearity, the transition from mode I to mode II cracking was already observed to have occurred. Although it was not visible at first, a 90° curve was observed when a small load was applied to open up the crack while under an optical microscope. Figure 4.24 shows the load/displacement record for the two interruptions. Although this crack was observed after the first interruption, the specimen was still able to carry an increased load. Therefore, although an R-curve could not be measured, the results were indicative of R-curve behavior.

4.2.2 Long Term Test Results

Long term studies were conducted via the procedure described in Chapter 3, namely, creep crack initiation and growth (interrupted constant load conditions) studies were done. The stresses for the initial tests were picked so as to be less than that of the first matrix cracking stress at that temperature. In many samples, delamination cracking occurred at the sample ends which may have been due to fixture alignment or insufficient span and/or sample length. Attempts at strain measurement were, for the most part, unsuccessful using the available methods which may have been in part due

to the uneven surface of the samples resulting from the presence of cut fibers on the surface. In addition, many of the long term studies done in this section relied on observation of the specimen surface. It should be realized that even the behavior of a specimen at elevated temperature may be dependent on the surface properties. As stated, most specimens had half cut fibers or fiber troughs exposed on the tensile surface and the effects of this have not been analyzed. Zok [32] states that care must be taken in making conclusions about fiber behavior from fibers exposed on the surface because such behavior might not be representative of the fibers completely embedded in the matrix, since the processes of cutting and polishing introduce defects which reduce the fracture stress of the fibers near the surface. The Appendix contains a summary of all the interruptions performed. A summary of the observations and behavior at elevated temperature follows.

Initial tests done at 1000° and 1200° C showed brittle behavior with cracks initiating in the matrix. Slow crack growth was not observed at these temperatures. This may have been due to the small sample sizes. Figure 4.25 (a) shows a matrix crack which initiated after 60 minutes exposure to 1000° C at 100 MPa. The whitish region indicated in regions in Figure 4.25 (b) was the first incipient matrix crack to form and suggested that heterogeneous regions in the matrix or matrix porosity may have served as sites for elevated temperature crack initiation. Time-dependent fiber bridging was observed at 1000° C with the fibers slowly pulling out of the matrix with time. This is indicative of a time-dependence in the bridging process at elevated temperature. A plot of this crack opening/time dependence is shown in Figure 4.26.

Although failure was due to cracks initiated in the matrix normal to the fibers, fiber fracture also occurred at 1200° C. Figure 4.27 is a view of fracture within a fiber which developed after 50 minutes exposure to 1200° C at 100 MPa. This type of fiber fracture was not clearly evident at 1000° C.

Once matrix cracks initiated at elevated temperatures, growth of the initiated crack occurred perpendicular to the fibers. Furthermore, Figures 4.16 (a) and (b) for the elevated temperature MOR case, crack growth left behind unbroken fibers in the crack wake. This was in contrast to the behavior at room temperature wherein cracks were deflected along the fiber/matrix interface and did not maintain a crack plane normal to the fibers or the applied load. In part, this difference in crack plane may be attributed to a changing residual stress state with increased temperature. At ambient temperatures, fiber/matrix interfaces are subjected to residual tension, whereas this tensile stress is relieved at elevated temperatures. This is due to the larger coefficient of thermal expansion of the SCS-6 fibers compared to the silicon nitride [31].

Interrupted tests were also done at temperatures of 1400° C, 1350° C, and 1300° C. The highest temperatures were tested first to see whether the material would exhibit slow crack growth at very high temperatures where the material was known, from the MOR tests, to deform significantly under load. The times to crack initiation and failure were obtained, and are summarized in Table 4.5. The times to matrix crack initiation indicated what appeared to be an increasing resistance to matrix crack initiation. This was consistent with results in a SiC whisker reinforced alumina [49] wherein the critical creep strain for crack initiation was increased as the temperature

was increased. Thus, as the temperature increased, the matrix exhibited more deformation and increased resistance to fracture initiation. It was also observed that, as the temperature increased, the matrix exhibited more deformation and increased resistance to crack initiation, consistent with increased fiber degradation at elevated temperature. Starting at around 1350° C there appeared to be a transition from matrix crack initiation to fiber crack initiation. Matrix cracks which ran a path where fiber defects were linked up, as shown in Figure 4.28. Figure 4.29 (a) and (b) show this behavior in finer detail clearly showing the movement of the matrix crack toward the fiber defects. In this case and at this temperature, failure seemed to be fiber degradation, cracking, controlled. There was only one crack at failure and it ran the whole width of the specimen. With subsequent interruptions, the oxidation took on the appearance of a cracked ceramic glaze.

Fiber cracks were also observed at 1400° C. At a stress of 125 MPa, the fibers appeared to be strongly bonded to the matrix and there was no fiber bridging or pullout perpendicular to the fibers. Several other cracks in addition to the main crack existed at failure. Matrix cracks appeared to have gravitated towards the fiber cracks. Figures 4.30 (a) and (b) show this crack gravitation clearly. This implies a strong fiber matrix bond. This was the same type of "linking up" that occurred at 1350° C. It appeared as if the fibers were degrading at these high temperatures. This, along with possible increased fiber/matrix bonding, higher τ, suggest that the fiber cracks may be the strength controlling flaws. Another observed feature at 1400° C was the quick formation, after the first interruption, of the glaze type cracks in the oxidation

layer. These are shown in Figure 4.31. It is not known what role they may play, if any, in the strength of the composite at elevated temperatures.

4.3 Monolithic Results

The room temperature bend strengths of the RBSN monolith used in this study were 262, 309, and 287 MPa for three samples. The manufacturer's reported flexural strength of this material is 200-250 MPa at room temperature to 250-275 MPa at 1500° C. Failure was brittle and the load/displacement plot was linear. The bend strength of this same refractory grade commercially available RBSN was 328 MPa at 1400° C. Even though the average strength of the composite at 1400° C was lower than that of the monolith, the work-of-fracture values for the composite were always higher than for the monolith. The behavior of the composite at high temperatures was extremely non-linear so although the ultimate strengths were lower the work-of-fracture remained high.

Notched specimens were also tested in bend at room temperature and at 1300° C. The resulting values of K_I as calculated from the previously mentioned fracture mechanics equation, gave values of 2.0 and 3.1 for the ambient and 1300° C tests respectively. The load/displacement curves for these notched tests had similar slopes and failure was catastrophic. In both specimens, one single crack grew out parallel to the notch, perpendicular to the fibers, and ran straight through to the end of the specimen. This was in stark contrast to even the composite specimens that exhibited initial mode I behavior. In the composite specimens, delamination always occurred at

some point and failure was never catastrophic with final failure occurring with a large work-of-fracture. The first load drop was, for most cases, not the last.

Two high temperature constant load tests were also performed on the monolith in an attempt to observe time dependent behavior as seen in the composite. Two samples were tested at 100 MPa for 60 minutes, one at 1000° C, the other at 1400° C. These short time, low stress regimes were chosen because the composite had showed crack initiation occurring under these conditions. The amount of strain in the monolithic samples was barely visible and except for some minor surface oxidation which was less than that seen in the composite, no damage, cracks, or other changes were noted. It was therefore concluded that the composite showed time-dependent crack initiation at time regimes much shorter than expected, even shorter than the corresponding monolithic material. However, it should be noted that initiation in the composite did not equal failure. This is in sharp contrast to brittle monolithic behavior. Further study is needed to be able to compare not just crack initiation time frames but final time dependent failure time frames. Within this study, no evidence for stable crack growth for either system was found.

The final monolithic study involved looking for a rate effect for a MOR test at elevated temperature, 1400° C. Instead of the MOR being run over the course of about 1 minute as was previously done, the rate was slowed to .0085 mm/min extending the test to over an hour. The same was also tried for a composite bar and the results are shown in Figure 4.32. When the testing rate for the monolith was slowed from 0.2 mm/min to 0.0085 mm/min, the strength values obtained at 1400° C

were 272 and 316 MPa. There was some initial non-linearity in the load/displacement records but this could not be distinguished from load train effects. When the composite sample was then tested at this slow rate, the ultimate strength was found to be 132 MPa with no first matrix cracking stress. The slopes of the load/displacement curves were nearly identical for both loading rates. Table 4.6 contains a summary of the monolithic results.

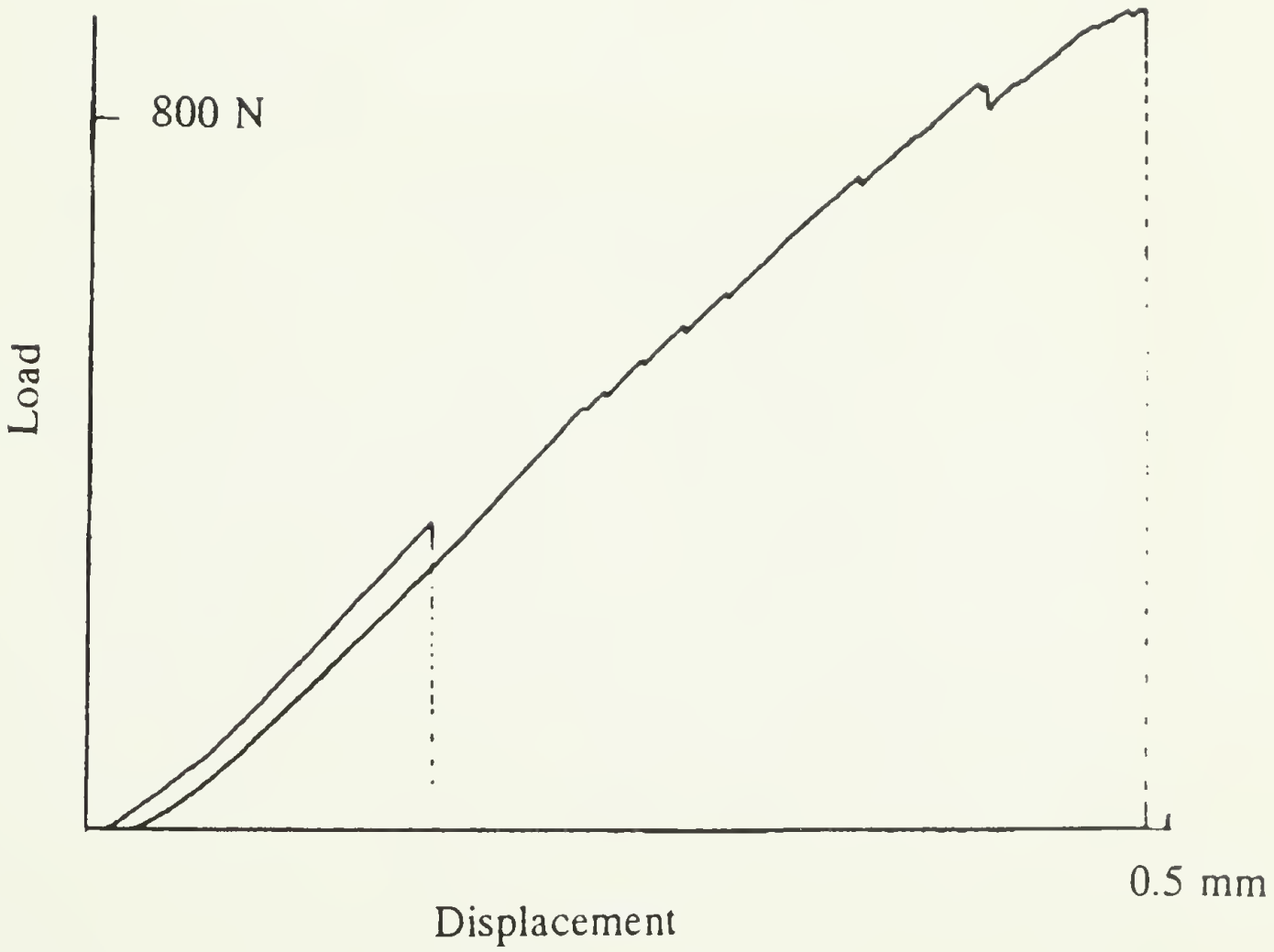

Figure 4.1 Load/Displacement plot of the SiC/RBSN composite and comparative monolithic RBSN showing increased strength and work of fracture of the composite. Both samples were of the same size.

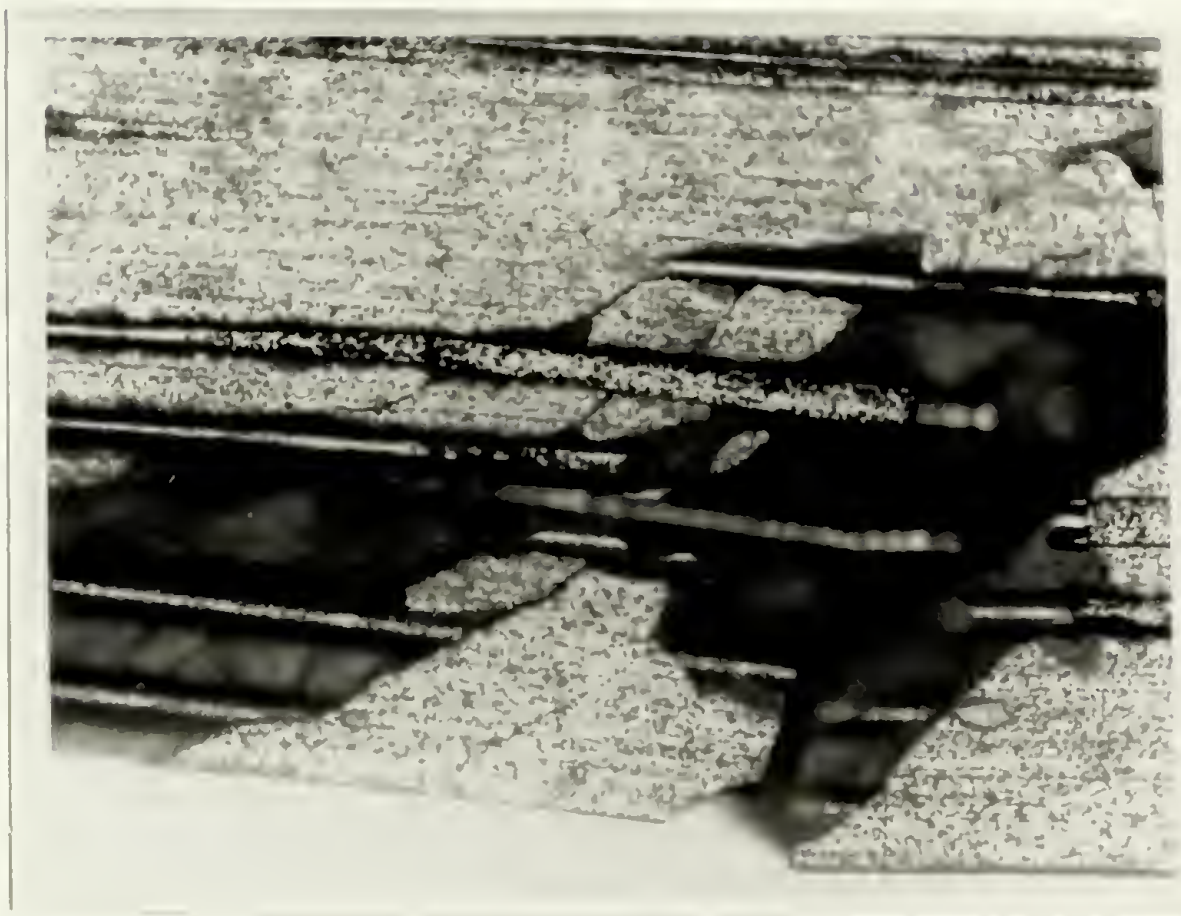

Figure 4.2 Surface normal to the tensile surface of MOR specimen tested at ambient temperature showing multiple crack formation and crack branching.

(A)

(B)

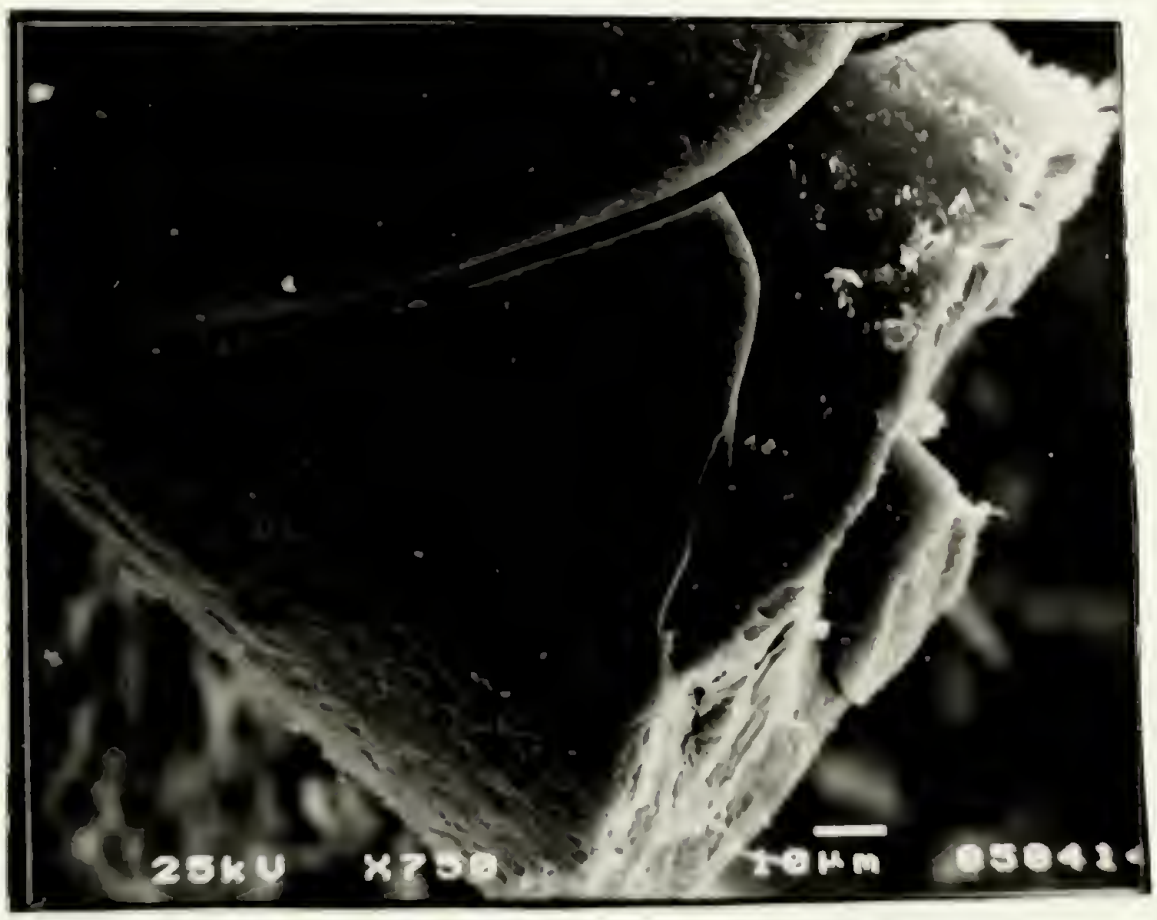

Figure 4.3 Scanning electron micrographs of SiC/RBSN fractured at ambient temperature showing (A) large amount of fiber pullout and (B) enlarged view showing that both coating layers remained on the fiber surface after pullout.

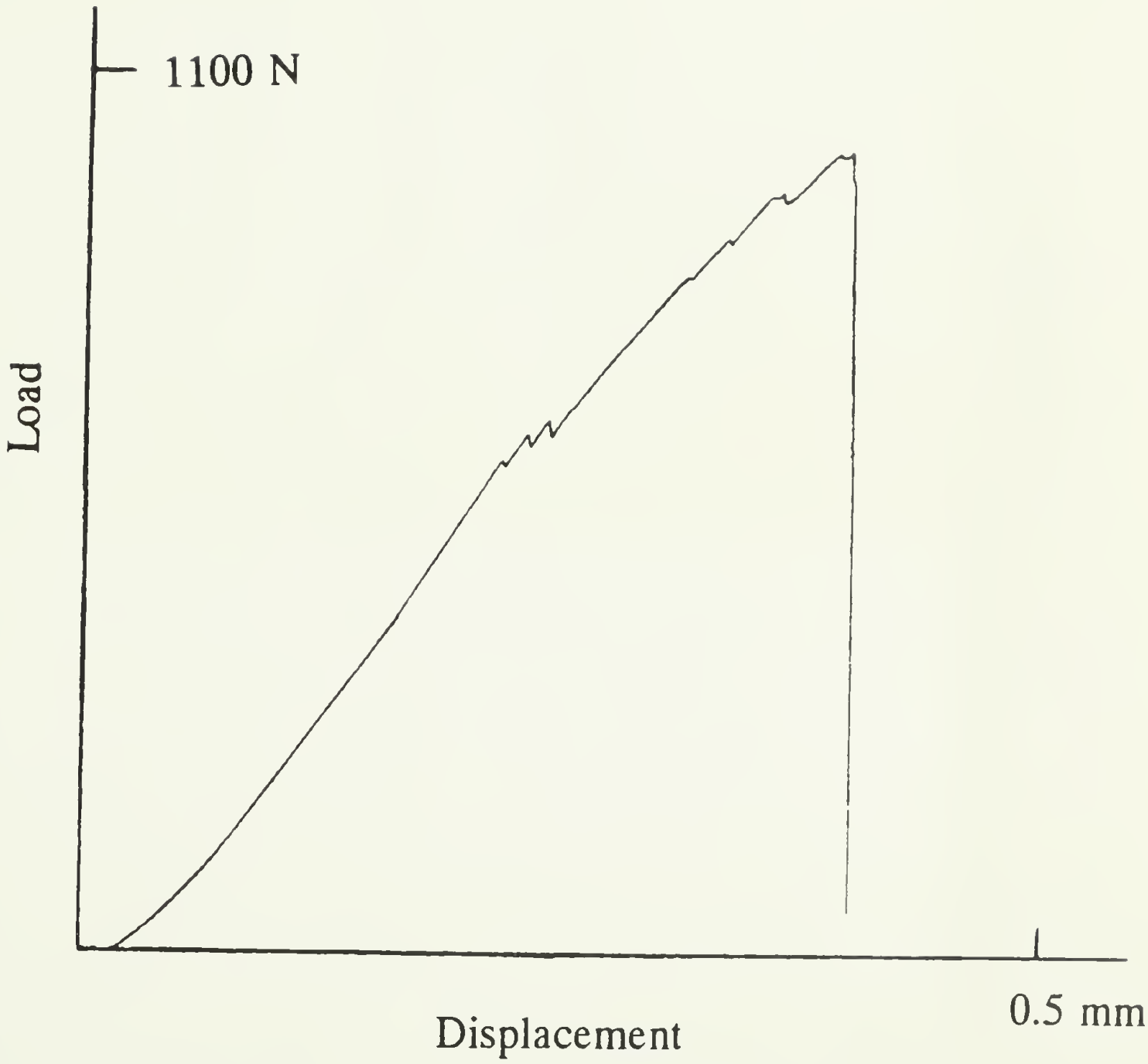

Figure 4.4 Load/displacement plot of SiC/RBSN at ambient temperature in alternate orientation. Specimen cross section is different than for the other orientation therefore results can not be directly compared.

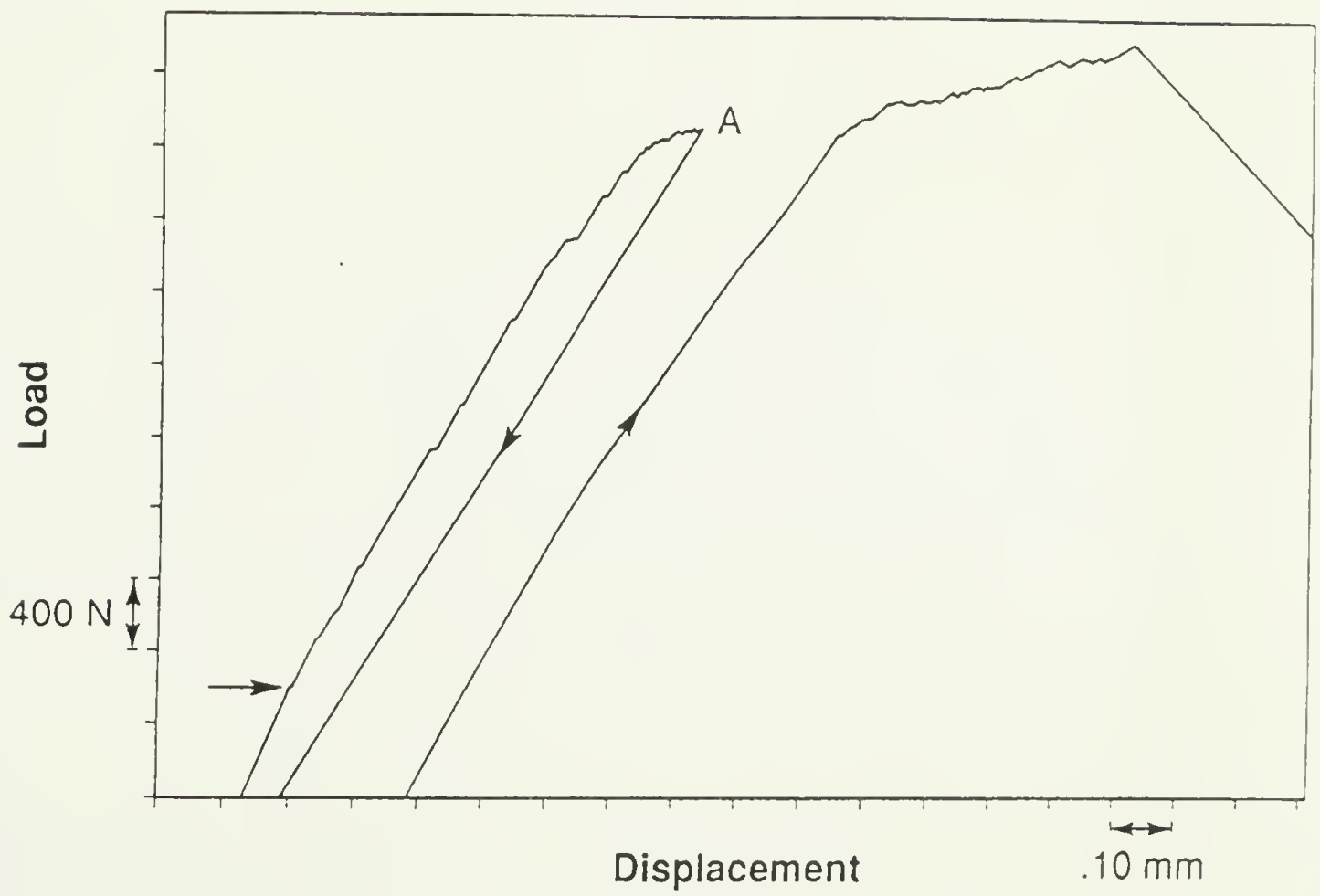

Figure 4.5 Typical load-displacement curve obtained during ambient temperature tensile test for the case of a notched specimen. The specimen was unloaded at point A and the second curve is for the subsequent reloading.

Figure 4.6 Micrograph showing fiber/matrix delamination of a notched specimen.

(A)

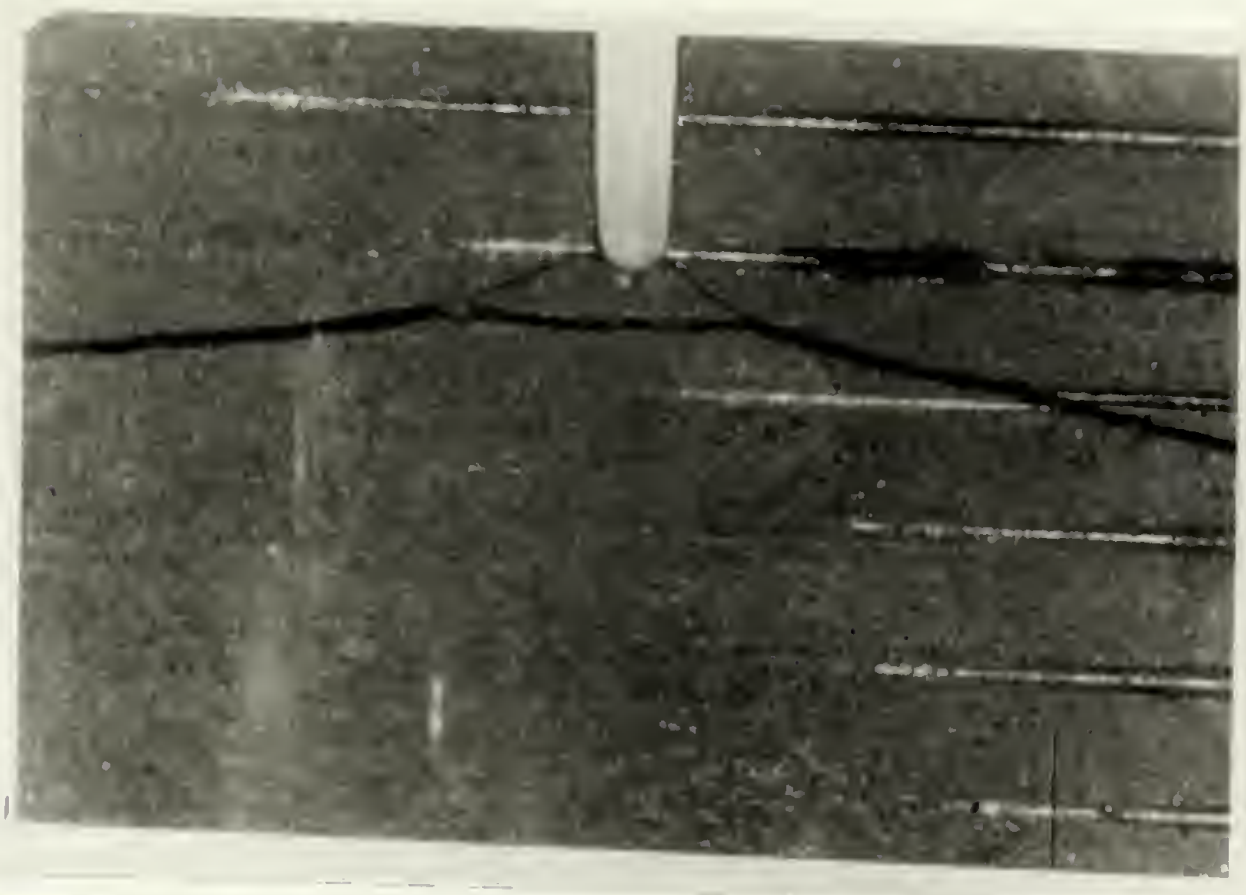

(B)

Figure 4.7 Micrographs showing both sides, (A) and (B), of a notched SiC/RBSN specimen (14b-3) tested in bend at room temperature. The mode II crack is visibly connected to the notch on one side but not the other.

Table 4.1 Bend strength data 25° - 1400° C for experimental SiC/RBSN.

specimen #	test temperature, °C	first matrix cracking stress, MPa	failure stress, MPa
14b-6	25	362	720
10a-3	25	347	573, alternate orient.
9b	1000	237	720
9d	1000	195	377
13c-7	1000	-	378
13a-4	1000	312	400
13c-6	1200	-	338
13c-6	1200	-	312
10a-?	1200	-	521
13c-10	1200	-	288
13c-9	1300	-	255
11c-8	1350	165	214
10a-9	1400	-	217
11c-16	1400	175	208
13c-3	1400	117	376

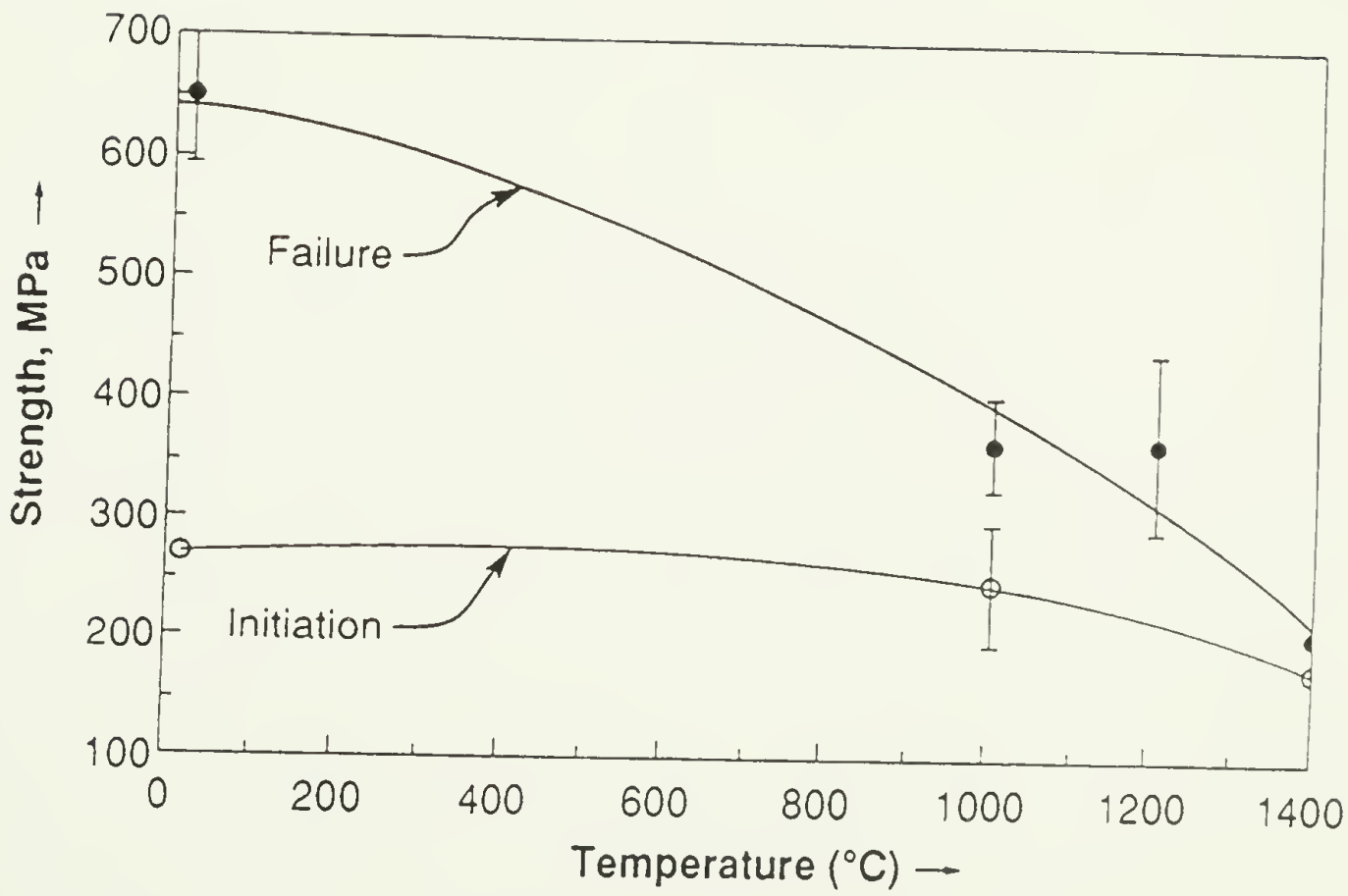

Figure 4.8 Variation of first matrix cracking stress and ultimate strength versus temperature.

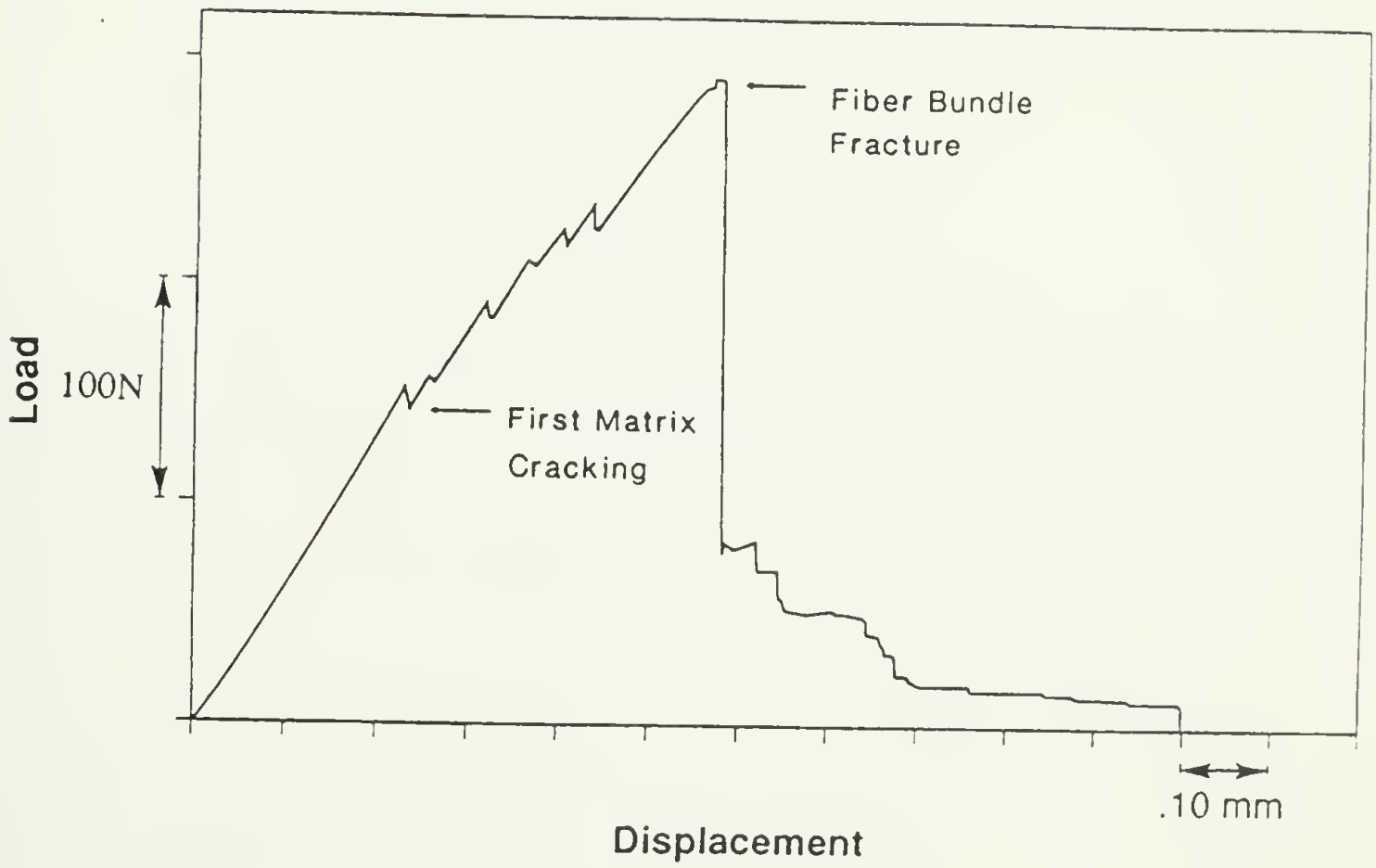

Figure 4.9 Load/displacement record of MOR test at 1000° C indicating the first matrix cracking load and the area of fiber bundle fracture.

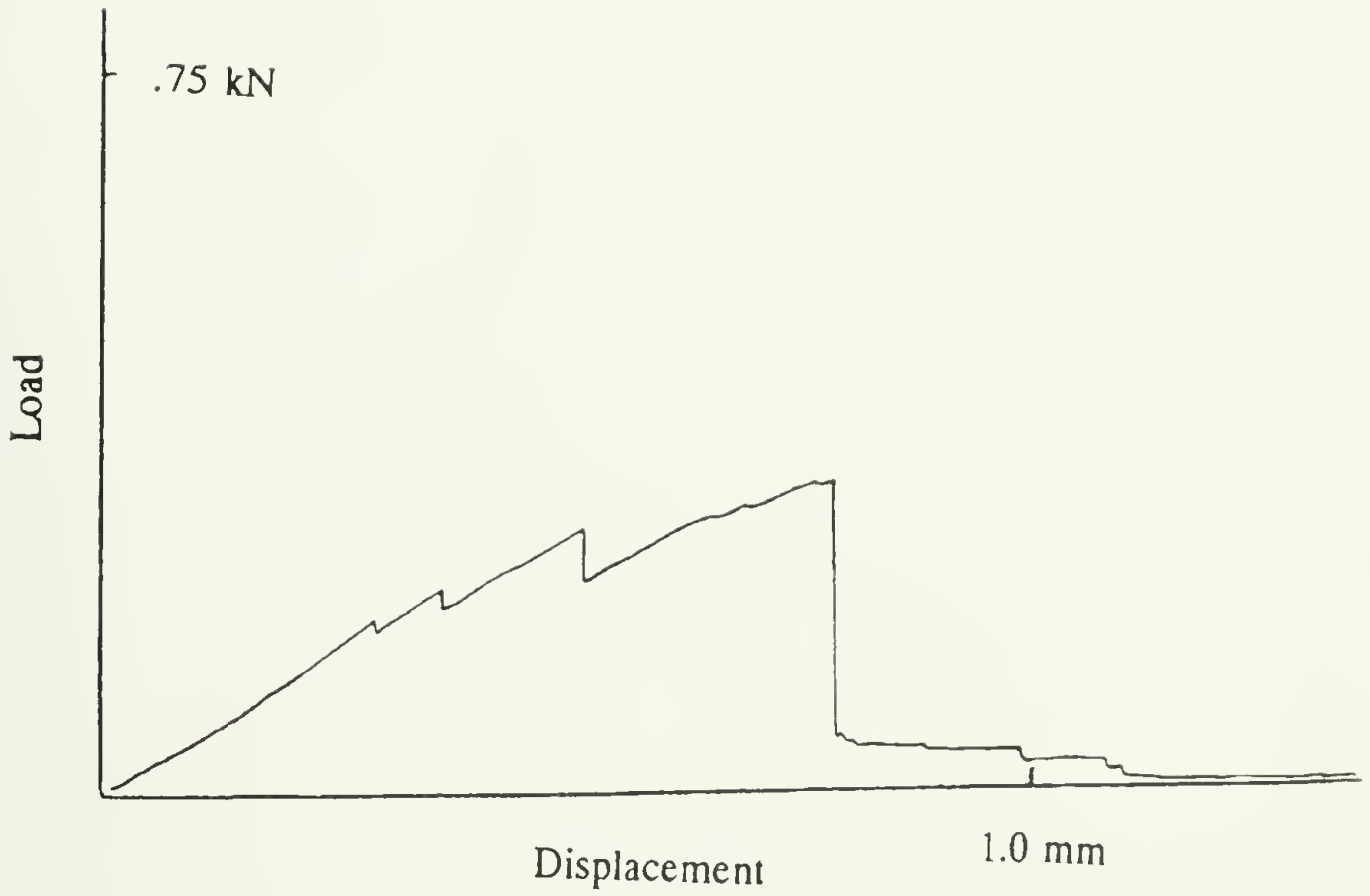

Figure 4.10 Load/displacement record of MOR test at 1000° C, sample 9c.

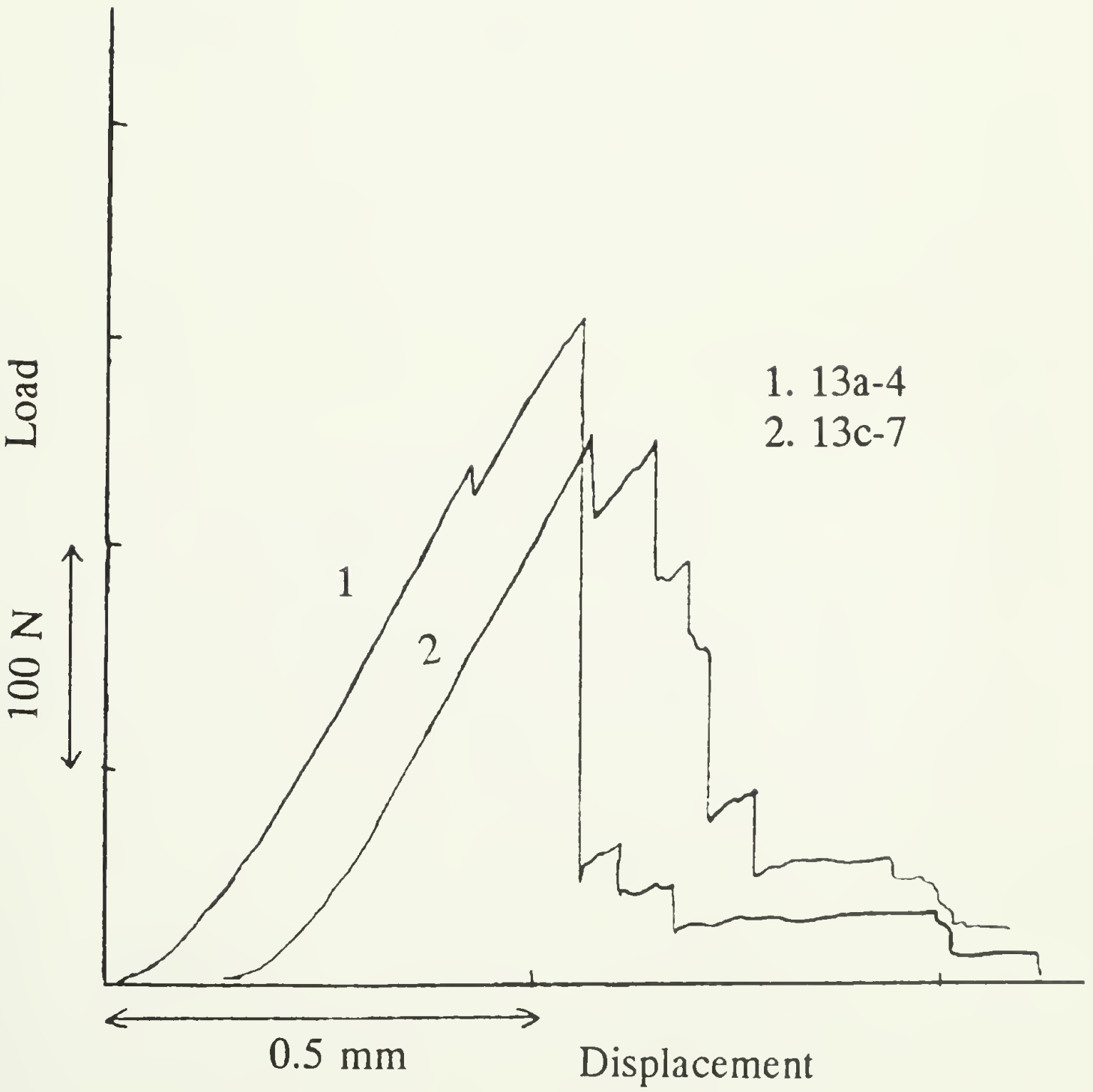

Figure 4.11 Load/displacement record of MOR test at 1000° C, two additional samples.

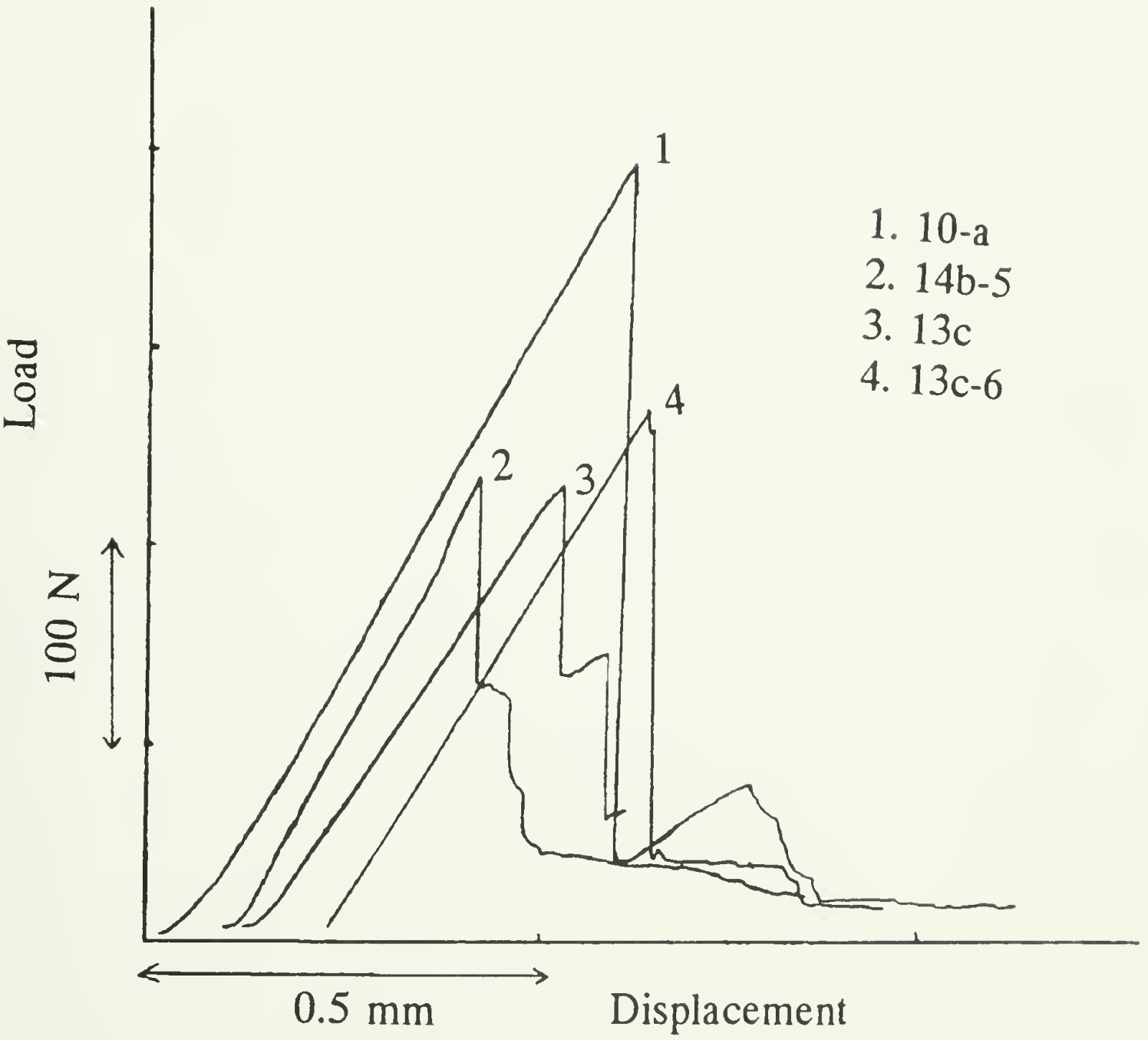

Figure 4.12 Load/displacement records of MOR tests at 1200° C. Note the absence of a first matrix cracking stress in all samples at this temperature.

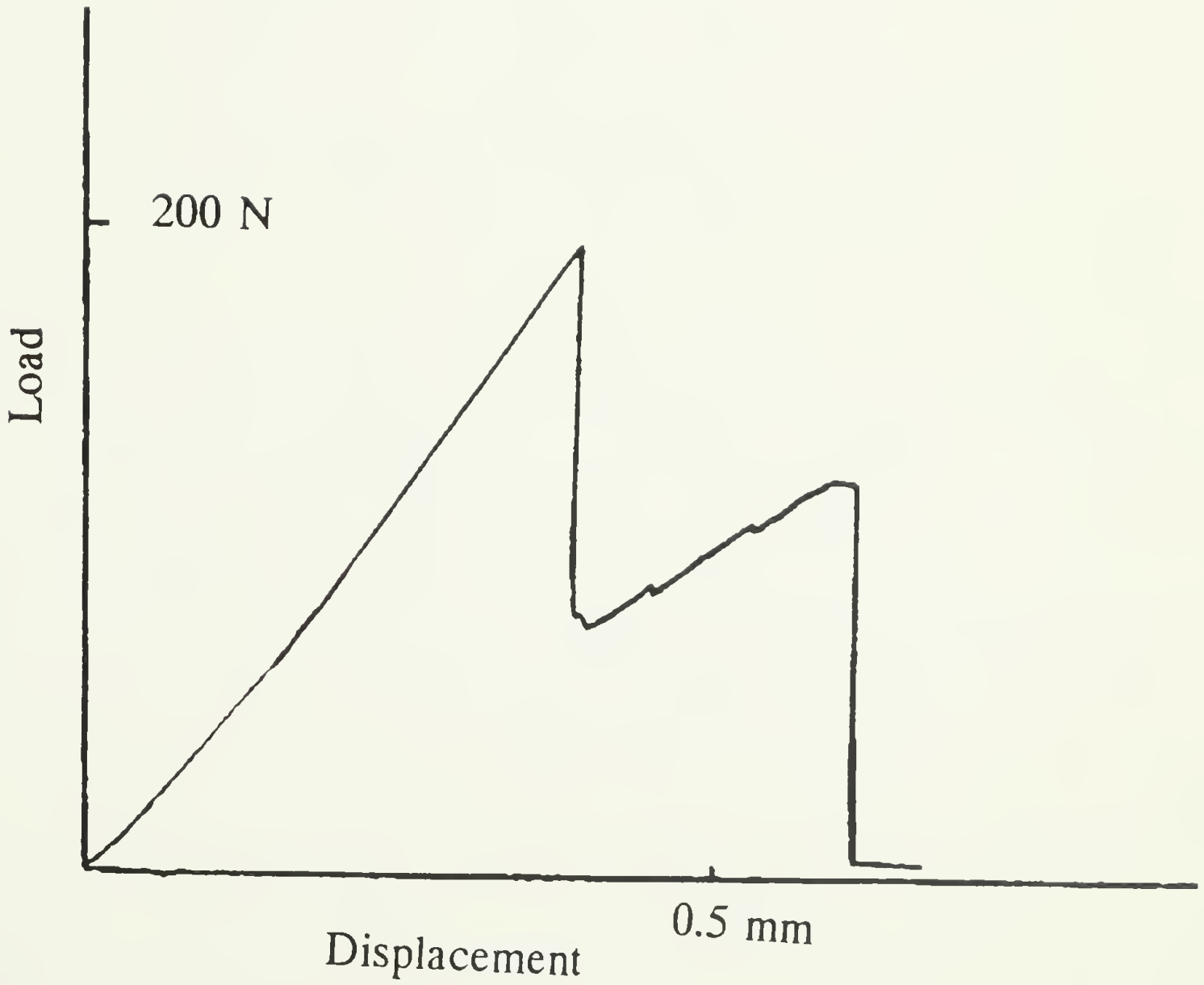

Figure 4.13 Load/displacement record of MOR test at 1300° C, sample 13c-9.

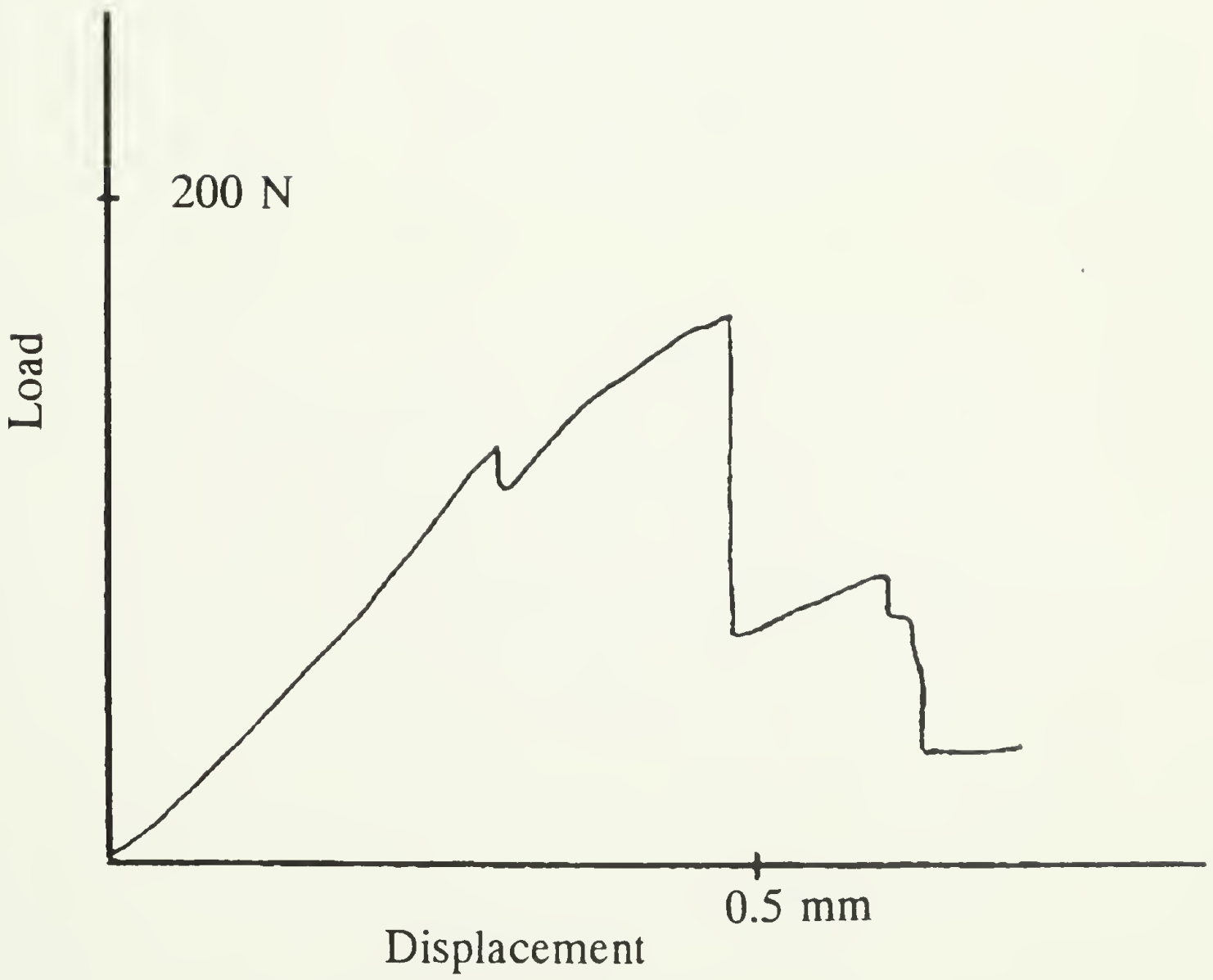

Figure 4.14 Load/displacement record of MOR test at 1350° C, sample 11c-8.

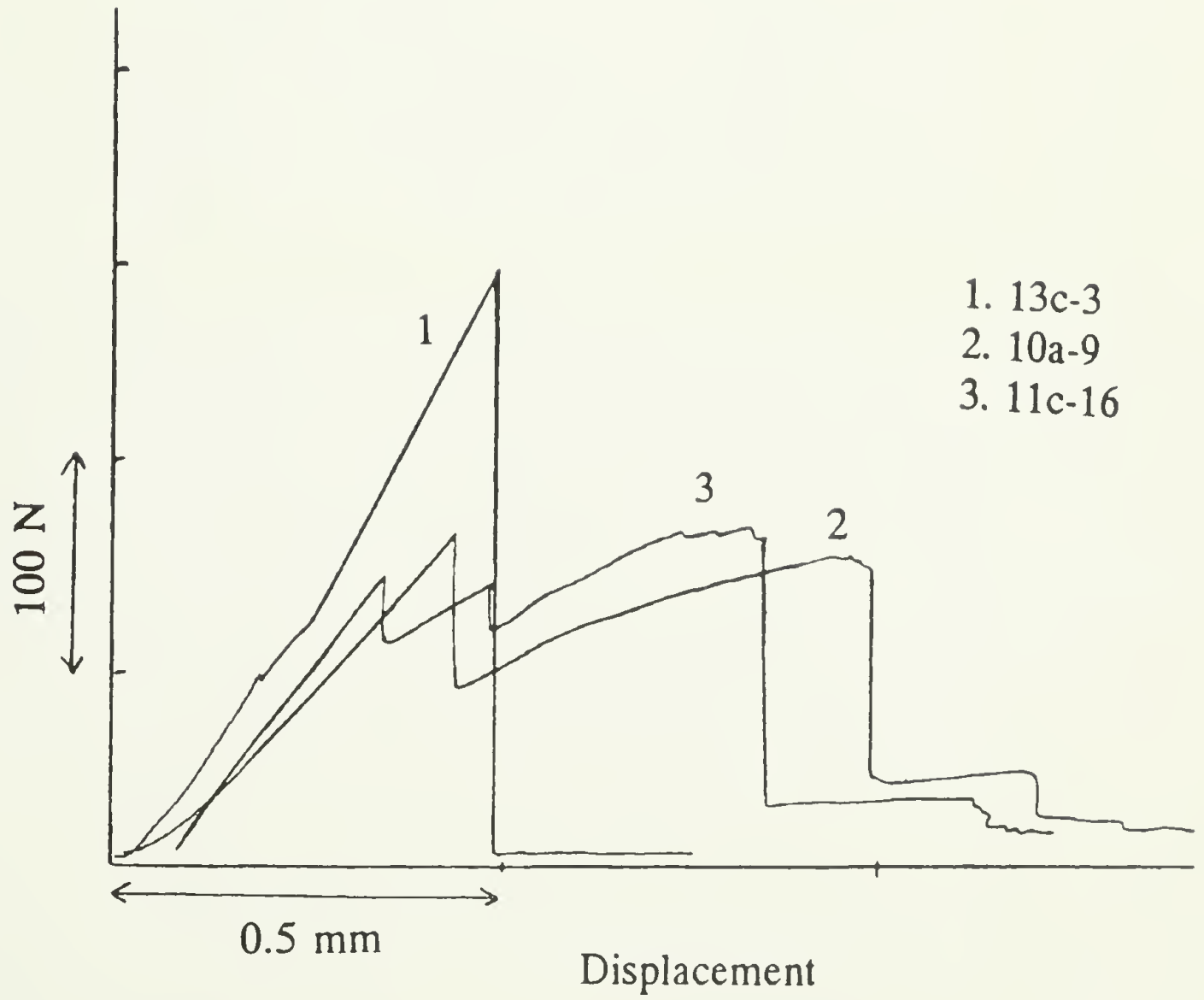

Figure 4.15 Load/displacement record of MOR tests at 1400° C.

(A)

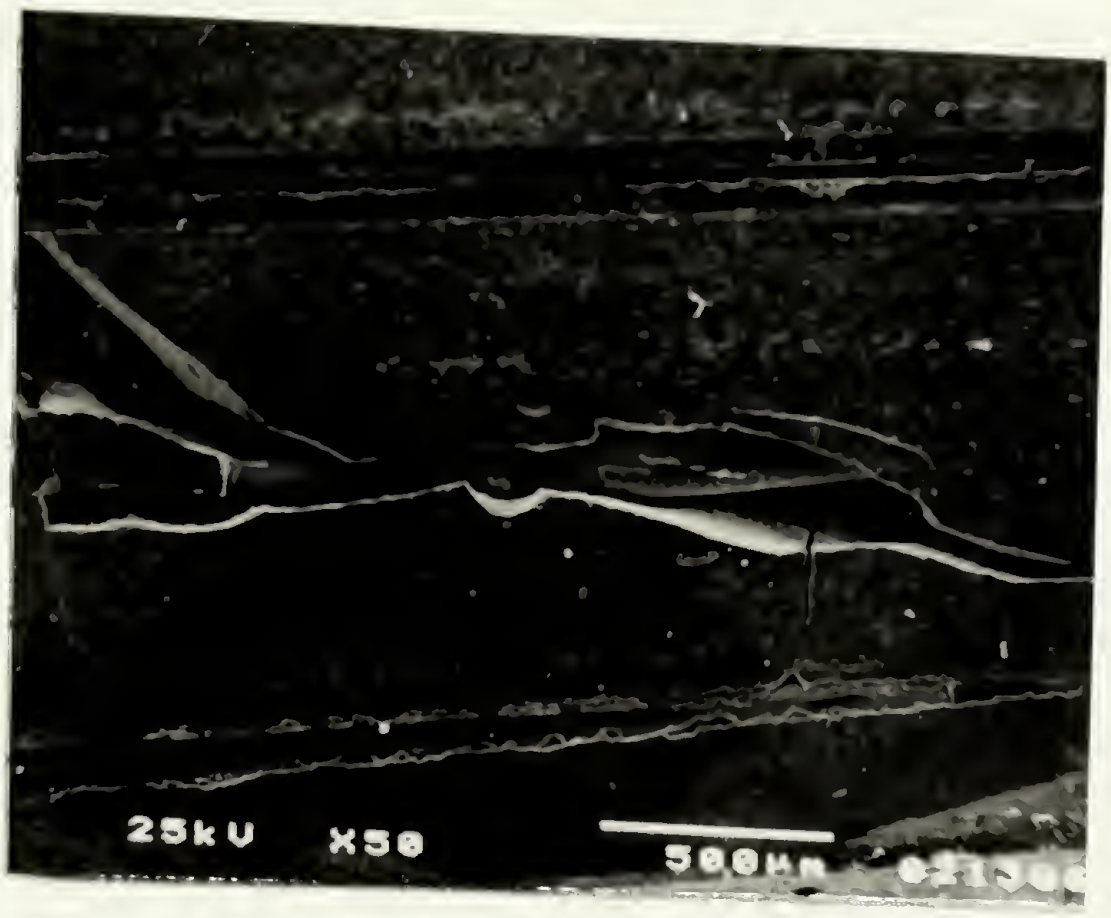

(B)

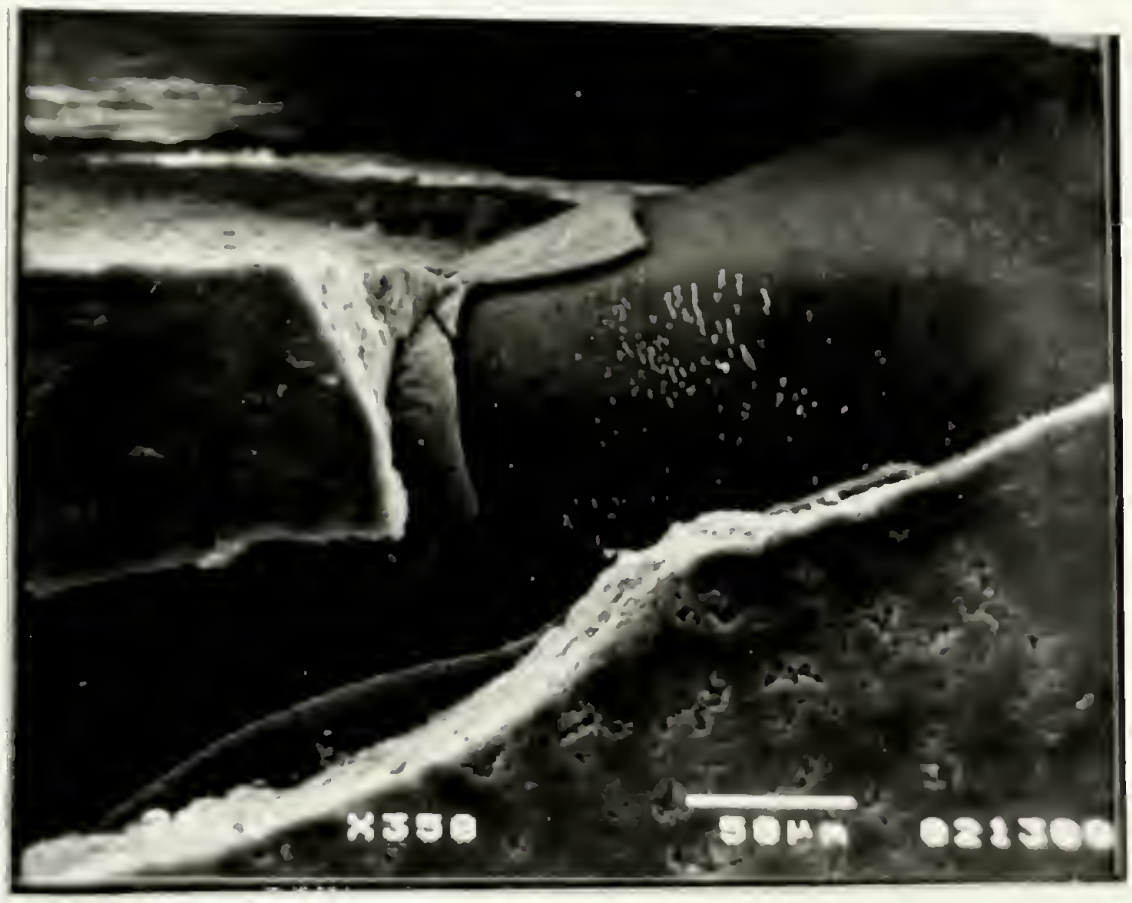

Figure 4.16 Scanning electron micrographs of SiC/RBSN fractured at 1000° C MOR test showing (A) fiber pullout at elevated temperature and (B) higher-magnification view showing that the coating layers are left behind in the matrix during fiber pullout.

(A)

(B)

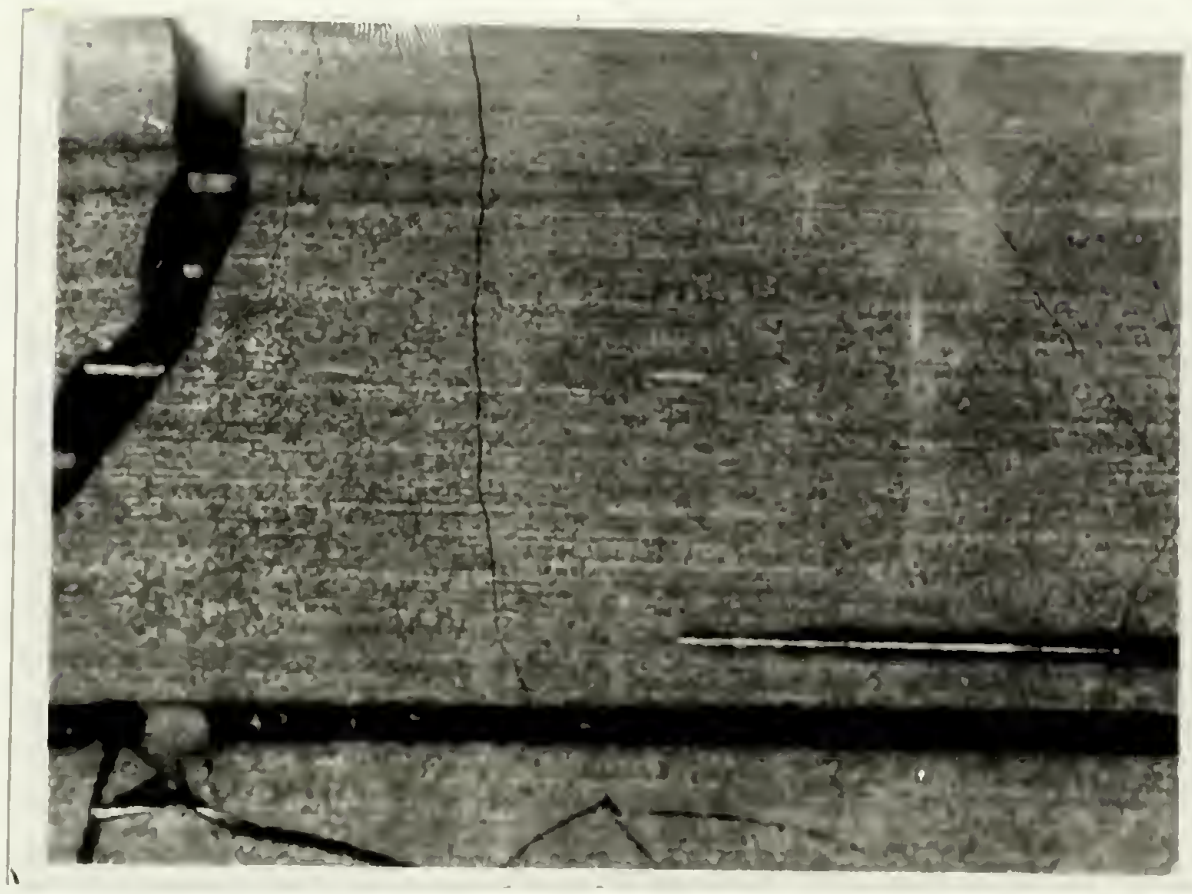

Figure 4.17 Photographs (35x) showing the tensile surface (A) and edge view (B) of a specimen (10a) tested in flexure at 1200° C. Note the multiple matrix cracking. This was not observed at lower temperatures.

Table 4.2 Interlaminar shear results at temperature.

Sample #	temperature	1st event	2nd event	failure stress
13c-2	25 °C	-	-	85 MPa
13c-11/I1	25	-	-	85
13c-11/I2	1000	17	31	63
13c-11/I3	1200	16	16/19	52
13c-11/I4	1400	16	21	36

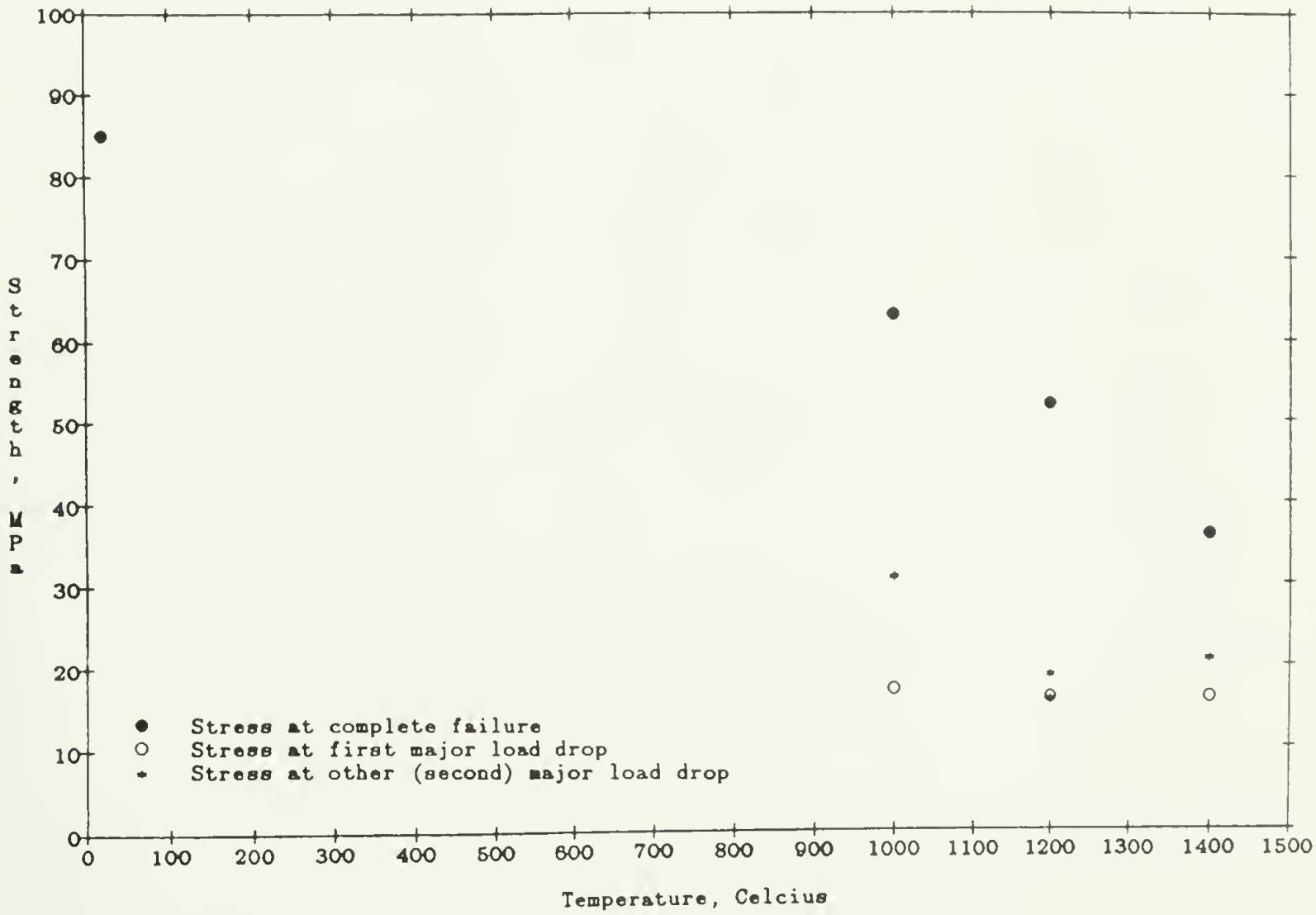

Figure 4.18 Interlaminar shear strength plotted against temperature for composite specimens made from sample 13c-11. All failure events are noted. While the ultimate stress at failure decreases with temperature, pre-failure events occur at approximately the same stress for all samples tested at elevated temperatures.

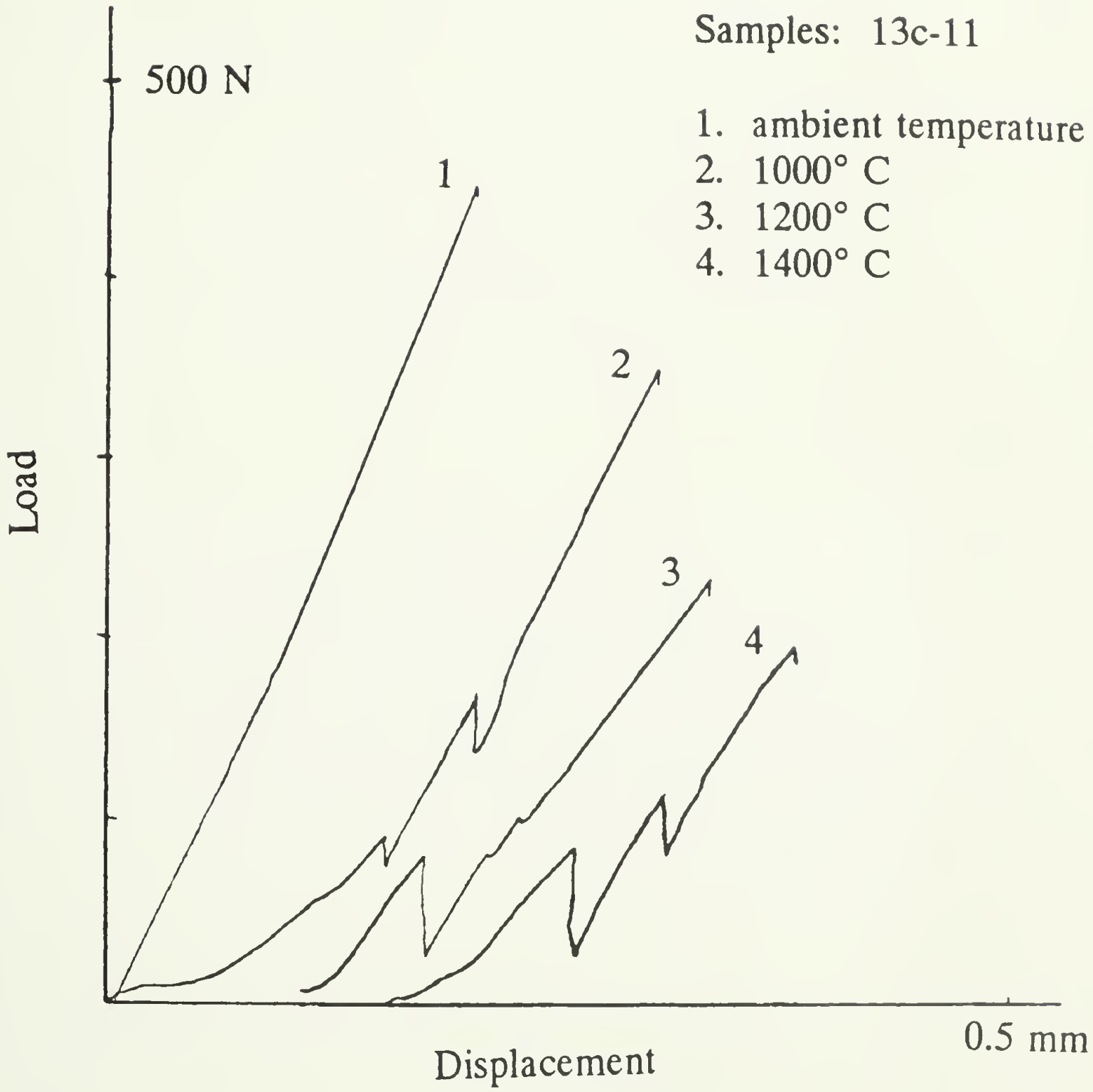

Figure 4.19 The load/displacement curves for the interlaminar shear tests done at temperature.

Table 4.3 Interlaminar shear results - pre-exposed.

Sample Number	PreExposure	Stress at Failure/MPa
10a-5/I1	none	42
10a-5/I2	1 hour @ 1000	39
10a-5/I3	1 hour @ 1200	38
10a-5/I4	1 hour @ 1400	43

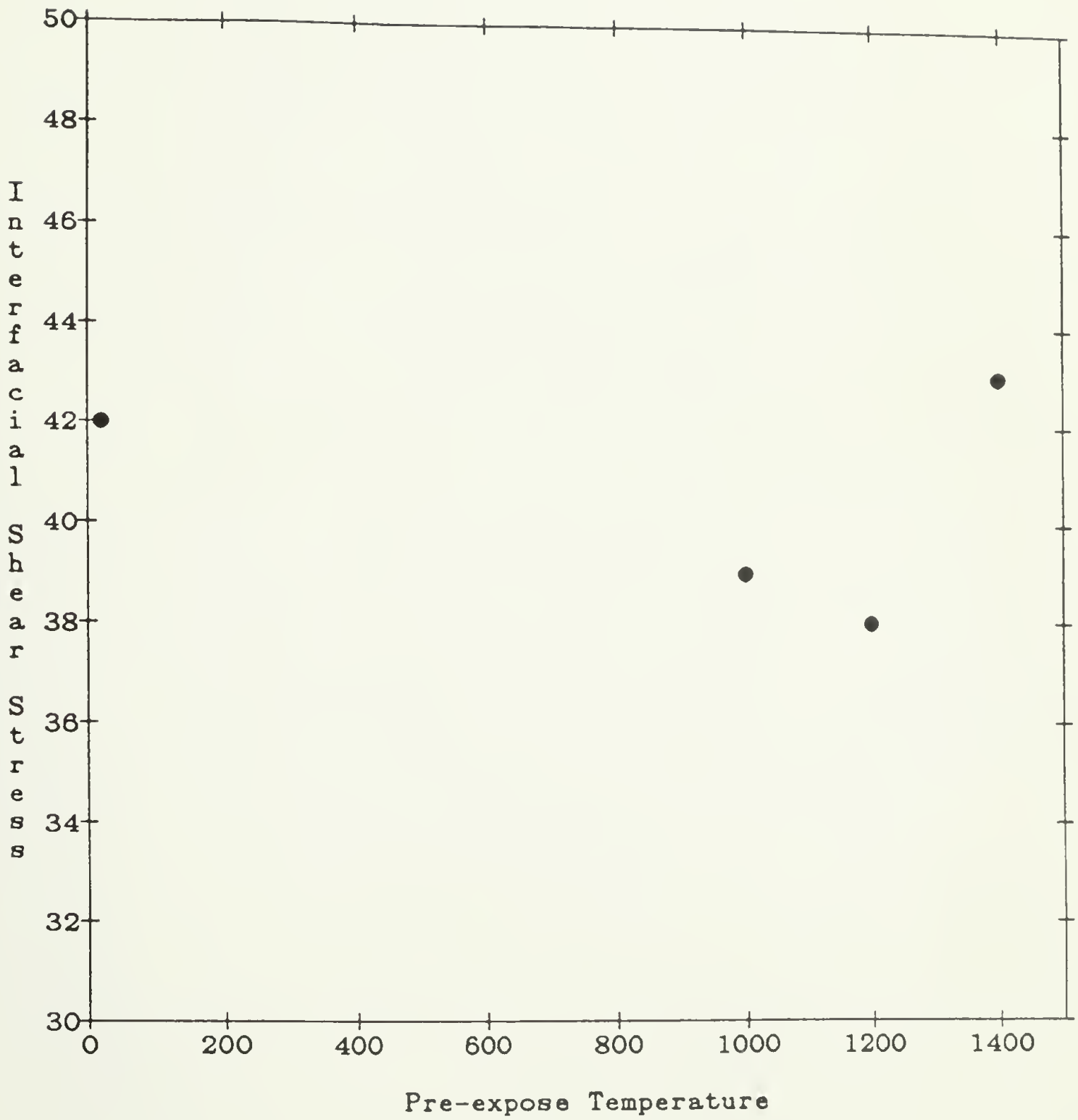

Figure 4.20 Interlaminar shear strength plotted against pre-exposure temperature.

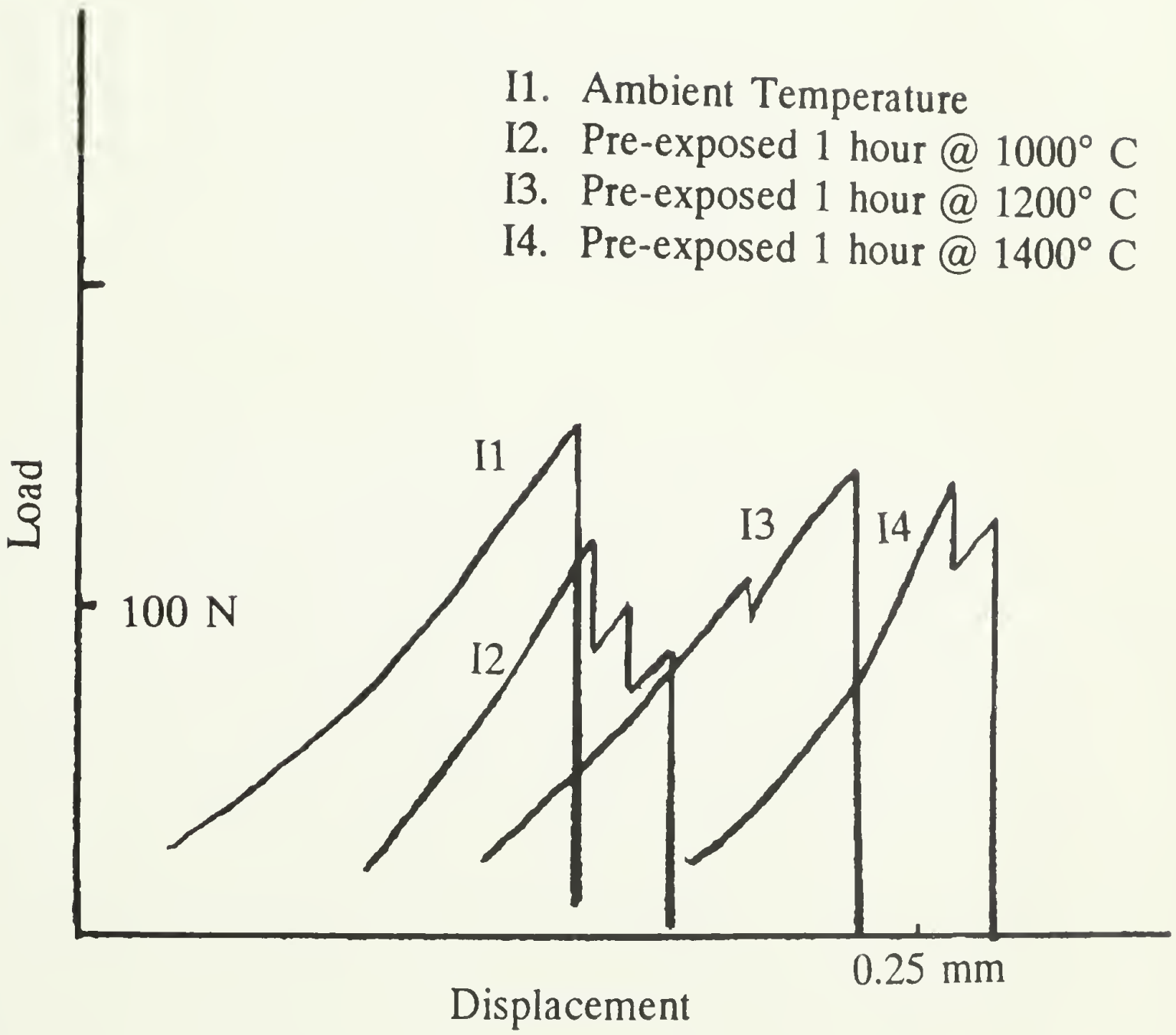

Figure 4.21 The load/displacement curves for the interlaminar shear tests after high temperature pre-exposure.

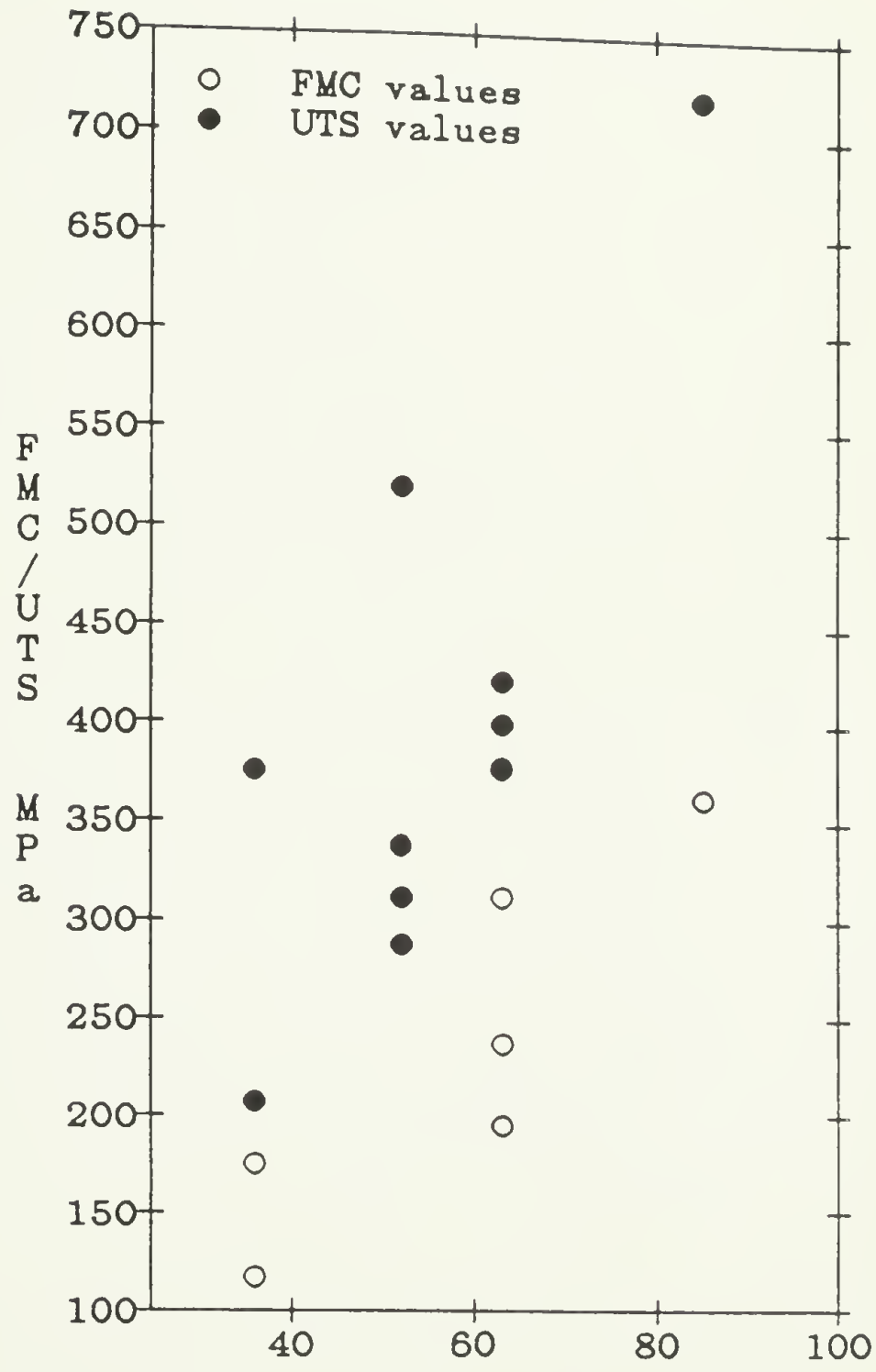

Figure 4.22 The first matrix cracking (FMC) and ultimate failure strengths (UTS) are plotted against their corresponding interlaminar shear strength results according to test temperature.

Table 4.4 Results of SENB tests at elevated temperature.

Temperature	Sample #	a/w	K_i
1000° C	10a-6	.26	2.8
	14b-4		3.6
1200° C	14b-7	.26	2.3
	13a-5		3.2
1300° C	10a-1	.23	3.5
	11c-11		3.0

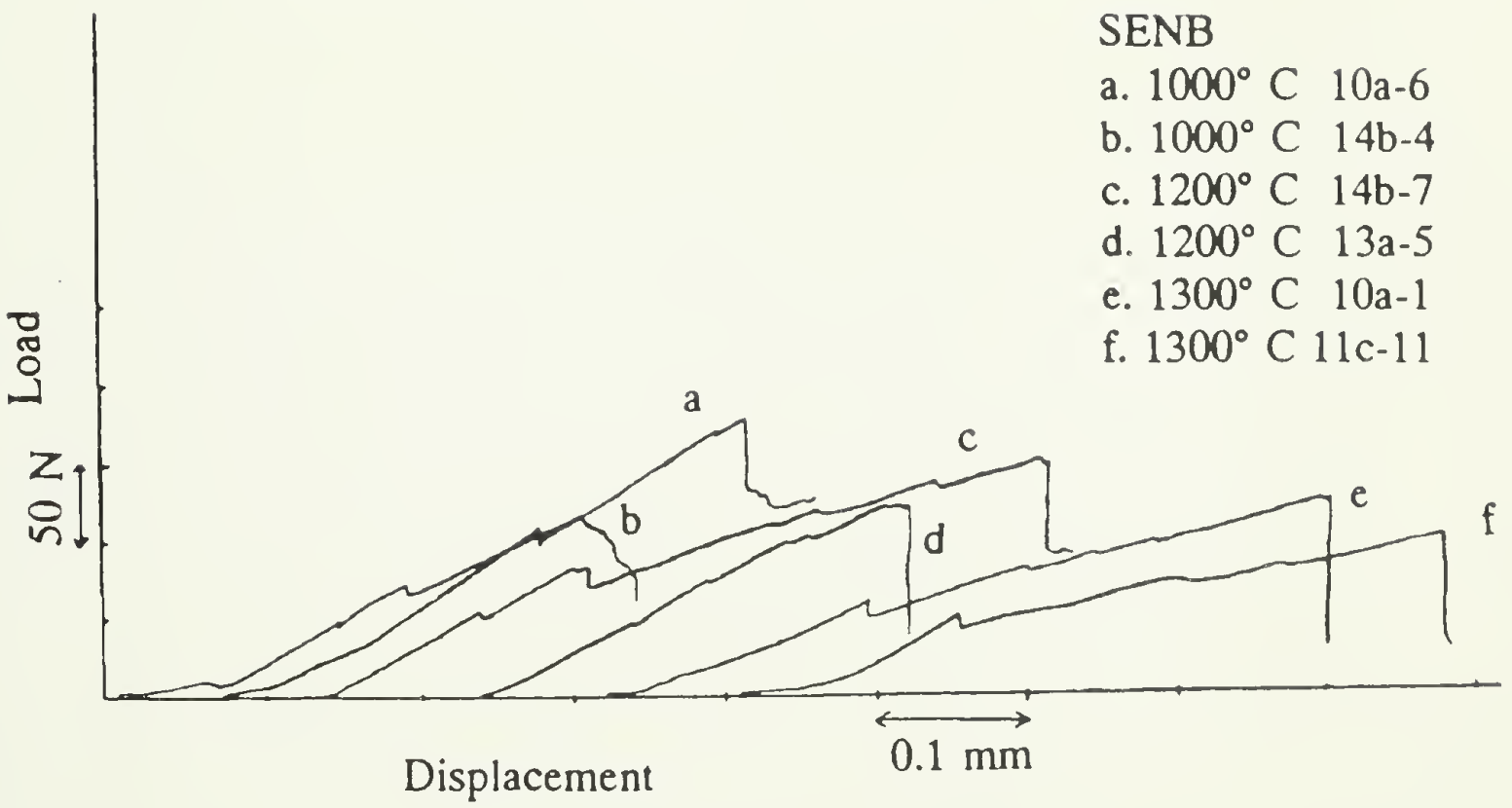

Figure 4.23 Load/displacement curves for single edge notched bend (SENB) tests at various temperatures.

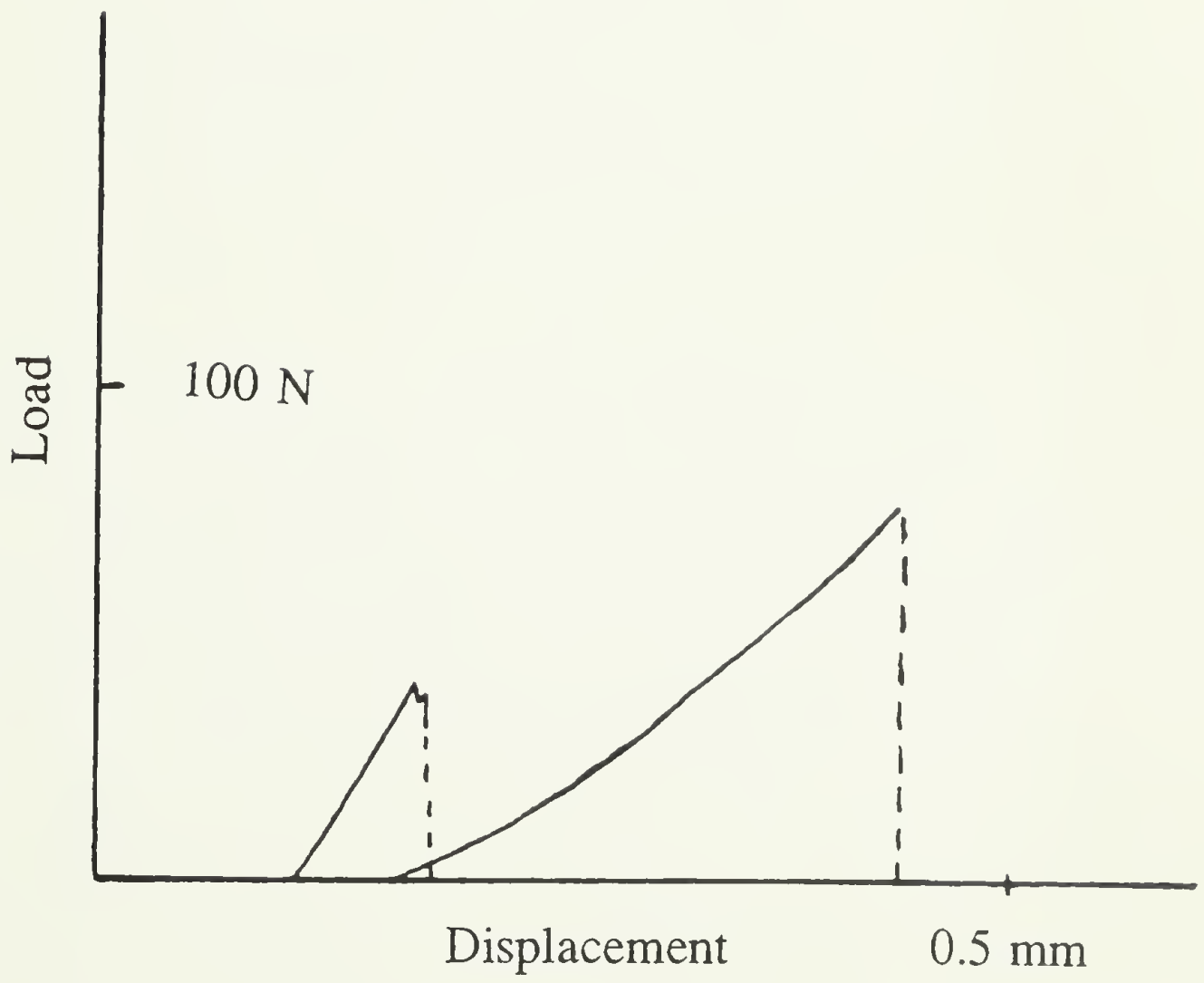

Figure 4.24 Load/displacement curve for 1300° C interrupted SENB test. After the first interruption, a crack extending from the notch was observed. Upon continuation of the test, however, the load sustained by the specimen was increased thus giving an indication of R-curve behavior.

Table 4.5 Times to crack initiation and failure at high temperature for SiC/RBSN specimens tested at one stress only.

Sample	Temperature	Stress	t_i	t_f
9c	1000 °C	100 MPa	127.5 min.	217.5 min.
11a	1000	100	61	206+ no failure
14b-9	1000	150	763+ no initiation	
11c-6	1000	200	120+ no initiation	
13c-1	1200	100	245+ no initiation	
13a-8	1350	125	30	45
13a-3	1350	100	785+ no initiation	
13a-7	1400	100	225.5+ no init.	
11c-4	1400	100	600+ no initiation	
11c-5	1350	125	13.5	stress changed
11c-7	1400	150	6	
13c-5	1400	125	300+ no initiation	

(A)

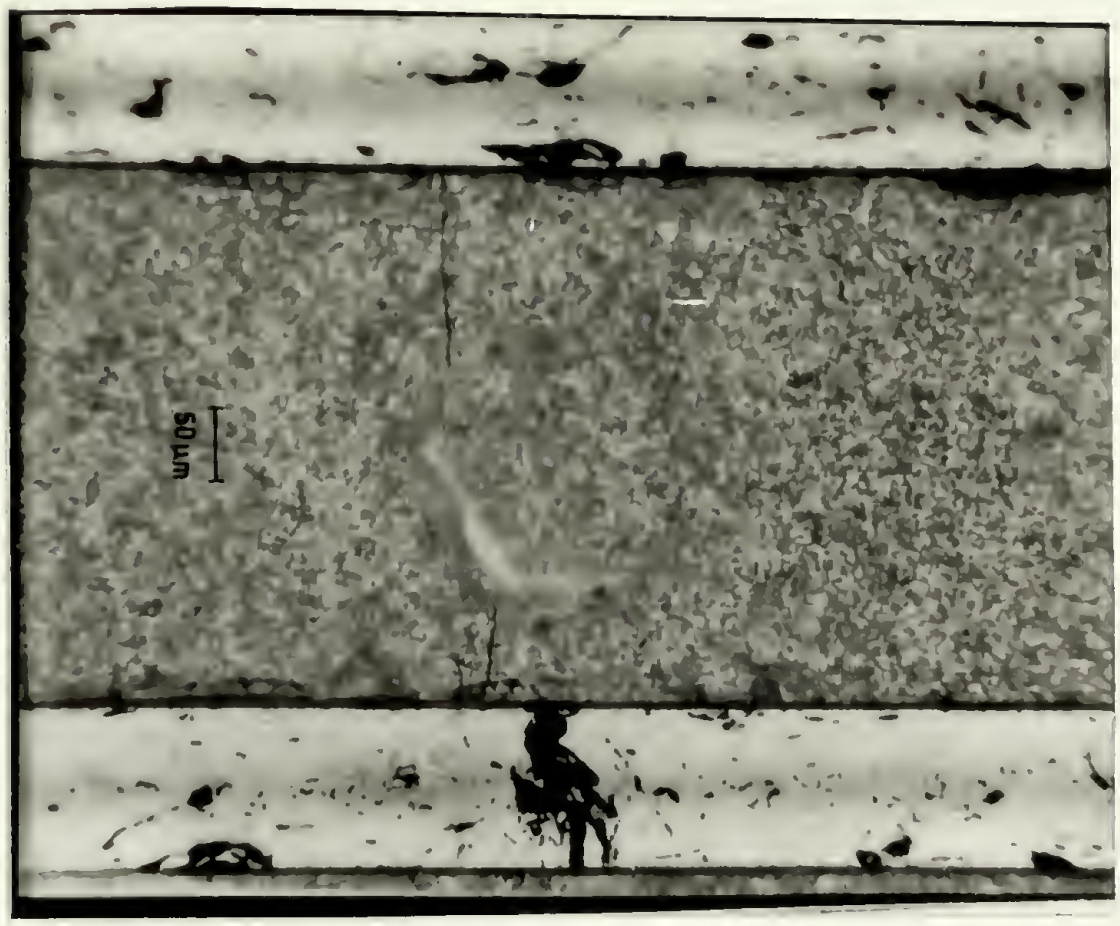

(B)

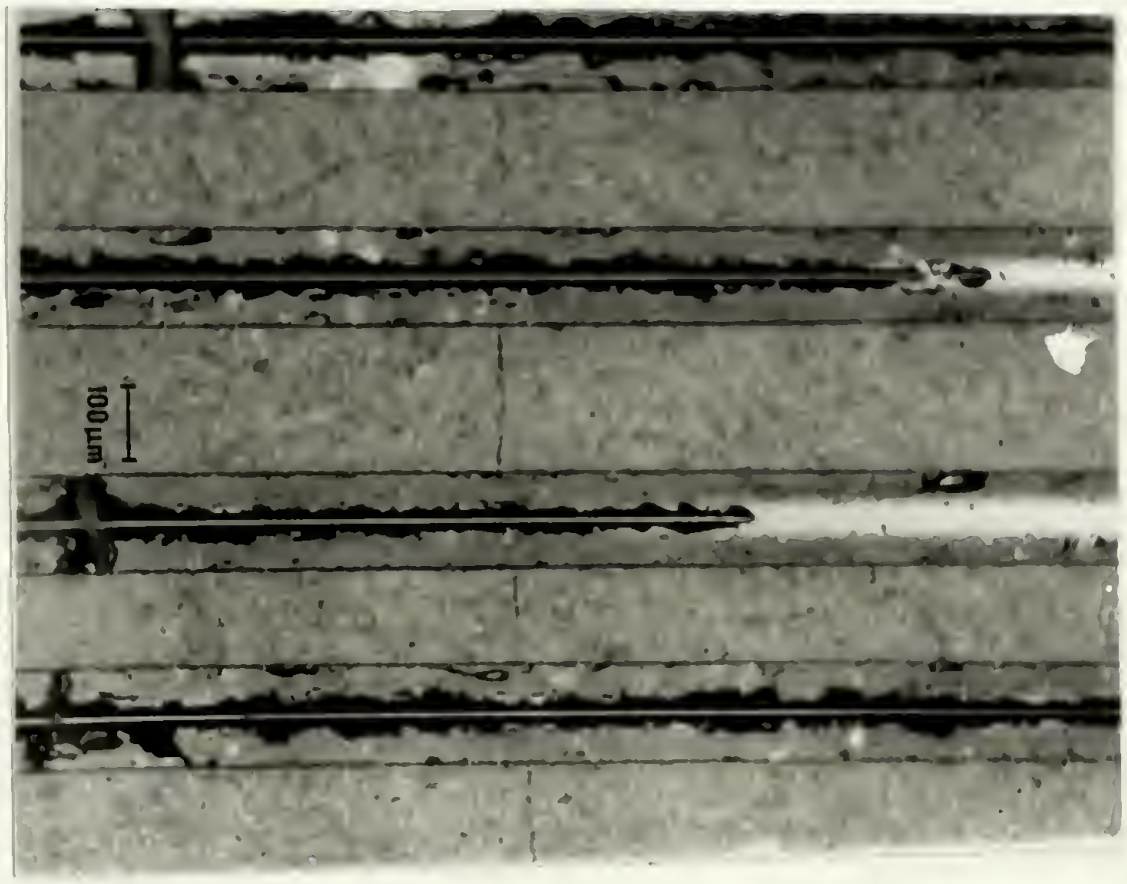

Figure 4.25 Optical micrographs of SiC/RBSN: (A) after 60-min and (B) after 206-minute creep test at 1000° C under 100 MPa stress showing crack initiation.

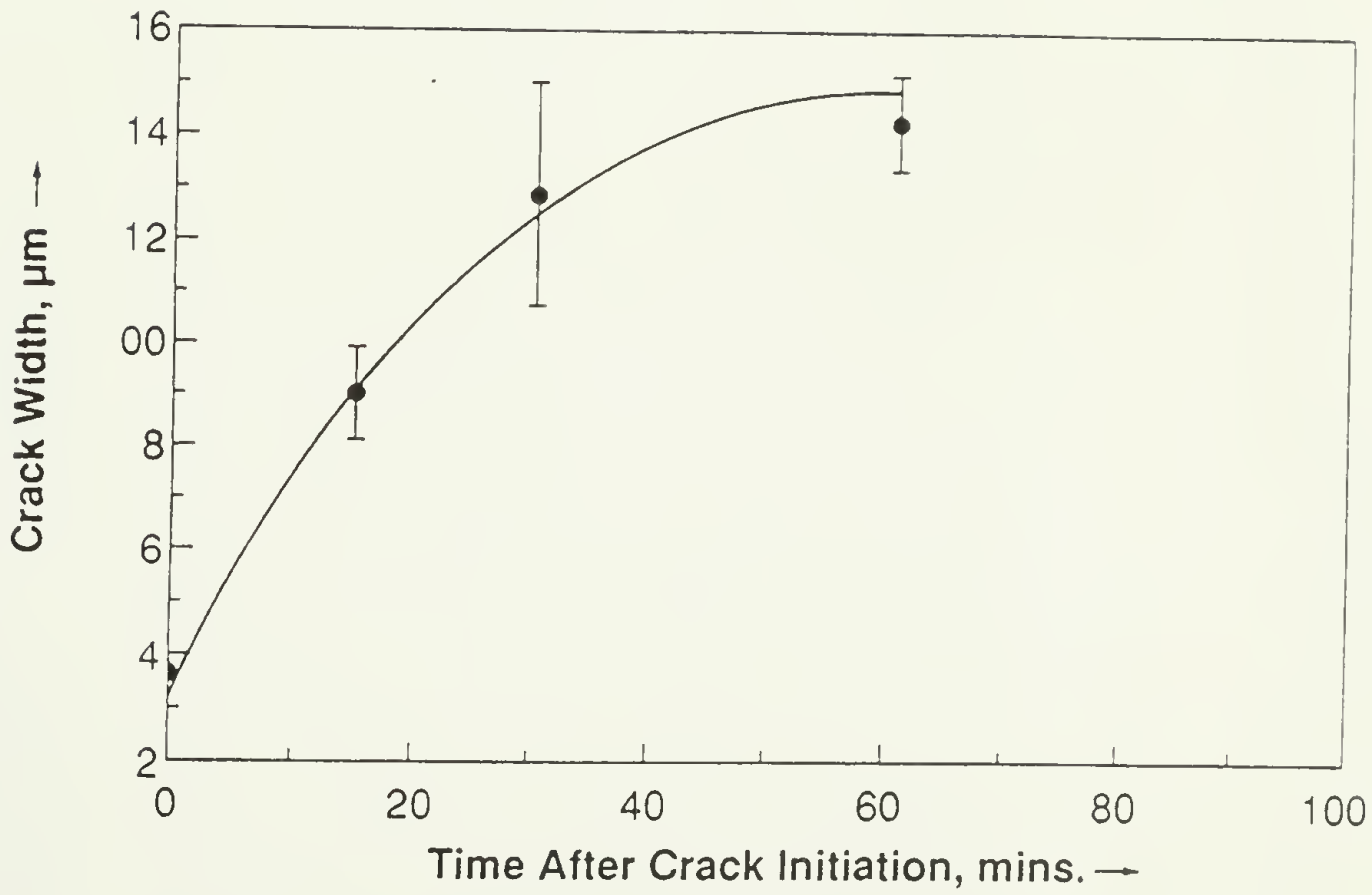

Figure 4.26 Variation of crack opening displacement vs time at 1000° C and applied 100 MPa.

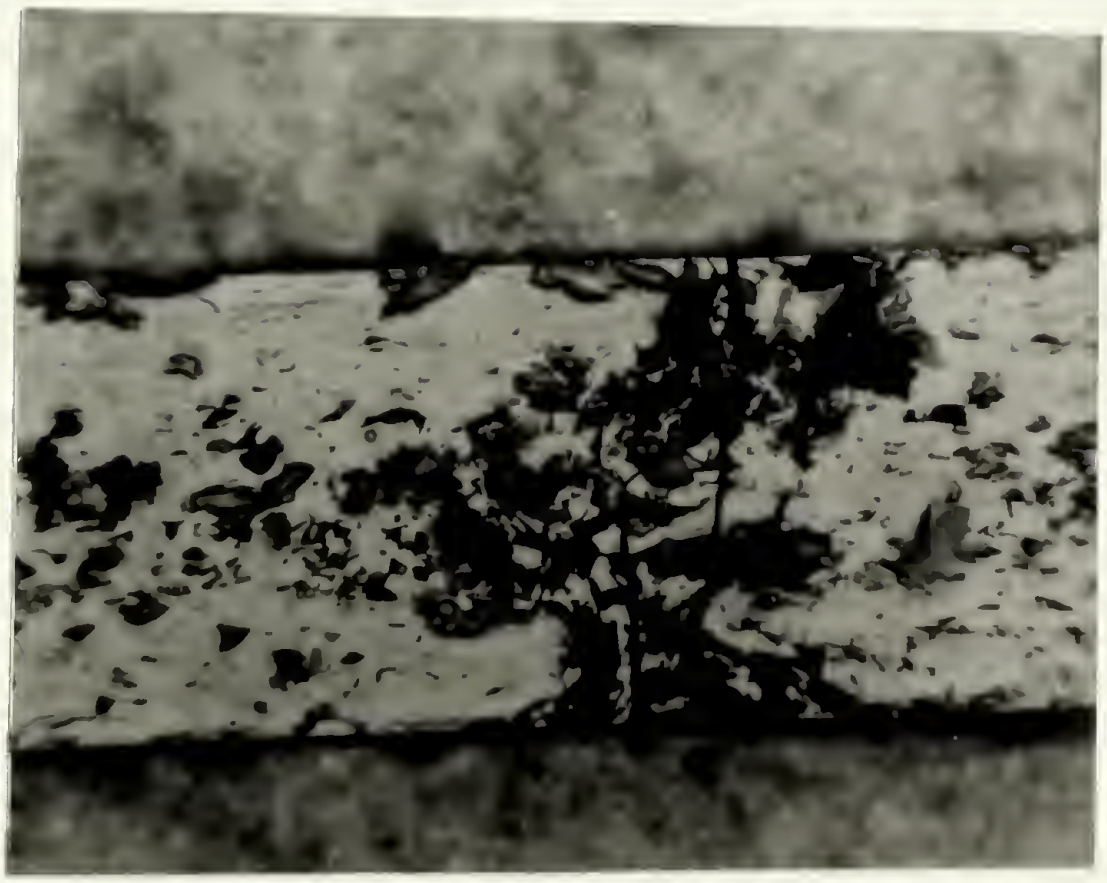

Figure 4.27 Optical micrograph of SiC/RBSN after 50-min creep test at 1200°C under 100 MPa stress showing fiber fracture.

Figure 4.28 Micrograph of specimen (13a-5) crept at 1350° C showing a fiber running through fiber and matrix and taking a path so as to link up areas of fiber damage and defects.

(A)

(B)

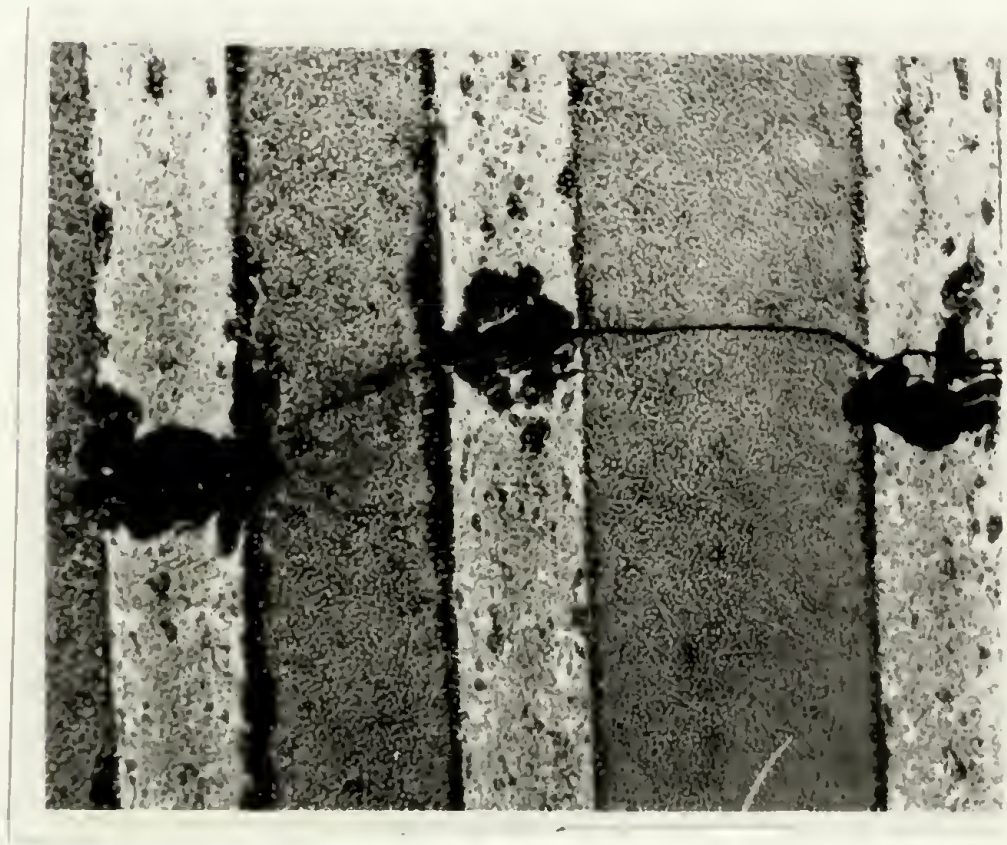

Figure 4.29 Sample 13a-8, (A) close-up of fiber breaking and (B) link-up of cracks.

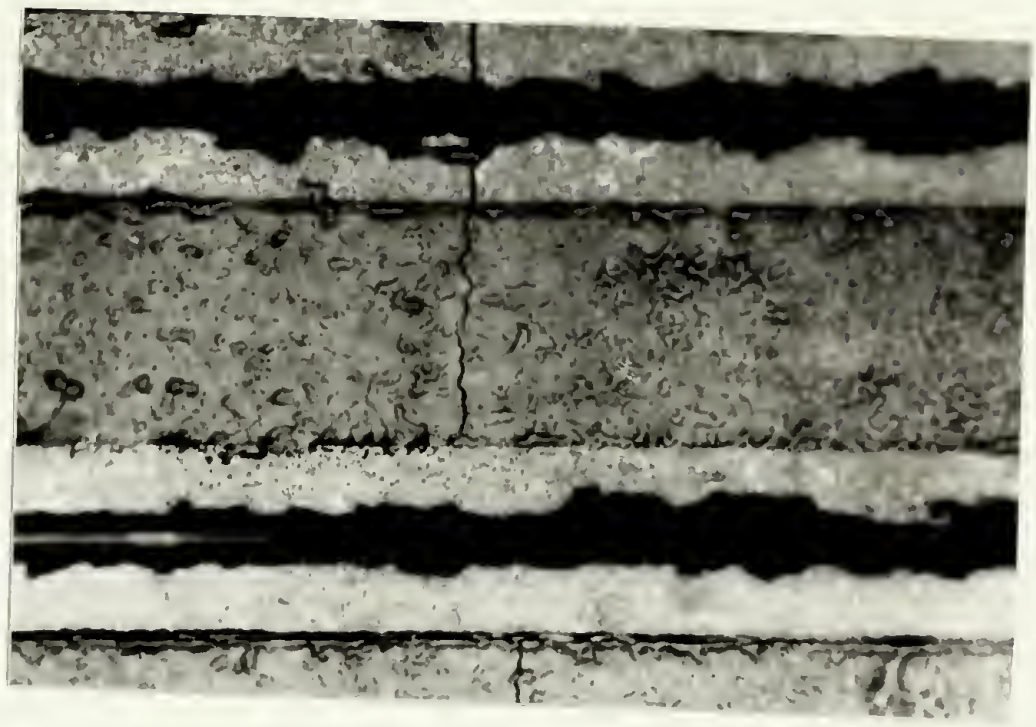

(A)

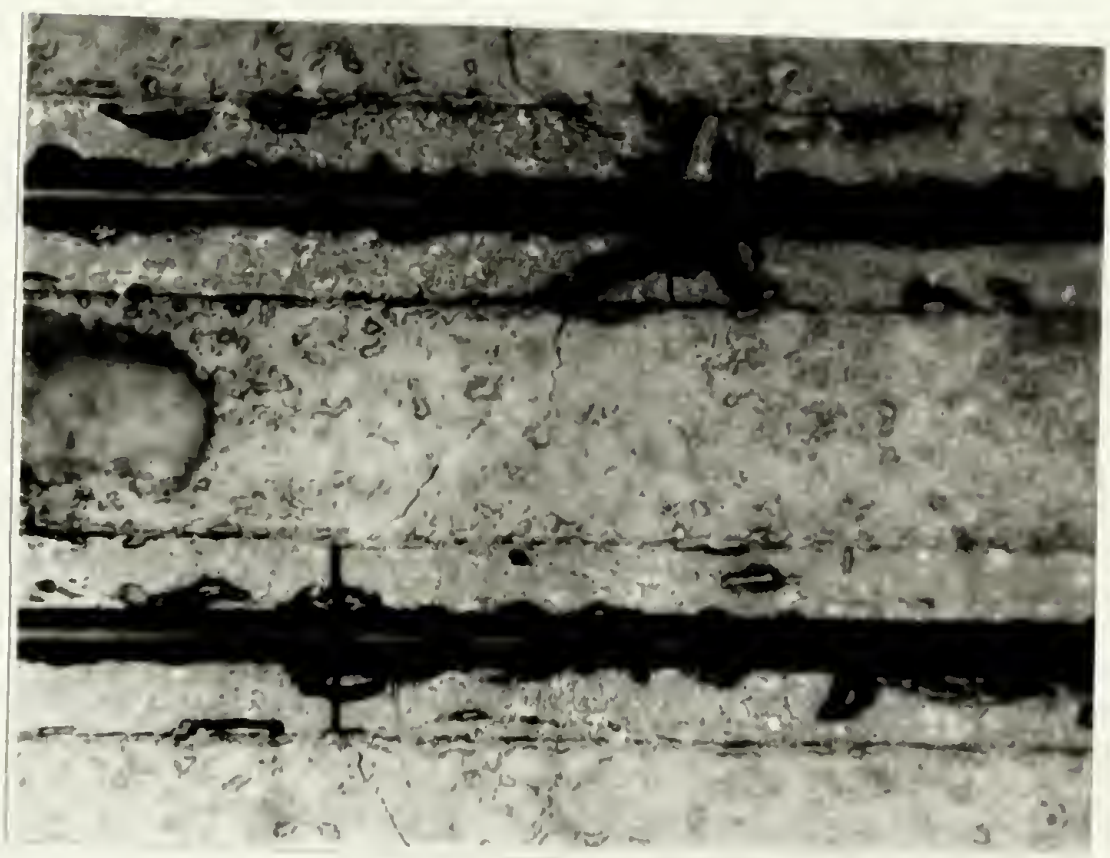

(B)

Figure 4.30 Micrographs of sample 11c5-16 showing crack gravitation to fiber defects at 1400° C.

Figure 4.31 Ceramic "glaze" cracking of the oxidation layer after testing at 1400° C.

Figure 4.32 Load/displacement curves of slow rate, .0085 mm/min, flexural tests of both monolithic RBSN and SiC/RBSN composite.

Table 4.6 Monolithic RBSN results.

Test	Rate/load	Temperature	Polished?	Result, Strength/K_i
MOR	0.2 mm/min	ambient	no	262 MPa
MOR	0.2	ambient	no	309 MPa
MOR	0.2	ambient	yes	287 MPa
MOR	0.2	1400° C	yes	328 MPa
MOR	0.0085	1400	yes	272 MPa
MOR	0.0085	1300	yes	316 MPa
SENB	0.1	ambient	-	2.0
SENB	0.1	1300	-	3.1
creep	100 MPa	1000	yes	no cracking
creep	100 MPa	1400	yes	no cracking

CHAPTER 5

MODELING AND ANALYSIS

5.1 Ambient Temperature and Short Term High Temperature Properties

From the results of SEM observation of the interface, it was concluded that the continuous-SiC-fiber-reinforced RBSN studied was processed with a minimum of fiber and fiber/matrix interface degradation. This was deduced from the improved load/displacement behavior when compared to that of the monolith and that of the ideal stress/strain curve for a fiber reinforced composite.

Llorca and Singh [50] in their parametric study of a SCS-6 fiber reinforced zirconia showed that by using fibers with high strength and large radius, and by using fiber matrix combinations with low interfacial shear stresses, composites with high strength and good ductility can be made. This was what was observed for the experimental composite studied here. Furthermore, larger fracture toughness values and stable crack growth have also been observed in composites with these properties [51] and this too has been demonstrated in this composite system.

The effect of the interface properties can not be underestimated in these composites. With a strongly bonded aligned fiber reinforced system, failure is catastrophic and characterized by a single mode I crack with the fibers not significantly affecting the fracture toughness [32]. If the interface is weak, Zok [32] states that multiple mode I matrix cracks may form followed by fracture of bridging fibers and high fracture toughness can be obtained. The MOR results often showed

more than one crack forming and toughness values were predicted to be higher. Although a weak interface is desirable, a large degree of delamination seems to be occurring. Llorca and Singh [50] stress that the minimum value of the interfacial shear stress is limited in two ways, (1) very low interfacial shear stresses may promote early matrix cracking thereby exposing the filaments to possible negative environmental effects and (2) low τ may induce failure due to interfacial delamination. In our case, interfacial delamination readily occurred even in tensile tests. Although interfacial shear measurements gave some idea of the interfacial strength, τ was not measured directly in this study. It has been measured, however, for SiC/RBSN [35]. The range of values for interfacial stress in that study was 5-15 MPa at 25° C.

The average pullout length for the composite in tension was high at room temperature, upwards of 1000 μm, with the average pullout length being about 600 μm. Pullout at higher temperatures was reduced although this was not as clearly apparent in the bend tests as the tensile. Reduction in pullout length often indicates an increase in τ [52]. The following equation has been derived from weakest link statistics and proposes a correlations between the strength of the interface and the average pullout length:

$$\bar{h}\ \tau^{m/(m+1)} = C \qquad (18)$$

This correlation agrees with the findings of this investigation.

In notched tensile tests, as stated above, delamination cracking was observed. This agreed with Zok [32] who stated that in notched specimens, failure occurs by a process of delamination parallel to the fiber axis and is occasionally accompanied by

mode I matrix cracking. In the case of the SiC/RBSN studied here, however, cracking other that delamination occurred as mixed mode I and II with the crack growing out 45 degrees from the notch. (Fiber/matrix debonding is primarily mode II).

Delamination can be studied further if the composite is considered to be a laminated composite which is true in the sense that the fibers are laid up as sheets (see Figure 3.1 on processing). Delamination in this case should be suppressed when the notch front is perpendicular to the laminate.

5.1.1 MOR

At ambient temperatures, the MOR results indicate that for the composite, mechanical properties were significantly improved over that of monolithic RBSN at the same porosity level. The strength of RBSN at 37% porosity is approximately 150 to 200 MPa [53], which is on the order of, or less than, the first matrix cracking strength of the composite. The substantially higher ultimate strengths and the presence of noncatastrophic failure provide the composite significant advantages over its monolithic counterpart.

A predicted value of the first matrix cracking strength can be calculated using the value for the ambient temperature matrix toughness, K_m, of 1.5 MPa·$m^{½}$ and Equation (3). Introducing E_f = 407 GPa [48], E_m = 60 GPa with 36% porosity [53], τ = 15 MPa, α_f = 4.4 x 10^{-6} /°C [31], and α_m = 3.3 x 10^{-5} /°C into Equations (3) through (6), the predicted value for σ_m^c is about 150 MPa and is smaller than the measured value, which may be due to choice of parameter values.

Orientation effects should also be considered. One MOR specimen was tested in the alternate, vertical, orientation. Its strength was lower but more tests would have to be run to determine if this was actually a result of laminate behavior.

5.1.2 Toughness

The toughening mechanisms for the composite have been identified. They include, at ambient temperature, crack bridging and pull-out, delamination crack growth and mixed mode crack growth, crack branching, and crack front microcracking occurring as mode II cracks ahead of the notch. As witnessed by the SENB tests, the samples were notch insensitive, an effect that has been seen in other composite systems that use uniaxial fibers. In the short term at elevated temperature, the mechanisms were bridging and pull-out. Delamination cracking was reduced. In the longer term high temperature tests, bridging was present but was time dependent as explained in the next section. Branching and delamination did not readily occur.

The initiation toughness at ambient temperature, including SENB data, gave a toughness result for five samples of 3.14 ± 0.2 $MPa \cdot m^{1/2}$. Direct observation revealed that initiation occurred by failure in the matrix ahead of the notch. On this basis, a predicted value of toughness was calculated according to Equation (7). Using a value of K_m of 1.5 $MPa \cdot m^{1/2}$ for RBSN with 36% porosity and the known value of E_c, the calculated value of K_c was 3.25 $MPa \cdot m^{1/2}$, which is close to the measured value. It therefore appears that there are no significant contributions to initiation toughness from

fiber/matrix debonding or fiber fracture ahead of the notch as was found to be the case in a different fiber-reinforced composite system [32].

Since cracks at room temperature extended in mixed mode I and II, actual values of the toughness could not be easily obtained. In addition it has been shown that cracks in this material close up very tightly and often invisibly upon unloading thereby. This could lead to erroneous assumptions about the amount of crack growth at a given stress.

5.1.3 R-Curve

R-curve behavior was shown to exist at ambient temperature for the SiC/RBSN composite as demonstrated by the interrupted notched tests. Even as the crack was shown to increase in length, the sample was able to carry an increasing load. Other clues to R-curve behavior, such as crack bridging and fiber pull-out were also present.

To evaluate the R-curve, crack extensions were measured as a function of load. It was found that, in all samples, crack extensions occurred at a steep angle to the notch, see schematic of Figure 5.1, which also shows a FEM that was generated by a coworker [54] to evaluate the corresponding stress-intensity values. Consequently, a new FEM mesh had to be generated at each value of the crack extension, which was why, as mentioned, R-curve results in this study were only obtained on one sample.

The FEM model was used to calculate the K_I and K_{II} components assuming that the solid was homogeneous with a modulus equal to that of the composite. The value of K_R was then obtained by

$$K_R = \sqrt{K_I^2 + K_{II}^2} \quad . \tag{19}$$

K_I and K_{II} were calculated using a crack opening displacement method [55]. The results of the R-curve are shown as triangular data points in Figure 5.2 in terms of the normalized fracture resistance K_R/K_o where K_o is the initiation toughness.

Superimposed on the results in Figure 5.2 are predicted theoretical R-curves using the very recent model explained in Chapter 2 which is based on fiber pull-out as being the major contributor to the overall toughening. The model provides for K_R Equation (8) as explained in Chapter 2. The following values were used to make the R-curve calculation: τ = 10 to 15 MPa, $\bar{h} \approx 600$ μm. From the comparison of the measured and predicted curves it appears that the data points provide the expected result for large-scale bridging [42] wherein the crack extensions are significant compared to the specimen widths. The predicted intrinsic steady-state toughness based on the pull-out model can be given by Equation (9). For the parameter values employed K_{ss1} is on the order of $12K_o$, or, with K_o of approximately 3 MPa·m$^{1/2}$, K_{ss1} = 36 MPa·m$^{1/2}$. Note however, that this steady-state value is only achieved when $\Delta a \approx 710\ \bar{h}$. This means that with $\bar{h} \approx 600$ μm the specimen widths would have to be greater than 430 mm before these high crack resistance values can be observed. If the specimen widths are smaller than this value the crack would completely travel the specimen width but not result in specimen failure because of bridging fractions.

We now evaluate the toughness predicted for the case where the major toughness contribution to the R-curve comes from elastic fiber bridging of matrix

cracks. The results for the steady-state toughness for this case, using another recent model [42], which was described by Equations (10) and (11) given in Chapter 2. The following values were used for this model; the known values for SCS-6 fiber of $\sigma_f = 3$ GPa [49], R = 70 μm, $\tau = 10$, taking $G_c = 4$ N·m/m^2 gives $K_{ss2}/K_o = 13.3$ or $K_{ss2} \approx$ 40 MPa·m^{½}. Based on this result, we conclude that, for the large diameter fiber reinforced composite, both fiber pull-out as well as elastic fiber bridging effects are important. We predict an overall composite steady-state toughness, K_{ssc}, as

$$K_{ssc} = \sqrt{K_{ss1}^2 + K_{ss2}^2} \qquad (20)$$

on which basis, $K_{ss2}/K_o \approx 18$ or $K_{ssc} \approx 54$ MPa·m^{½}. This number is an estimate of the toughness potential in the composite of this study and suggests that large diameter fibers offer the maximum potential for toughness increases. However, the difference between the potential toughness and the experimental results is due to the fact that the dimension of the specimen is not large enough to accommodate the large crack extensions prior to attaining the steady state toughness value.

5.1.4 Interlaminar Shear

From observations of the interface of failed specimens at ambient and elevated temperature, and from the crack growth behavior at temperatures above 1300° C, interlaminar shear strength of the composite would be expected to rise with temperature due to increased interfacial strength and bonding at elevated temperatures. This anticipated increase of interlaminar shear strength did not occur however as was

clearly shown in Figure 4.18. Likewise, when the first matrix cracking stresses and ultimate stresses were plotted against the interlaminar shear strength, Figure 4.22, the general trend was upward. One would have expected the opposite to be true if the interface was becoming more strongly bonded at higher temperatures and if the matrix strength did not have a large effect, which it should not since the strength of RBSN does not dramatically change with temperature due to its lack of sintering additives. Also, researchers [35] have shown that the interfacial strength in push-out tests of a SiC/RBSN does rise with temperature. This apparent contradiction may be the result of the stress concentrations occurring at the notch tips which could give rise to misleading results.

A closer examination of the interlaminar shear load/displacement records shows what might have been a separate initiation event occurring during the elevated temperature tests. The value of the stress at this initiation event, which is evident on Figure 4.18, was less sensitive to temperature. A finite element analysis of this geometry showed that the shear stress at the notch tip is high and decreases significantly beyond the notch. Furthermore, the average of the nodal stresses between the notch tips added up to the average shear stress as calculated by force divided by the area sheared. This average, F/A, stress explains nothing about the true stress state of the specimen which is in fact quite complex. Therefore the delamination phenomenon may not correspond well with the interlaminar shear strength results but it may with the interlaminar shear initiation. Further studies would be needed to relate UTS and FMC to the interlaminar initiation stress. Even so, a decrease in interlaminar

shear strength may not indicate an increased tendency for delamination cracking because of the complicated stress state in the composite.

5.2 Long Term Elevated Temperature Studies

5.2.1 Crack Growth

The mechanics of crack growth at elevated temperatures include a strong time-dependence to the fiber bridging process. Figure 4.26 is a plot of the crack opening as a function of time at temperature obtained in this study. It appears that the fibers slid out of the matrix in a time dependent fashion which allowed the crack widths to increase. This result was similar to the result obtained previously in a SiC-fiber-reinforced alumina ceramic [49]. In that study, the time-dependent opening was found to be enhanced by the presence of glassy interfacial phases, suggesting the presence of amorphous phases at the interface may contribute to the time-dependent sliding of bridging fibers out of the matrix.

Recently, a model [14] was developed to evaluate the time dependence of the crack opening for the case where the fiber/matrix interface is viscous and exhibits Newtonian viscous deformation. The crack opening displacement was shown to be

$$\delta = \delta_0 \{1 - \exp\left(\frac{t}{\beta^2 t_0}\right) erfc\left[\left(\frac{t}{\beta^2 t_0}\right)^{1/2}\right]\} \qquad (21)$$

where δ_0 is the crack opening at the mouth of the crack for the case of no fiber bridging; $\beta = 4(1 - \nu_c^2)fE_f/\pi E_c$ and $t_0 = 2a^2/RE_f\varepsilon_0$, in which a is the crack length and ε_0 is the ratio of the viscous interface thickness, Δ, to the viscosity, μ. This form of

the predicted crack opening equation as a function of time is similar to the observed result.

Provided viscous time-dependent sliding of the fibers is significant, crack growth at elevated temperatures can arise as a result of the increase in crack tip stress-intensity factor as the fibers slip out of the matrix. In fact, model derivations predict stable crack growth rate of magnitude

$$\frac{da}{dt} = \frac{R\,\Delta\,\pi^2 E_c^{\,2}\,\sigma^2_{app}}{8\,(1-\nu_c^{\,2})\,f^2 E_f K_m^{\,2}\,\mu} \tag{22}$$

where σ_{app} is the applied stress and R is the fiber radius. Because the actual crack growth rate was not measured in this study, the prediction of Equation (22) cannot be directly verified. However, the observation of time-dependent stable cracking accompanied with time-dependent fiber pullout is qualitatively consistent with model predictions.

5.2.2 Modeling for Creep

Because of the high variability of the crack initiation times, a relation between time to initiation or failure as a function of stress and temperature could not be determined for the composite material. Attempts were made to look at the trends only for specific batches but variability occurred even within a batch. As can be seen even from the MOR results, there was a high degree of batch to batch variability and even variability between batches thus making any batch strength correlations difficult. This variability could be caused by processing variations, surface finish, i.e. the placement

of fibers on the surface, as well as machining damage and polishing, internal defects and other surface and volume flaws.

The values of the log of the stress versus log of the initiation and failure times did not yield the appearance of an emerging steady state creep rate, see Figure 5.3. The Monkman-Grant equation therefore would not give any useful result or give an accurate description of the system behavior.

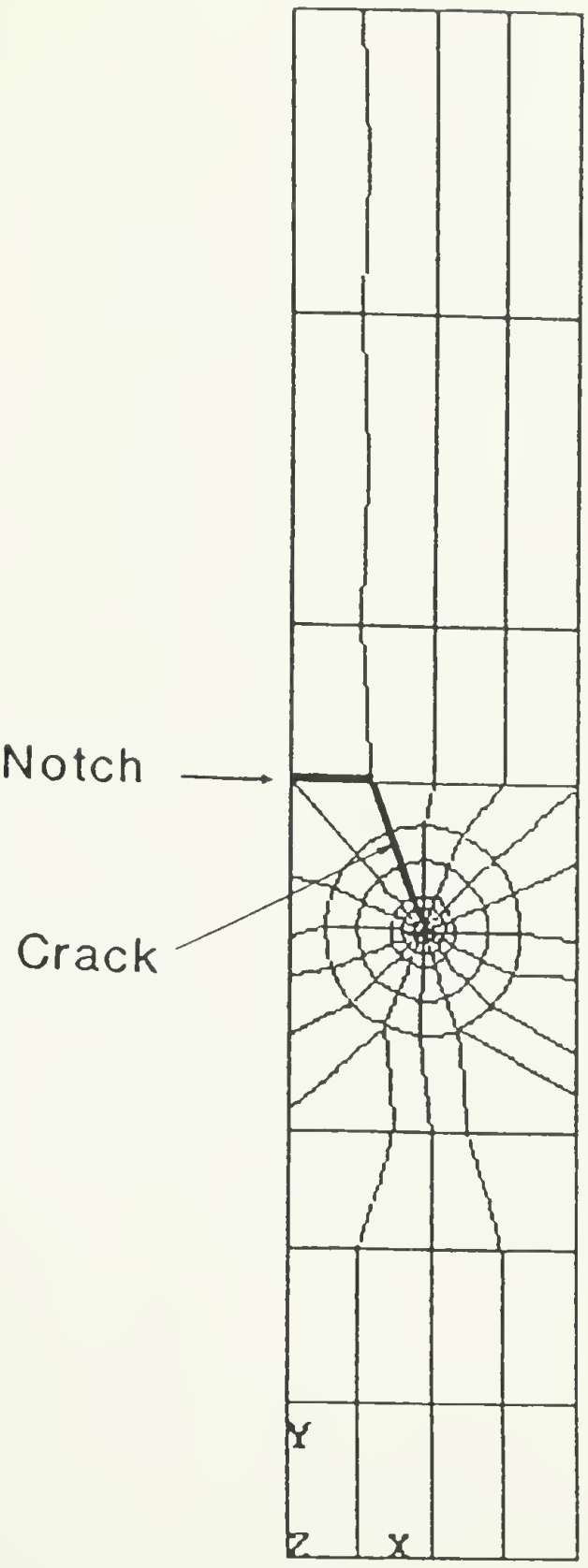

Figure 5.1 Mesh generated for finite element model in order to analyze the fracture toughness at ambient temperature. The crack extension is shown to occur at a steep angle to the initial notch.

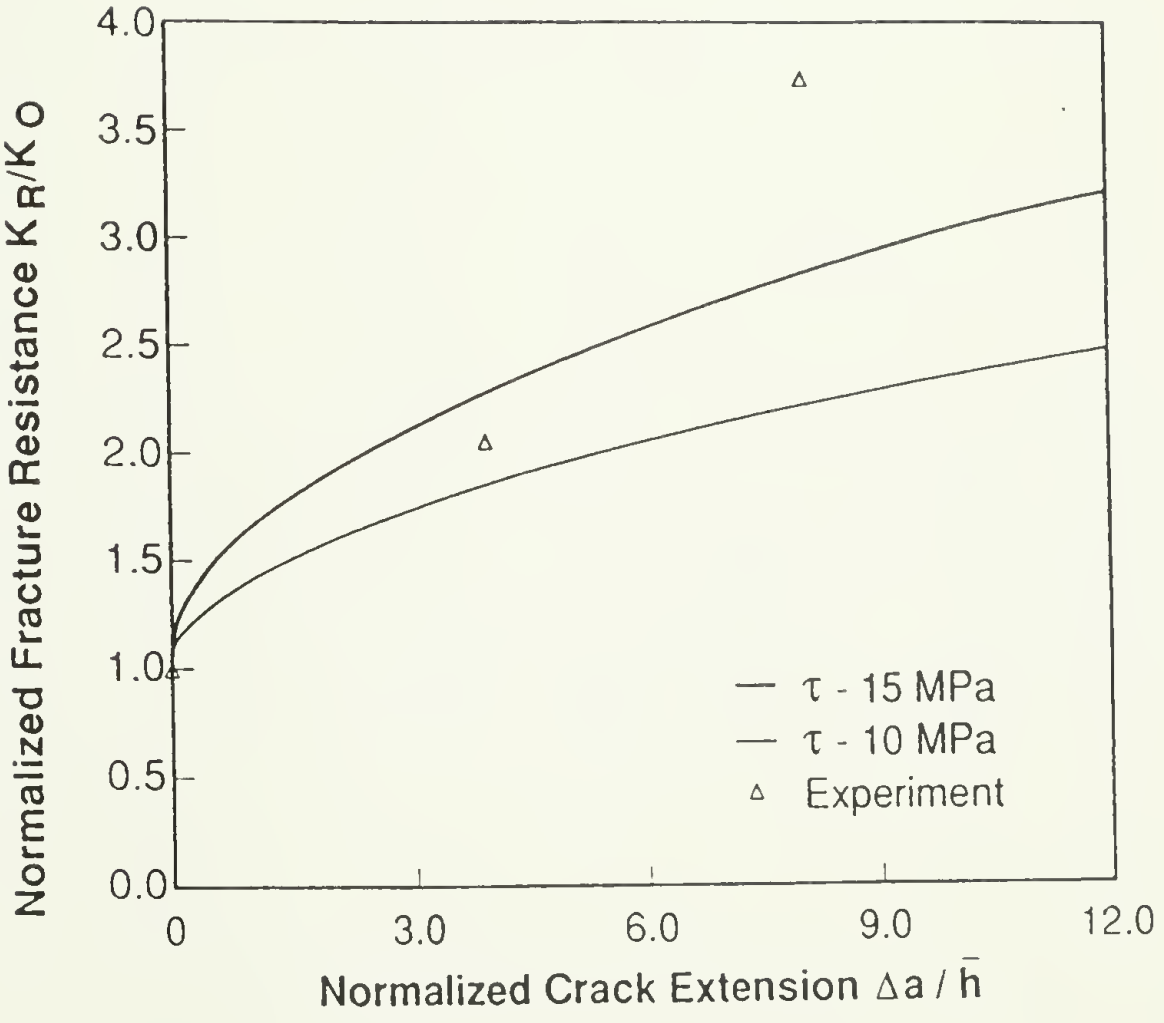

Figure 5.2 Experimental R-curve results for one specimen compared with the analytical solution based on a fiber pullout model [Zok].

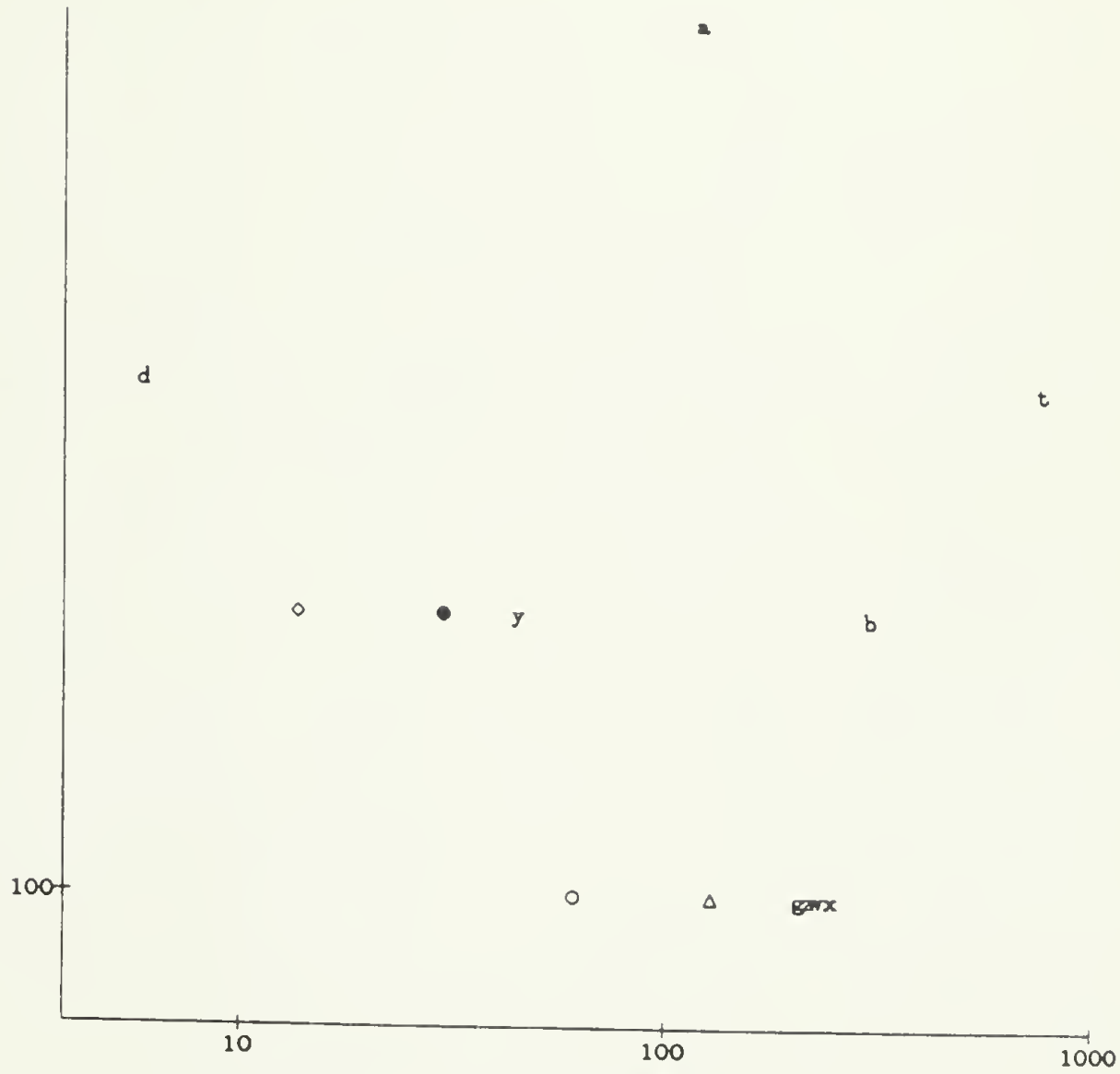

Figure 5.3 Log of the stress plotted against initiation and failure times for various specimens tested under constant load conditions.

CHAPTER 6

SUMMARY AND CONCLUSIONS

The purpose of the following research was to obtain an understanding of both ambient and elevated temperature mechanical behavior of a SiC fiber reinforced RBSN composite. At ambient temperature, applicability of available mechanics models to describe the stress-strain curve were examined. Emphasis was also placed on fracture toughness and R-curve behavior, toughening mechanisms and the applicability of available fracture mechanics models to describe toughening behavior. At elevated temperature, an attempt was made to characterize the short term and long term effects on the composite. The applicability of empirical predictive models for lifetime was investigated. The material used was a RBSN reinforced with large diameter continuous SiC fibers. A limited investigation of the mechanical behavior of a commercially available RBSN monolith was also performed for comparison purposes with the reinforced material. The results were compared to those of the composite in an attempt to estimate the degree of improvement.

The continuous SiC fiber reinforced RBSN used in this study was processed with minimum fiber and fiber/matrix interface degradation. The strength and stiffness of the composite, however, were limited by the existence of many large voids and the high porosity levels in the composite matrix which contributed to the lowering of matrix strength. Ambient temperature toughening mechanisms were explored through the evaluation of the toughness and R-curve behavior of the composite. The

composite exhibited noncatastrophic failure and analysis of the results suggested that fiber pullout as well as elastic fiber bridging effects may both provide significant contributions to the overall toughness, with the overall potential for toughness calculated to be on the order of 54 $MPa \cdot m^{1/2}$. Analysis of the toughness based on these mechanisms was complicated, however, by the large amount of delamination that took place in this composite. At temperatures below 1350°C, matrix strength degradation seemed to be the reason for crack initiation. At higher temperatures, 1350° C and up, degradation of the fibers seemed to be the cause for ultimate failure. Linking up of fiber cracks also occurred above 1350° C.

Toughening occurred as pullout, bridging, mixed mode failure at room temperature. During long term elevated temperature exposure, bridging became a time dependent process. At elevated temperatures, crack initiation under constant load occurred in the matrix at temperatures on the order of 1000° C, but occurred in the fiber itself as the temperatures increased past 1350° C. The elevated temperature cracks were normal to the reinforcing fibers and were associated with unbroken bridging fibers in the crack wake. Furthermore, it was observed that the fibers pulled out of the matrix in a time-dependent fashion, thus making bridging a time dependent process during elevated temperature exposure. It was determined that the composite material behaved in a brittle manner at all temperatures. It did not exhibit slow crack growth. Fiber reinforcement did, however, contribute to strength.

APPENDIX

SUMMARY OF CONSTANT LOAD TESTS

Sample: 9c
Temperature: 1000 °C

Interruption	Stress,MPa	Duration, min.	Comments
1	100	15	change in fibers (oxidation) noted
2		30	visible deformation, long interlaminar cracks extending from sample ends, white marks noticed.
3		60	continued delamination.
4		22.5	crack initiation, through white areas also.
5		15	crack opening continues to increase, approx. 30 white 'cracks'.
6		15	again, crack opening continues to increase.
7		30	total time = 187.5, around 53+/-5 white 'cracks'
8		30	total time = 217.5

Sample: 11a
Temperature: 1000 °C

Interruption	Stress,MPa	Duration, min.	Comments, pretest observation of pits, voids
1	100	30	observation of white lines/marks. no I.S. cracks or end cracks.
2		31	sample visibly deformed. initiation, whole width. there is also another crack between the inner and outer spans.
3		15	no real changes or thermal (end) cracks.
4		30	observation of white marks outside inner span.
5		20	
6		35	there are a couple of extra thin cracks
7		45	total time = 206

Sample: 14b-9
Temperature: 1000 °C

Interruption	Stress, MPa	Duration	Comments
1	150	255	
2		508	total time = 763, no initiation

Sample: 11c-6
Temperature: 1000 °C

Interruption	Stress, MPa	Duration	Comments
1	200	120	
2		<2min	error trip. no change

Sample: 13c-1
Temperature: 1200 °C

Interruption	Stress,MPa	Duration, min.	Comments
1	100	20	pre-test: no evidence of 'white lines' many voids avg size approx 50 um diameter and voids seem to be concentrated in areas 'between' fibers. a few fiber 'cracks' around 10, i.e. chunks of fiber missing. after 1st, carbon core burned out. popout of matrix near interface.
2		30	visible permanent deformation.
3		25	
4		45	there are a couple of large parallel cracks on the compressive ends. there is a crack between the fibers where the roller was on the tensile side. the interface is getting 'worse'. there is also an edge crack on the tensile side end.
5		45	large splitting, delamination, cracks at ends of the sample.
6		80	245 minutes total-no inner span cracks noted.

Sample: 14b-1
Temperature: 1300 °C

Interruption	Stress, MPa	Duration	Comments, pretest-note voids.
1	125	30	multiple fiber cracking, in inner span around 38 fiber crack areas
2		20	parallel cracking outside inner span, some new fiber cracks
3		60	no change
4		180	"
5	150	60	"
6	165	60	"
7	175	60	noticeably deformed, no inner span cracks. it is hard to tell if oxidation is increasing, splitting is observable.

Sample: 13a-8
Temperature: 1350 °C

Interruption	Stress, MPa	Duration, min.	Comments
1	125	30	crack initiated through entire width
2		15	specimen failure, total time 45 min. one crack whole width. note fiber defect hopping at this temperature. this is perhaps evidence for fiber failure control at 1350. transition temperature from matrix crack initiation to fiber crack initiation. failure is perhaps fiber-cracking controlled

Sample: 13a-6
Temperature: 1350 °C

Interruption	Stress,MPa	Duration, min.	Comments
1	100	105	not much happened. observation of cracked 'glaze'
2	125	30	
3		88	some indication of interface related matrix crack. actually this is just this glaze cracking
4		84	fiber cracks, low strain.

Sample: 13a-3
Temperature: 1350 °C

Interruption	Stress, MPa	Duration	Comments
1	150	120	visible strain, few (2) fiber cracks
2		242	no visible changes from last int.
3		423	fiber cracks only - total time = 785 minutes.

Sample: 11c-4
Temperature: 1400 °C

Interruption	Stress, MPa	Duration	Comments
1	100	160	visible permanent strain, no cracks in matrix, small cracks in fibers, no end cracks
2		440	surface heavily oxidized, total time = 600 minutes

fine fiber cracks

Sample: 13a-7
Temperature: 1400 °C

Interruption	Stress, MPa	Duration	Comments
1	100	39.5	1-6 GWO
2		18	
3		17	
4		20.5	
5		24.5	
6		46	total time (gwo) 165.5
7	nn.	60	total 225.5

Sample: 11c-5
Temperature: 1400 °C

Interruption	Stress.MPa	Duration. min.	Comments.initially, lots of voids
1	125	13.5	initiation in matrix between inner and outer span lots of oxidation - much more so than at 1200°C. no cracking at ends.
2		16.5	no noticeable changes
3		60	no noticeable changes
4		90	
5		60	
6	150	1.0	total time = 240 min. cracked "glaze" finish specimen failure main crack occurred under loading pin, several other cracks also exist. fibers appear to be strongly bonded to the matrix and there was no fiber bridging or pullout at this main crack. sample quite deformed. near other loading pin there is another crack that goes through some fibers and bridges others. note how crack gravitates toward weaknesses in the fibers. evidence of a strong fiber matrix bond.

Sample: 13c-5
Temperature: 1400 °C

Interruption	Stress, MPa	Duration	Comments
1	125	300	no cracks

Sample: 11c-7
Temperature: 1400 °C

Interruption	Stress, MPa	Duration	Comments
1	150	6	initiation

REFERENCES

1. A. J. Moulson, "Review: Reaction-Bonded Silicon Nitride: Its Formation and Properties," Journal of Materials Science, 14 1017-1051 (1979).

2. B. J. Dalgleish and P. L. Pratt, Proc. Brit. Ceram. Soc., 25 295 (1975).

3. G. Grathwohl and F. Thummler, "Creep of Reaction-Bonded Silicon Nitride," J. of Mat. Sci., 13 1177-1186 (1978).

4. R. T. Bhatt, "Mechanical Properties of SiC Fiber-Reinforced Reaction-Bonded Silicon Nitride Composites," NASA Technical Memorandum 87085 USAAVSCOM Technical Report 85-c-14 July 1985.

5. R. T. Bhatt, "Effects of Fabrication Conditions on the Properties of SiC Fiber Reinforced Reaction-Bonded Silicon Nitride Matrix Composites (SiC/RBSN)," NASA Tech Memorandum 88814 AVSCOM Tech. Report 86-C-2 January 1986.

6. N. D. Corbin, G. A. Rossetti, Jr., and S. D. Hartline, "Microstructure/Property Relationships for SiC Filament-Reinforced RBSN," Ceramic Eng. & Sci. Proc., 7 [7-8] 958-968 (1986).

7. N. D. Corbin, C. A. Wilkens, and S. D. Hartline, "RBSN Matrix Composites Reinforced with Polymer Derived Fibers," NASA Conference Proceedings on Metal Matrix, Carbon, and Ceramic Matrix Composites, Cocoa Beach, FL, January 1987.

8. D. Jablonski and R. Bhatt, "High Temperature Tensile Properties of Fiber Reinforced Reaction Bonded Silicon Nitride," Presented at ASTM Symposium on Thermal and Mechanical Behavior of Ceramic and Metal Matrix Composites, Atlanta, Georgia, November 7, 1988.

9. R. Lundberg, R. Pompe, R. Carlsson, and P. Goursat, "Fiber Reinforced Silicon Nitride Composites," Composites Science and Technology, 37 165-176 (1990).

10. A. Lightfoot, L. Ewart, J. S. Haggerty, Z. Q. Cai, J. E. Ritter, and S. V. Nair, "Processing and Properties of SiC Whisker and Particulate Reinforced Reaction Bonded Silicon Nitride," Proceedings of the 15th Annual Conference on Composites and Advanced Ceramics, Engineering Ceramics Division Meeting, American Ceramic Society, Cocoa Beach, FL, January 1991.

11. A. Lightfoot, H. L. Ker, and J. S. Haggerty, "Properties of RBSN and RBSN-SiC Composites," Ceram. Eng. Sci. Proc., 11 [7-8] 842-856 (1990).

12. F. D. Gac, "Synthesis and Characterization of VLS Silicon Carbide Whisker Reinforced Reaction Bonded Silicon Nitride," Ph.D. Thesis, Department of Materials Science and Engineering, University of Washington, Seattle, WA, 1989.

13. A. G. Evans, "Perspective on the Development of High-Toughness Ceramics," J. Am. Ceram. Soc., 73 [2] 187-206 (1990).

14. S. V. Nair, K. Jakus and T. Lardner, "The Mechanics of Matrix Cracking in Fiber-Reinforced Ceramic Composites Containing a Viscous Interface," Accepted for Publication in Mechanics of Materials Journal, 1991.

15. J. S. Haggerty, "Ceramic-Ceramic Composites with Reaction Bonded Matrices," Proceedings of Symposium "Interface Phenomena in Composites: Processing, Characterization and Mechanical Properties", J. Mat. Sci. Eng., Nov., 1988.

16. H. C. Cao, E. Bischoff, O. Sbaizero, Manfred Ruhle, and A. G. Evans, "Effect of Interfaces on the Properties of Fiber-Reinforced Ceramics," J. Am. Ceram. Soc., 73 [6] 1691-99 (1990).

17. R. N. Singh, "Influence of Interfacial Shear Stress on First-Matrix Cracking Stress in Ceramic-Matrix Composites," J. Am. Ceram. Soc., 73 2930-37 (1990).

18. J. Aveston, G. A. Cooper, and A. Kelly, "Single and Multiple Fracture," pp. 15-26 in The Properties of Fiber Composites, Conference Proceedings, National Physical Laboratory. IPC Science and Technology Press, London, U.K., 1971.

19. M. Sutcu and W. B. Hillig, "The Effect of Fiber- Matrix Debond Energy on the Matrix Cracking Strength and Debond Shear Strength,"; to be published in Acta Metall.

20. R. T. Bhatt and R. E. Phillips, "Laminate Behavior for SiC Fiber-Reinforced Reaction-Bonded Silicon Nitride Matrix Composites," Journal of Composites Technology & Research, 12 [1] 13-23 (1990).

21. E. Y. Luh and A. G. Evans, "High-Temperature Mechanical Behavior of a Ceramic Matrix Composite," J. Am. Ceram. Soc., 70 [7] 466-69 (1987).

22. A. Chulya, J. P. Gyekenyesi, and R. T. Bhatt, "Mechanical Behavior of Fiber Reinforced SiC/RBSN Ceramic Matrix Composites: Theory and Experiment," NASA Technical Memorandum 103688 AVSCOM Technical Report 91-C-004, Prepared for the 36th International Gas Turbine and Aeroengine Congress and Exposition sponsored by the American Society of Mechanical Engineers, Orlando, Florida, June 3-6, 1991.

23. G. Y. Baaklini and R. T. Bhatt, "In-Situ X-Ray Monitoring of Damage Accumulation in SiC/RBSN Tensile Specimens," NASA Technical Memorandum 103733 AVSCOM Technical Report 91-C-019 Prepared for the 15th Annual Conference on Composites and Advanced Ceramics sponsored by the American Ceramic Society, Cocoa Beach, Florida, January 13-16, 1991.

24. R. T. Bhatt and R. E. Phillips, "Laminate Behavior for SiC Fiber-Reinforced Reaction-Bonded Silicon Nitride Matrix Composites," Journal of Composites Technology & Research, 12 [1] 13-23 (1990).

25. T. Mah et al., "Recent Developments in Fiber Reinforced High Temperature Ceramic Composites," Amer. Ceram. Soc. Bull., 66 [2] 304 (1987).

26. H. Bhatt, K. Y. Donaldson, and D. P. H. Hasselman, "Role of the Interfacial Barrier in the Effective Thermal Diffusivity/Conductivity of SiC-Fiber-Reinforced Reaction- Bonded Silicon Nitride," J. Am. Ceram. Soc., 73 [2] 312-316 (1990).

27. R. T. Bhatt, "Effects of Fabrication Conditions on the Properties of SiC Fiber Reinforced Reaction-Bonded Silicon Nitride Matrix Composites," NASA Technical Report 86-C-2, January 1986.

28. R. T. Bhatt, J. D. Kiser, "Matrix Density Effects on the Mechanical Properties of SiC Fiber-Reinforced Silicon Nitride Matrix Properties," Ceram. Eng. Sci. Proc., 11 [7-8] 974-994 (1990).

29. D. C. Larsen, S. L. Stuchly, and J. W. Adams, "Evaluation of Ceramics and Ceramic Composites for Turbine Engine Applications," Final report to Air Force AFWAL-TR-4202, December 1988.

30. J. Laughner, R. T. Bhatt, "Measurement of Interfacial Shear Strength in SiC-Fiber Si3N4 Composites," J. Am. Ceram. Soc.,72 [10] 2017-19 (1989).

31. M. K. Brun and M. P. Borom, "Thermomechanical Properties of Chemically Vapor Deposited Silicon Carbide Filaments," J. Am. Ceram. Soc., 72 [10] 1993-1996 (1989).

32. F. Zok, O. Sbaizero, C. L. Hom, and A. G. Evans, "The Mode I Fracture Resistance of a Laminated Fiber Reinforced Ceramic," J. Am. Ceram. Soc., 74 [1] 187-93 (1991).

33. Hironori Kodama, Hiroshi Sakamoto, and Tadahiko Miyoshi, "Silicon Carbide Monofilament-Reinforced Silicon Nitride or Silicon Carbide Matrix Composites," J. Am. Ceram. Soc., 72 [4] 551-58 (1989).

34. D. B. Marshall and A. G. Evans, "Failure Mechanisms in Ceramic-Fiber/Ceramic-Matrix Composites," J.Am. Ceram. Soc., 68 [5] 225-231 (1985).

35. G. M. Morscher, P. Pirouz, and A. H. Heuer, "Temperature Dependence of Interfacial Shear Strength in SiC-Fiber-Reinforced Reaction-Bonded Silicon Nitride," J. Am. Ceram. Soc., 73 [3] 713-720 (1990).

36. J. W. Holmes, "Tensile Creep Behavior of a Fiber- Reinforced SiC/Si3N4 Composite," In Press J. Mater. Sci.

37. J.-M. Yang, R. B. Thayer, S. T. Chen, and W. Lin, "Creep of Fiber-Reinforced Ceramic Matrix Composites," Published in the Proceedings of the International Conference on Composite Materials, 1991.

38. B. Budianski, J. W. Hutchinson, and A. G. Evans, "Matrix Fracture in Fiber-Reinforced Ceramics," J. Mech. Phys. Solids, 34 [2] 167-89 (1986).

39. A. G. Evans, "Engineering Property Requirements for High Performance Ceramics," Mater. Sci. Eng., 71 3-21 (1985).

40. C. H. Hsueh and P. F. Becher, "Thermal Expansion Coefficients of Unidirectional Fiber-Reinforced Ceramics," J. Am. Ceram. Soc., 71 C438-C441 (1988).

41. P. G. Charalambides and A. G. Evans,"Debonding Properties of Residually Stressed Brittle-Matrix Composites," J. Am. Ceram. Soc, 72 [5] 746-53 (1989).

42. S. V. Nair, "Crack Wake Debonding and Toughness in Fiber or Whisker Reinforced Brittle-Matrix Composites," J. Am. Ceram. Soc. 73 [10] 2839-47 (1990).

43. D. B. Marshall, B. N. Cox, and A. G. Evans, "The Mechanics of Matrix Cracking in Brittle-Matrix Composites," Acta Metall., 33 [11] 2013-2021 (1985).

44. P. F. Becher, P. Angelini, W. H. Warwick, and T. N. Tiegs, "Elevated-Temperature-Delayed Failure of Alumina Reinforced with 20vol% Silicon Carbide Whiskers," J. Am. Ceram. Soc., 73 [1] 91-96 (1990).

45. G. W. Hollenberg, G. R. Terwilliger, R. S. Gordon, "Calculation of Stresses and Strains in Four-Point ending Creep Tests," J. Am. Ceram. Soc. 54 [2] 196-199 (1971).

46. M. Godin, Master's Thesis, Department of Mechanical Engineering, University of Massachusetts at Amherst, May 1990.

47. R. T. Bhatt and M. D. Kraichman, "Environmental Effects on the Tensile Strength of Chemically Vapor Deposited Silicon Carbide Fibers," NASA TM-86981, NASA Lewis Research Center, Cleveland, OH, April 1985.

48. T. F. Foltz, "SiC Fibers for Advanced Ceramic Composites," Ceram. Eng. Sci. Proc., 6 [9-10] 1206-20 (1985).

49. S. V. Nair, K. Jakus, and C. Ostertag, "Role of Glassy Interface in High Temperature Crack Growth in SiC Fiber Reinforced Alumina," Ceram. Eng. Sci. Proc., 9 [7-8] 681 (1988).

50. J. Llorca and R. N. Singh, "Influence of Fiber and Interfacial Properties on the Fracture Behavior of Fiber-Reinforced Ceramic Composites," 74 [11] 2882-90 (1991).

51. J. Llorca and M. Elices, "Fracture Toughness, Ductility and Crack Growth Resistance of Fiber Reinforced Ceramics"; Structural Ceramics - Processing, Microstructure and Properties; pp. 403-11 in proceedings of the 11th Riso International Symposium on Metallurgy and Materials Science (Riso, Denmark, Sept., 1990), Edited by J.J. Bentzen et al. In press.

52. M. D. Thouless and A. G. Evans, Acta Metall., 36 (1988) 517.

53. W. A. Dunlay, "Mechanical Properties of Laser Synthesized Reaction Bonded Silicon Nitride"; Master's Thesis. Mechanical Engineering Department, University of Massachusetts, Amherst, MA, September 1987.

54. H. G. Kim, University of Massachusetts at Amherst, presented at the American Ceramic Society Cocoa Beach Conference, January 1990.

55. R. D. Cook, Concepts and Application of Finite Element Analysis. Wiley, New York, 1981.

BIBLIOGRAPHY

Averston, J., G. A. Cooper, and A. Kelly, "Single and Multiple Fracture," pp. 15-26 in The Properties of Fiber Composites, Conference Proceedings, National Physical Laboratory. IPC Science and Technology Press, London, U.K., 1971.

Baaklini, G. Y. and R. T. Bhatt, "In-Situ X-Ray Monitoring of Damage Accumulation in SiC/RBSN Tensile Specimens," NASA Technical Memorandum 103733 AVSCOM Technical Report 91-C-019 Prepared for the 15th Annual Conference on Composites and Advanced Ceramics sponsored by the American Ceramic Society, Cocoa Beach, Florida, January 13-16, 1991.

Baldoni, J. G. and s. T. Buljan, "Creep and Crack Growth Resistance of Silicon Nitride Composites," Ceramic Materials & Components for Engines, p. 785-795.

Becher, P. F., P. Angelini, W. H. Warwick, and T. N. Tiegs, "Elevated-Temperature-Delayed Failure of Alumina Reinforced with 20vol% Silicon Carbide Whiskers," J. Am. Ceram. Soc., 73 [1] 91-96 (1990).

Bhatt, H., K. Y. Donaldson, and D. P. H. Hasselman, "Role of the Interfacial Barrier in the Effective Thermal Diffusivity/Conductivity of SiC-Fiber-Reinforced Reaction- Bonded Silicon Nitride," J. Am. Ceram. Soc., 73 [2] 312-316 (1990).

Bhatt, R. T., "Mechanical Properties of SiC Fiber-Reinforced Reaction-Bonded Silicon Nitride Composites," NASA Technical Memorandum 87085 USAAVSCOM Technical Report 85-c-14 July 1985.

Bhatt, R. T., J. D. Kiser, "Matrix Density Effects on the Mechanical Properties of SiC Fiber-Reinforced Silicon Nitride Matrix Properties," Ceram. Eng. Sci. Proc., 11 [7-8] 974-994 (1990).

Bhatt, R. T. and M. D. Kraichman, "Environmental Effects on the Tensile Strength of Chemically Vapor Deposited Silicon Carbide Fibers," NASA TM-86981, NASA Lewis Research Center, Cleveland, OH, April 1985.

Bhatt, R. T., "Effects of Fabrication Conditions on the Properties of SiC Fiber Reinforced Reaction-Bonded Silicon Nitride Matrix Composites (SiC/RBSN)," NASA Tech Memorandum 88814 AVSCOM Tech. Report 86-C-2 January 1986.

Bhatt, R. T. and R. E. Phillips, "Laminate Behavior for SiC Fiber-Reinforced Reaction-Bonded Silicon Nitride Matrix Composites," Journal of Composites Technology & Research, 12 [1] 13-23 (1990).

Bordia, R. K., B. J. Dalgleish, P. G. Charalambides, and A. G. Evans, "Cracking and Damage in a Notched Unidirectional Fiber-Reinforced Brittle Matrix Composite," J. Am. Ceram. Soc., 74 [11] 2776-80 (1991).

Brun, M. K. and M. P. Borom, "Thermomechanical Properties of Chemically Vapor Deposited Silicon Carbide Filaments," J. Am. Ceram. Soc., 72 [10] 1993-1996 (1989).

Budianski, B., J. W. Hutchinson, and A. G. Evans, "Matrix Fracture in Fiber-Reinforced Ceramics," J. Mech. Phys. Solids, 34 [2] 167-89 (1986).

Cao, H. C., E. Bischoff, O. Sbaizero, Manfred Ruhle, and A. G. Evans, "Effect of Interfaces on the Properties of Fiber-Reinforced Ceramics," J. Am. Ceram. Soc., 73 [6] 1691-99 (1990).

Carroll, D. F., and R. E. Tressler, "Effect of Creep Damage on the Tensile Creep Behavior of a Siliconized Silicon Carbide," J. Am. Ceram. Soc., 72 [1] 49-53 (1989).

Charalambides, P. G. and A. G. Evans,"Debonding Properties of Residually Stressed Brittle-Matrix Composites," J. Am. Ceram. Soc, 72 [5] 746-53 (1989).

Chatterjee, A., Capt., J. W. Moschler, R. J. Kerans, N. J. Pagano, S. Mall, "Residual Stresses and Damage in Unidirectional Model Composites," Ceram. Eng. Sci. Proc. 10 [9-10] pp. 1179-1190 (1989).

Chuck, L., S. M. Goodrich, N. L. Hecht, and D. E. McCullum, "High-Temperature Tensile Strength and Tensile Stress Rupture Behavior of Norton/TRW NT-154 Silicon Nitride," Ceram. Eng. Sci. Proc., 11 [7-8] pp. 1007-1027 (1990).

Chulya, A., J. P. Gyekenyesi, and R. T. Bhatt, "Mechanical Behavior of Fiber Reinforced SiC/RBSN Ceramic Matrix Composites: Theory and Experiment," NASA Technical Memorandum 103688 AVSCOM Technical Report 91-C-004, Prepared for the 36th International Gas Turbine and Aeroengine Congress and Exposition sponsored by the American Society of Mechanical Engineers, Orlando, Florida, June 3-6, 1991.

Cook, R. D., Concepts and Application of Finite Element Analysis. Wiley, New York, 1981.

Corbin, N. D., G. A. Rossetti, Jr., and S. D. Hartline, "Microstructure/Property Relationships for SiC Filament-Reinforced RBSN," Ceramic Eng. & Sci. Proc., 7 [7-8] 958-968 (1986).

Corbin, N. D., C. A. Wilkens, and S. D. Hartline, "RBSN Matrix Composites Reinforced with Polymer Derived Fibers," NASA Conference Proceedings on Metal Matrix, Carbon, and Ceramic Matrix Composites, Cocoa Beach, FL, January 1987.

Dalgleish, B. J. and P. L. Pratt, Proc. Brit. Ceram. Soc., 25 295 (1975).

Dunlay, W. A., "Mechanical Properties of Laser Synthesized Reaction Bonded Silicon Nitride"; Master's Thesis. Mechanical Engineering Department, University of Massachusetts, Amherst, MA, September 1987.

Evans, A. G., "Engineering Property Requirements for High Performance Ceramics," Mater. Sci. Eng., 71 3-21 (1985).

Evans, A. G., "Perspective on the Development of High-Toughness Ceramics," J. Am. Ceram. Soc., 73 [2] 187-206 (1990).

Evans, A. G. and S. M. Wiederhorn, "Crack Propagation and Failure Prediction in Silicon Nitride at Elevated Temperatures," J. Mat. Sci. 9 270-278 (1974).

Evans, R. W., T. Murakami, and B. Wilshire, "Rate Controlling Processes During Creep of Silicon Nitride Ceramics," Br. Ceram Trans. J., 87 54-57 (1988).

Fett, T., K. Keller, D. Munz, "An Analysis of the Creep of Hot Pressed Silicon Nitride in Bending." J. Mat. Sci., 23 467-474 (1988).

Foltz, T. F., "SiC Fibers for Advanced Ceramic Composites," Ceram. Eng. Sci. Proc., 6 [9-10] 1206-20 (1985).

Foulds, W., J. F. LeCostaouec, C. Landry, and S. DiPietro, "Tough jSilicon Nitride Matrix Composites Using Textron Siloicon Carbide Monofilaments," Ceram. Eng. Sci. Proc. 10 [9-10] pp. 1083-1099 (1989).

Gac, F. D., "Synthesis and Characterization of VLS Silicon Carbide Whisker Reinforced Reaction Bonded Silicon Nitride," Ph.D. Thesis, Department of Materials Science and Engineering, University of Washington, Seattle, WA, 1989.

Ghosh, A., M. G. Jenkins, K. W. White, A. S. Kobayashi, and R. C. Bradt, "Elevated-Temperature Fracture Resistance of a Sintered Silicon Carbide," J. Am. Ceram. Soc., 72 [2] 242-47 (1989).

Godin, M., Master's Thesis, Department of Mechanical Engineering, University of Massachusetts at Amherst, May 1990.

Grathwohl, G. and F. Thummler, "Creep of Reaction-Bonded Silicon Nitride," J. of Mat. Sci., 13 1177-1186 (1978).

Haggerty, J. S., "Ceramic-Ceramic Composites with Reaction Bonded Matrices," Proceedings of Symposium "Interface Phenomena in Composites: Processing, Characterization and Mechanical Properties", J. Mat. Sci. Eng., Nov., 1988.

Haggerty, J. S., A. Lightfoot, J. E. Ritter, P. A. Gennari, and S. V. Nair, "Oxidation and Fracture Strength of High-Purity Reaction-Bonded Silicon Nitride," J. Am. Ceram. Soc., 72 [9] 1675-79 (1989).

Hawk, D. E. and J. L. Bassani, "Transient Crack Growth Under Creep Conditions," J. Mech. Phys. Solids. 34 [3] 191-212 (1986).

Hollenberg, G. W., G. R. Terwilliger, R. S. Gordon, "Calculation of Stresses and Strains in Four-Point ending Creep Tests," J. Am. Ceram. Soc. 54 [2] 196-199 (1971).

Holmes, J. W., "Tensile Creep Behavior of a Fiber- Reinforced SiC/Si3N4 Composite," In Press J. Mater. Sci.

Hsueh, C. H., "Interfacial Debonding and Fiber Pull-out Stresses of Fiber-reinforced Composites," Materials Science and Engineering, A123 1-11 (1990).

Hsueh, C. H. and P. F. Becher, "Thermal Expansion Coefficients of Unidirectional Fiber-Reinforced Ceramics," J. Am. Ceram. Soc., 71 C438-C441 (1988).

Jablonski, D., and R. Bhatt, "High Temperature Tensile Properties of Fiber Reinforced Reaction Bonded Silicon Nitride," Presented at ASTM Symposium on Thermal and Mechanical Behavior of Ceramic and Metal Matrix Composites, Atlanta, Georgia, November 7, 1988.

Jakus, K. J. E. Ritter, Jr., and W. P. Rogers, "Strength of Hot-Pressed Silicon Nitride After High-Temperature Exposure," J. Am. Ceram. Soc., 67 [7] 471-475 (1984).

Jakus, K. and S. M. Wiederhorn, "Creep Deformation of Ceramics in Four-Point Bending," J. Am. Ceram. Soc., 71 [10] 832-36 (1988).

Jakus, K., S. M. Wiederhorn, and B. J. Hockey, "Nucleation and Growth of Cracks in Vitreous-Bonded Aluminum Oxide at Elevated Temperatures," J. Am. Ceram. Soc. 69 [10] 725-731 (1986).

Jakus, K. and S. V. Nair, "Nucleation and Growth of Cracks in SiC/Al2O3 Composites," Composites Science and Technology 37 279-297 (1990).

Kim, H. G., University of Massachusetts at Amherst, presented at the American Ceramic Society Cocoa Beach Conference, January 1990.

Kodama, Hironori, Hiroshi Sakamoto, and Tadahiko Miyoshi, "Silicon Carbide Monofilament-Reinforced Silicon Nitride or Silicon Carbide Matrix Composites," J. Am. Ceram. Soc., 72 [4] 551-58 (1989).

Lange, F. F., "High-Temperature Strength behavior of Hot-Pressed Si3N4: Evidence for Subcritical Crack Growth," J. Am. Ceram. Soc., 57 [2] 84-87 (1974).

Larsen, D. C., S. L. Stuchly, and J. W. Adams, "Evaluation of Ceramics and Ceramic Composites for Turbine Engine Applications," Final report to Air Force AFWAL-TR-4202, December 1988.

Laughner, J., R. T. Bhatt, "Measurement of Interfacial Shear Strength in SiC-Fiber Si3N4 Composites," J. Am. Ceram. Soc.,72 [10] 2017-19 (1989).

Lightfoot, A., L. Ewart, J. S. Haggerty, Z. Q. Cai, J. E. Ritter, and S. V. Nair, "Processing and Properties of SiC Whisker and Particulate Reinforced Reaction Bonded Silicon Nitride," Proceedings of the 15th Annual Conference on Composites and Advanced Ceramics, Engineering Ceramics Division Meeting, American Ceramic Society, Cocoa Beach, FL, January 1991.

Lightfoot, A., H. L. Ker, and J. S. Haggerty, "Properties of RBSN and RBSN-SiC Composites," Ceram. Eng. Sci. Proc., 11 [7-8] 842-856 (1990).

Llorca, J. and R. N. Singh, "Influence of Fiber and Interfacial Properties on the Fracture Behavior of Fiber-Reinforced Ceramic Composites," 74 [11] 2882-90 (1991).

Llorca, J. and M. Elices, "Fracture Toughness, Ductility and Crack Growth Resistance of Fiber Reinforced Ceramics"; Structural Ceramics - Processing, Microstructure and Properties; pp. 403-11 in proceedings of the 11th Riso International Symposium on Metallurgy and Materials Science (Riso, Denmark, Sept., 1990), Edited by J.J. Bentzen et al. In press.

Luh, E. Y. and A. G. Evans, "High-Temperature Mechanical Behavior of a Ceramic Matrix Composite," J. Am. Ceram. Soc., 70 [7] 466-69 (1987).

Lundberg, R., R. Pompe, R. Carlsson, and P. Goursat, "Fiber Reinforced Silicon Nitride Composites," Composites Science and Technology, 37 165-176 (1990).

Mah, T. et al., "Recent Developments in Fiber Reinforced High Temperature Ceramic Composites," Amer. Cer. Soc. Bull., 66 [2] 304 (1987).

Mall, S., R. P. Vozzola, and L. P. Zawada, "Characterization of Fracture in Fiber-Reinforced Ceramic Composites under Shear Loading," J. Am. Ceram. Soc., 72 [7] 1175-78 (1989).

Marshall, D. B., B. N. Cox, and A. G. Evans, "The Mechanics of Matrix Cracking in Brittle-Matrix Composites," Acta Metall., 33 [11] 2013-2021 (1985).

Marshall, D. B. and A. G. Evans, "Failure Mechanisms in Ceramic-Fiber/Ceramic-Matrix Composites," J.Am. Ceram. Soc., 68 [5] 225-231 (1985).

Morscher, G. M., P. Pirouz, and A. H. Heuer, "Temperature Dependence of Interfacial Shear Strength in SiC-Fiber-Reinforced Reaction-Bonded Silicon Nitride," J. Am. Ceram. Soc., 73 [3] 713-720 (1990).

Moulson, A. J., "Review: Reaction-Bonded Silicon Nitride: Its Formation and Properties," Journal of Materials Science, 14 1017-1051 (1979).

Nair, S. V., "Crack Wake Debonding and Toughness in Fiber or Whisker Reinforced Brittle-Matrix Composites," J. Am. Ceram. Soc. 73 [10] 2839-47 (1990).

Nair, S. V., K. Jakus, and C. Ostertag, "Role of Glassy Interface in High Temperature Crack Growth in SiC Fiber Reinforced Alumina," Ceram. Eng. Sci. Proc., 9 [7-8] 681 (1988).

Nair, S. V., K. Jakus and T. Lardner, "The Mechanics of Matrix Cracking in Fiber-Reinforced Ceramic Composites Containing a Viscous Interface," Accepted for Publication in Mechanics of Materials Journal, 1991.

Ohji, T., Y. Yamauchi, W. Kanematsu, S. Ito, "Tensile STrength and Fracture Defects Expanded by Subcritical Crack Growth of Silicon Nitride at High Temperatures, "J. Mat. Sci. Letters, 9 1266-1268 (1990).

Okada, A. and N. Hirosaki, "Subcritical Crack Growth in Sintered Silicon Nitride Exhibiting a Rising R-Curve," J. Am. Ceram. Soc., 73 [7] 2095-6 (1990).

Pezzotti, G., I. Tanaka, and T. Okamoto, "Si3N4/SiC-Whisker Composites without Sintering Aids: III, High-Temperature Behavior," J. Am. Ceram. Soc. 74 [2] 326-32 (1991).

Porz, F., and F. Thummler, "Oxidation Mechanism of Porous Silicon Nitride," J. Mat. Sci. 19 1283-1295 (1984).

Pysher, D. J., K. C. Goretta, R. S. Hodder, Jr., and R. E. Tressler, "Strengths of Ceramic Fibers at Elevated Temperatures," J. Am. Ceram. Soc., 72 [2] 284-88 (1989).

Quinn, G. D. and R. N. Katz, "Stepped Temperature Stress-Rupture Testing of Silicon-Based Ceramics," J. Am. Ceram. Soc., 57 [11] 1057-1058 (1978).

Quinn, G. D., "Static Fatigue in High-Performance Ceramics," Special Technical Testing Publication 844, ASTM (1984).

Rice, R. W., "Mechanisms of Toughening in Ceramic Matrix Composites," Ceramic Eng. Sci. Proc. [7-8] 661-702 (1981).

Rice, R. W., "Ceramic Matrix Composite Toughening Mechanisms: An Update," Ceram. Eng. Sci. Proc., [7-8] 589-606 (1985).

Ritter, J. E., P. A. Gennari, S. V. Nair, J. S. Haggerty, and A. Lightfoot, "Strength of Reaction Bonded Silicon Nitride After High Temperature Air Exposures," Ceram. Eng. Sci. Proc. 10 [7-8] pp. 625-631 (1989).

Shetty, D. K., M. R. Pascucci, B. C. Mutsuddy, and R. R. Wills, "SiC Monofilament-Reinforced Si3N4 Matrix Composites," Ceram. Eng. Sci. Proc.

Singh, R. N., "Influence of Interfacial Shear Stress on First-Matrix Cracking Stress in Ceramic-Matrix Composites," J. Am. Ceram. Soc., 73 2930-37 (1990).

Singh, R. N., "High-Temperature Mechanical Properties of a Uniaxially Reinforced Zircon-Silicon Carbide Composites," J. Am. Ceram. Soc., 73 [8] 2399-2406 (1990).

Smith, E., "Crack Tip Reinforcement by Bridging Elements: Modelling the Fracture of the Matrix Material," J. Mat. Sci. 25 1632-35 (1990).

Sutcu, M. and W. B. Hillig, "The Effect of Fiber- Matrix Debond Energy on the Matrix Cracking Strength and Debond Shear Strength,"; to be published in Acta Metall.

Swab, J., G. D. Quinn, D. J. Snoha, "Mechanical Behavior of a SiC-Fiber/Si3N4 Composite," MTL TN 90-2, September 1990.

Thouless, M. D. and A. G. Evans, Acta Metall., 36 (1988) 517.

Thouless, M. D., O. Sbaizero, L. S. Sigl, and A. G. Evans, "Effect of Interface Mechanical Properties on PUllout in a SiC-Fiber-Reinforced Lithium Aluminum Silicate Glass-Ceramic," J. Am. Ceram. Soc., 72 [4] 525-32 (1989).

Weihs, T. P., O. Sbaizero, E. Y. Luh, and W. D. Nix, "Correlating the Mechanical Properties of a Continuous Fiber-Reinforced Ceramic-Matrix Composite to the Sliding Resistance of the Fibers," J. Am. Ceram. Soc., 74 [3] 535-40 (1991).

Yang, J.-M., R. B. Thayer, S. T. Chen, and W. Lin, "Creep of Fiber-Reinforced Ceramic Matrix Composites," Published in the Proceedings of the International Conference on Composite Materials, 1991.

Zok, F., O. Sbaizero, C. L. Hom, and A. G. Evans, "The Mode I Fracture Resistance of a Laminated Fiber Reinforced Ceramic," J. Am. Ceram. Soc., 74 [1] 187-93 (1991).